UNIVERSITÀ DEGLI STUDI DI PADOVA

PhD School in Industrial Engineering

Chemical, Materials and Mechanical Engineering - XXVIII cycle

Characterization of the micro injection molding of micro and nanostructured polymer surfaces

Supervisor: Prof. Giovanni Lucchetta

PhD. Student: Marco Sorgato

UNIVERSITÀ
DEGLI STUDI
DI PADOVA

Sede Amministrativa: Università degli Studi di Padova

Dipartimento di Ingegneria Industriale

SCUOLA DI DOTTORATO DI RICERCA IN : INGEGNERIA INDUSTRIALE

INDIRIZZO: IINGEGNERIA CHIMICA, DEI MATERIALI E MECCANICA

XXVIII CICLO

CHARACTERIZATION OF THE MICRO INJECTION MOLDING OF MICRO- AND NANO- STRUCTURED POLYMER SURFACES

Direttore della Scuola: Ch.mo Prof. PAOLO COLOMBO

Coordinatore d'indirizzo: Ch.mo Prof. ENRICO SAVIO

Supervisore: Ch.mo Prof. GIOVANNI LUCCHETTA

Dottorando: MARCO SORGATO

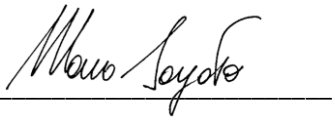

An expert is a person who has made all the
mistakes that can be made in a very narrow field.

Niels Bohr

SOMMARIO

Tra i processi per la produzione di componenti micro e nano strutturati, il processo di micro stampaggio a iniezione presenta una serie di vantaggi che lo rendono commercialmente interessante. Tale tecnologia è caratterizzata da un elevato grado di riproducibilità, che la rende idonea alla produzione di massa di micro componenti in materiale termoplastico. Parlando di micro prodotti, la qualità del pezzo stampato risulta essere di fondamentale importanza e per questo, negli ultimi decenni, lo studio dei fattori che influenzano la qualità del prodotto finito, sono stati al centro di numerose indagini. Questo lavoro di tesi si pone come obbiettivo l'analisi del processo di micro stampaggio per la produzione di componenti micro e nano strutturati aventi features ad elevato rapporto di forma. Lo studio si concentra soprattutto sulle limitazioni del processo, utilizzando come casi studio delle geometrie particolarmente critiche per il micro stampaggio a iniezione. La caratterizzazione del processo e l'individuazione dei sui limiti sono stati indagati non solo considerando i parametri che influenzano la qualità del prodotto finito, ma anche le proprietà dei materiali termoplastici impiegati, l'interazione tra materiale plastico e stampo, e l'utilizzo di tecnologie ausiliarie come il riscaldamento e raffreddamento rapido dello stampo e l'evacuazione forzata dell'aria dalla cavità. I risultati confermano quanto riportato in letteratura e contribuiscono ad estendere lo stato dell'arte sul processo di micro stampaggio a iniezione, il quale rappresenta ad oggi una tecnologia affidabile ed economicamente efficace per la produzione su larga scala di micro componenti in materiale plastico in diversi settori industriali.

ABSTRACT

The micro injection moulding process has a set of advantages that makes it commercially interesting, with potential for further developments in the future. In this sense, its application to the replication of surfaces characterized by micro and nano-structures has been the focus of many researches. In this work, the micro injection moulding process for the manufacturing of nanofeatures and high AR microfeatures was characterized, focusing on the challenges and limitations in the replication.

This research completely characterized the μIM technology, not only considering the process parameters, but also considering the material properties, the interaction between polymer and mould material, and the use of auxiliary technologies like cavity air evacuation and rapid heat cycle moulding. The carried out work confirms previous findings and contributes to extend the state-of-the-art knowledge about the μIM process, which is considering nowadays a reliable and cost effective means of producing a wide range of micro components in thermoplastics materials.

CONTENTS

LIST OF TABLES

INTRODUCTION

The integration of functional micro- and nanostructures on polymeric surfaces offers a wide range of potential applications for different markets, because a variety of surface properties can be adapted without changing the chemical composition of the material, which is of particular relevance for the life science and medical diagnostics sector. The interaction of surface topographies with cells is of particular interest for tissue engineering and implant surfaces, and also in the context of bactericidal surfaces. Moreover, there is growing industrial interest in optical structures for anti-reflection, redirection of sunlight and diffractive and holographic structures for decorative and anti-counterfeit applications. Realization of these applications in polymers requires fast and efficient mass production methods that allow functional structures to be integrated into the product in a versatile and cost-effective manner. In this sense, polymer micro injection moulding (μIM), has been identify as key enabling technology for the mass production of nano and micro structured components.

When replicating micro- and nano features, surface quality is one of the most important process characteristics and it constitutes a manufacturing constrain in applying the μIM process to a wider range of micro-engineering applications. Consequently, the study of factors that affects the replication capabilities is very important in order to gain insight of the process and overcome technological limitations that still persists.

Even if in the last decades, many research group focused their attention on the factors that affect the replication quality during the μIM process, the complete replication of both micro- and nanofeatures poses over a large substrate, remain a critical task. This is due to the fact that in micro injection moulding, the polymer flow is characterized by a high surface-to-volume ratio, which leads to a high cooling speed of the polymer melt in the mould cavity. The polymer melt near the wall of the cavity cool down to a solid skin and reduced the cross section of the flow, precluding the complete filling.

This is more evident when moulding:

- Features with *cross section* in the order of few micrometers and *high apect ratio (AR)* (Figure 0.1a);
- Features with *cross section* in the order of few hundreds nanometer (Figure 0.1b).

In this work, the micro injection moulding process for the manufacturing of nanofeatures and high AR microfeatures was characterized, focusing on the challenges and limitations in the replication.

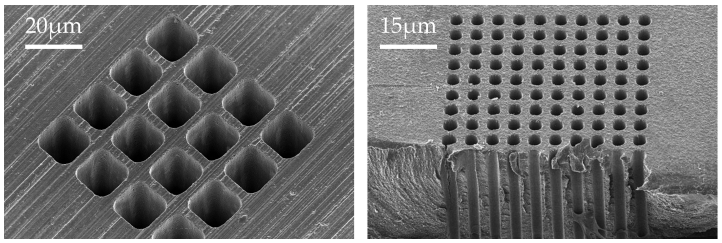

(a)

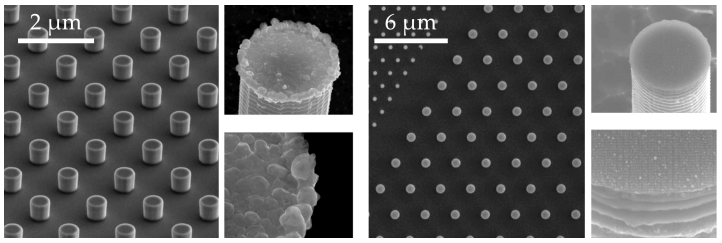

(b)

Figure 0.1: SEM pictures of (a) High aspect ratio micro features and (b) nanofeatures.

Two different projects were considered as case studies: the *Cell-Diasp project* and the *NanoBones project*. Both these projects required the replication of challenging micro- and nanofeatures, posed over a larger surface, via micro injection moulding.

The ErytroChip device is characterized by a great lenght-to-thickness (L/t) ratio of the main flow region, covered by more than 5700 high aspect ratio micro-channels, while the support for the NanoBones the features has a cross section of few hundreds of nanometers and aspect ratio 1:2.

In this section the two projects are briefly presented, in order to understand what are the objectives that they poses and how these brought up micro injection moulding related issues.

THE CELLDIASP PROJECT

The *CellDiasp* or *ErytroChip* project (Cell - Diagnostics Sample - Preparation BioMEMS) aims to develop a micro-fluidic device for the depletion of red blood cells (RBCs) in blood analysis. The device should permit the isolation and extraction of rare cells contained in the blood.

The basic principle of the filtering device (Figure 0.2) is the idea of using the gravity to favor the entrapment of RBCs in micro-channels realized over the micro-fluidic chip. RBCs are characterized by a diameter of $6.2 \div 8.2$ μm, a thickness of $2 \div 2.5$ μm in the sides and of $0.8 \div 1$ μm in the center. The nucleated cells have greater diameters, $8 \div 24$ μm, and have a spherical shape. Therefore, due to their dimensions and shape, the nucleated cells cannot enter the micro-cavities

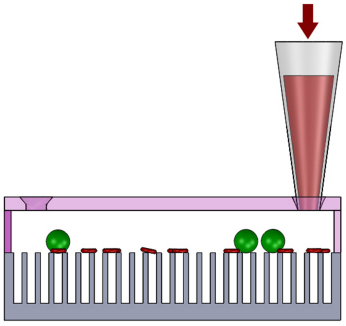

(a)

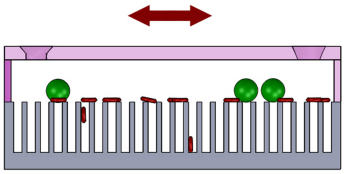

(b)

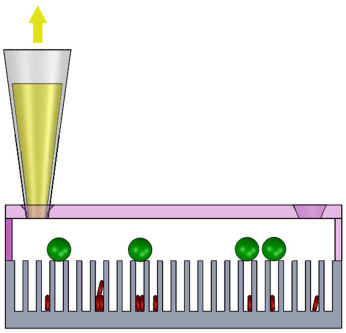

(c)

Figure 0.2: Schematic of the filtering device (ErytroChip): (a) sample introduction, (b) cells filtering, (c) selective retrieval.

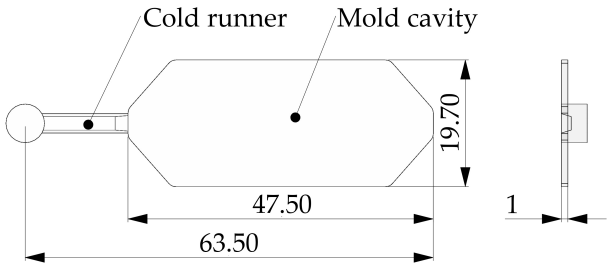

Figure 0.3: Dimensions of the ErytroChip.

and so can be extracted. Thus the final blood sample contains almost only nucleated cells, that are what will be analyzed.

According to its functionality the device should have:

1. an adequate volume between micro-channels for the accumulation of the RBCs, and to avoid them to exit;

2. an uniform distribution of micro-channels along the chip.

The micro injection moulding process was chosen for the manufacturing of the device, due to its capabilities in replicating micro structured surface. In terms of manufacturing the focus was on the replication of the microstructures, that because of their aspect ratio are a manufacturing constraint.

From a manufacturing point of view, the functional objectives become:

1. the replication of high aspect ratio micro-features via micro-injection moulding;

2. the achievement of a low standard deviation in the replicated height of micro-channels.

The ErytroChip is characterized by more than 5700 micro-channels, that have a width of 5 μm and an height of 15 μm (aspect ratio: 3). These microfeatures are oriented perpendicular to the flow direction and located at an increasing distance from the injection location. The main dimension of the ErytroChip are shown in Figure 0.3, its thickness is 1 mm.

THE NANOBONES PROJECT

The main objective of the project is the realization of micro-and nanostructured surfaces to induce the differentiation of stem cells into osteoblasts, with the intent to improve bone replacement technologies.

Bone replacement procedures are commonly used to replace bone structures. To achieve a functional and long-term repair, the bone

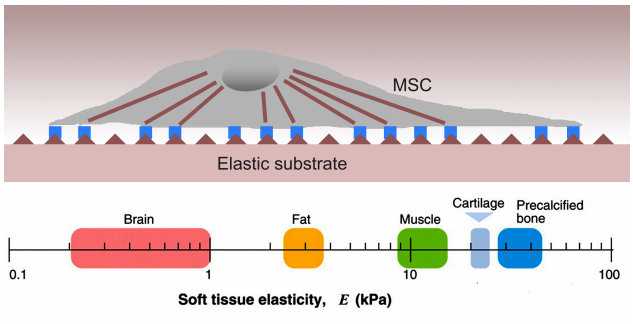

Figure 0.4: Influence on cell culture of the elasticity of the substrate.

substitutes must firmly join to the natural bone. This process, named *osseointegration*, is a consequence of the migration of undifferentiated cells from the host to the surrounding tissues to the prosthesis and their differentiation towards mature bone cells (*osteoblasts*) producing bone tissue that firmly anchor the implant in place. When cells fail to do this, a soft capsule surrounds the implant resulting in the dislodgement of the prosthesis or low quality repair. Traditionally, substrate materials were simply considered as inert context that carry biochemical supplements for cell growth and/or differentiation promotion. However recently studies found out that cells interact with surfaces typically through the creation of attachment points linking the cytoskeleton to extracellular binding sites. For this reason the basic understanding of cell–substrate interaction represents a crucial factor in the fields of tissue engineering. Moreover intrinsic material properties that mimic physiologically relevant extracellular matrix characteristics have been proven to regulate stem cell fate (from adhesion to proliferation and differentiation). In particular, substrate mechanical stiffness and micro and nanometre-scale topography have been reported to play a fundamental role in driving human mesenchymal stem cell differentiation (Figure 0.4).

Starting from this basis, the general aim of the project is to develop the technology to produce potentially transplantable osteoinductive devices for bone replacement. This is concerned with the development of the design rules for nano structured surfaces for cell differentiation, the development and the implementation of a suitable manufacturing process chain for the mass production of substrates for cell differentiation including the optimization of tooling as well as replication process.

The polymer samples dimensions were selected according to the cells culture wells and represented in Figure 0.5.

Concerning the design rules for nano-structured surfaces for cell differentiation, a literature review was performed. As the result that among different substrate parameters such as, surface topographies, feature shape, feature dimensions and inter-pillar gap sizes, the inter-pillar gap size and their dimensions have the largest influence on cell

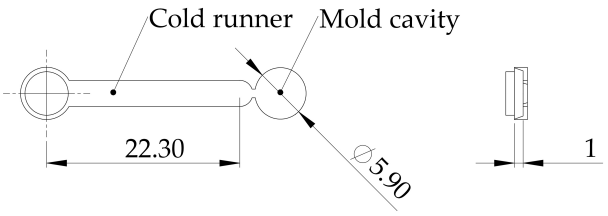

Figure 0.5: Dimensions of the polymeric substrate for the NanoBones project.

behaviour, while the specific shape of the pillars does not have any significant effect.

In this work we have opted for cylindrical pillars with fixed aspect ratio and variable diameter and interspaces as shown in Figure 0.6. These geometries were used for analyzed the effect of the interaction substrate/stem cell on their adhesion, proliferation and differentiation.

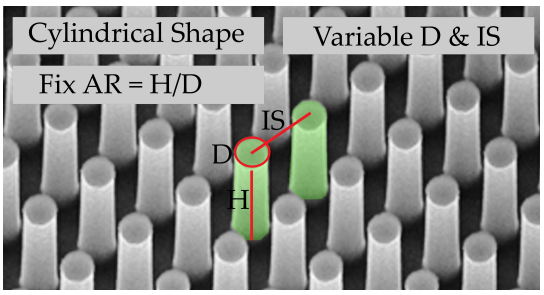

Figure 0.6: Nanopillars geometrical parameters.

Part I

OVERVIEW OF MICRO-MANUFACTURING

1

MICRO MANUFACTURING

Micro-products and components are almost everywhere in our lives, and their demand is constantly increasing. The utilization of micro-systems covers very large and differentiated fields of applications; the most popular application markets are summarized in Figure 1.1.

Manufacture of these products has received great attention during recent years. At the same time, as nanotechnology becomes more and more mature and influential, more nano technology-based products have emerged, such as nano-devices for sensors, communication and medical treatment, nano-materials and coating/ functionalized surfaces for enhanced performances.

Micro- manufacturing concerns manufacturing methods, technologies, equipment, organizational strategies and systems for the manufacture of products and/or features that have at least two dimensions that are within sub-millimeter ranges. Micro-manufacturing engineering is a general term which concerns a series of relevant activities within the chain of manufacturing micro-products/ features, including design, analysis, materials, processes, tools, machinery, operational management methods and systems.

There is a huge diversity in micro-products, the main types being micro-electronics products, micro-optical electronics systems (MOES), micro-electronics mechanical systems (MEMS) and micro-optical electronics mechanical systems (MOEMS), depending on the combination of product functionalities and/or working principles. Correspondingly, there are different methods and strategies which could be used to manufacture these products. Micro-manufacturing, in a wider context, should cover all these aspects relating to manufacturing these products.

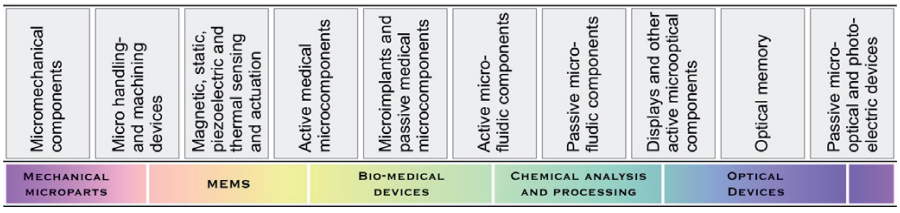

Figure 1.1: Micro product categories.

1.1 MICRO-PRODUCTS DESIGN AND FABRICATION

Design of products for micro- manufacturing needs to address production issues fully, compared with the prototype products based on micro-technologies.

High volume production of micro-components should be a target for design for micro-manufacturing. When these products are designed, not only will functional requirements need to be considered but also micro- manufacturing related factors will have to be taken into account. This is because, as briefly describe above, manufacturing these products renders more significant challenges, compared to the manufacture of macro-products. The following are some typical issues to be addressed at the design stage:

- **Overall dimensions of the part/products.** Overall dimensions of a part, like diameters, widths, lengths and thicknesses, are very much constrained by the overall capabilities of the processes and manufacturing facility (machines, handling devices, tool, etc.). Both maximum and minimum dimensions are the parameters to be checked with reference to the manufacturing system's capabilities. Complexity around dimensional scale issues is a dominant factor in micro-/ nano- manufacturing.

- **Part component local features.** Design of local features, such as hole/ pocket radii and aspect ratios, widths/ depths of channels or aspect ratios, wall thickness, area reductions, density of the local features, will be largely constrained by the processing capability in micro-/ nano-manufacturing, especially those relying on the use of tools such as replicating processes. Manufacture of local features spread over a large area also renders challenges to many micro-manufacturing processes and equipment.

- **Shape capability.** Shape capability considers the capability/ limitation of a manufacturing process in dealing with the shapes to be produced. For example, a lot of processes are only able to deal with 2D/2.5D shapes while 3D shapes may need much more significant efforts such as new processes and expensive equipment. Conventional rules on shape capability of manufacturing may not be applicable to micro-manufacturing largely due to the sizes to be considered and limitation of the tool shapes that could be produced.

- **Tolerance and surface quality capability.** Design of a macro-product would expect the designer to consult handbooks/standards before specifying a grade of tolerance and surface quality requirements. Design for micro-manufacturing may not be as straightforward as the design of a macro-product. Standards on

manufacturing tolerances for design for micro-manufacturing have not been established fully, while most of the data is *in-house* determined.

- **Material capability.** Selection of a material for micro- manufacturing will be constrained largely by availability of the material for volume production, due to the limited number of the suppliers currently operating in this field; however, the trend is improving, such as with nano-material suppliers, the number of which has increased significantly recently. New study/ qualification of material properties may be needed if the material suppliers are not able to provide the material data relevant to micro-manufacturing, such as size effects and material property descriptions. The properties will have to be qualified for design uses, with consideration of size effects, and these have to be available with the inclusion of mechanical, thermal, electrical and magnetic properties, as appropriate, and others including biocompatibility, chemical compatibility, hydrophilic and hydrophobic properties, etc.

- **Part/component material properties after processing.** Involvement of large plastic deformations, damages, possible significant local temperature rise and thermal stresses during mechanical and thermal processes may result in alteration of the material properties after processing. The micro-part/ component material properties will play significant roles in determining part/component performance under working conditions than that for macro-components, such as those used in micro-sensors and medical implants. Part/component design is, therefore, constrained by the applicability of certain micro-manufacturing processes, e.g. chemical and high temperature processes, due to considerations of possibly adverse effects on the material properties.

The design of micro-products is still a challenging task due to lack of sufficient standards, design/ manufacturing rules and understanding of the manufacturing process themselves. Compared to the manufacture of macro-products, manufacturing methods and strategies in micro-manufacturing may be different. Manufacturing macro-products may be carried out by manufacturing individual components/ parts by removing and/or deforming and/or adding materials, and then assembling them. These can be carried out either at a single industrial site or at different sites.

Manufacturing micro-products may be carried out with patterning, deposition and layering methods within a single machine/ manufacturing platform, e.g. integrating components/ parts fabrication with assembly/ packaging is often used in MEMS and micro-systems manufacturing. Micro-manufacturing largely uses non-traditional manu-

facturing methods or scaling down or modifying the traditional methods, as appropriate, to fully address issues related to manufacturing in the micro-world. Further, manufacturing chains may also be different, compared to traditional manufacturing. Moreover, the increased demand for micro-products has led to rapid development of other technologies for micro-manufacturing of individual parts and systems, following the paths of downscale existing manufacturing processes or develop new processes in the cross field of existing technologies. Although on the technological side the development has moved very fast, it is a continuous challenge to create the operational basis for an industrial production of micro products, process reliability and stability must be targets for the design for micro-manufacturing.

In recent years plastic moulding techniques such as injection moulding have been adapted for the necessities of micro- components fabrication. Injection moulding is a process technology that has been well established in the production of polymer parts in the macro-dimensional range for decades, therefore, vast know-how and machine technology is available to be made use of in micro injection moulding (μIM). Parts fabricated by micro injection moulding, even from high end materials, are suitable for applications requiring low cost and disposable components. In fact, peculiar characteristics such as production capability, disposability, biocompatibility, optical properties, just to mention a few, pose plastics as the best choice for numerous micro-products. As result plastic products manufactured by micro- injection moulding have made successful entry into the market; a large variety of applications is already known and many more are expected to arise in the future.

1.2 MICRO INJECTION MOULDING

Micro injection moulding technology was firstly introduced from conventional injection moulding since late eighties, to satisfy the specific functional and technical requirements of new emerging micro-products. At that time no appropriate technology was available and only modified commercial units of traditional injection moulding machine could be used. Only in the middle nineties (March 1997) *Battenfeld* started the project for the *Microsystem* 50, subsequently new machines were developed specifically addressing micro-moulding parts.

Among the variety of micro-manufacturing processes, μIM possesses the advantage of having a vast know-how available from conventional plastics technology. The advantages that micro injection moulding inherited from the conventional process, in addition to the considerable technological developments witnessed in the recent years, made it an ideal process for producing micro-moulded plastic components for a wide range of applications.

1.2.1 *Applications*

A broad variety of applications is already known for the micro moulding of thermoplastic polymers (Table 1.1) and many more are expected to arise in the near future.

Markets which need micro-parts are the following:

- Automotive (e.g. micro-switch, sensors, ABS-Systems);
- Computer (e.g. head of an ink-jet printer);
- Telecommunication (e.g. mobile phone, SIM card connector);
- Connectors (e.g. plug connectors, couplers);
- Electronics Micro-parts on circuit boards;
- Micro-equipment (e.g. valve technology);
- Medical technology (e.g. micro-fluidic devices with micro- channels hearing aids, implants, devices for DNA analysis, bio-MEMS, tissue scaffolds, vascular clamp);
- Sensors (e.g. airbag sensors, sensor disk, bio-sensors);
- Micro-mechanics (e.g. micro-motor, rotor, micro-gears, micro-switch, locking lever, catch wheel, operating pins, sleeve);
- Optics (e.g. lenses, displays);
- Optical gratings (CD, DVD);
- Watches (e.g. gear wheels, latches, micro-transmissions)
- Glass fiber conductors (ferrules, connectors);
- Micro-structured micro-parts (lab on the chip, data carrier, self-cleaning surfaces, sensor disk structure);
- Patterned adhesives;
- Precise suppliers;
- Special materials (e.g. PIM (MIM/CIM), PTFE);
- Institutes, Universities (e.g. material, technology for research).

In general miniaturized parts fabricated with micro injection moulding, even from high end materials, are suitable for applications requiring low cost, mass production, flexibility, geometrical quality, and disposable components.

APPLICATION FIELDS	EXAMPLES
Micromechanical parts	• Locking lever for micro mechanical industry or micro switch; • Latch for the watch industry; • Catch wheel for micro switch; • Operating pin; • Gear plate for motive power engineering.
Micro gear wheel	• Dented wheel for watch industry; • Rotor with gear wheel for watch industry; • Gear wheel for micro gear; • Spur wheel in the field of electrical technology; • Spiral gear in the field of electrical technology/metrology; • Spline in the field of electrical technology/metrology.
Medical industry	• Micro filter for acoustics, hearing aid; • Implantable clip; • Bearing shell/bearing cap; • Sensor housing implantable; • Aseptic expendable precision blade.
Optical and Electronic industries	• Coax plug/switch MID for mobile phone; • SIM card connector for mobile phone; • Pin connector for mobile phone; • Single mode and multi mode ferrules.

Table 1.1: Application fields of the micro injection moulding process [1].

1.2.2 *Micro Injection Moulding Machines and Process Steps*

Injection moulding is the process of transferring a thermoplastic raw material in the form of granules (pellets) from a hopper into a heated barrel so that it becomes molten and soft. The material is then forced under pressure inside a mould cavity where it is subjected to holding pressure for a specific time to compensate material shrinkage. The material solidifies as the mould temperature is decreased below the glass-transition temperature of the polymer. After sufficient time, the material freezes into the mould shape and gets ejected, then the cycle is repeated. A typical cycle lasts between few seconds to few minutes.

Conventional injection moulding machines are comprised of the following parts:

THE PLASTICIZING AND INJECTION UNIT: their major tasks are to melt the polymer, fed it to the screw chamber, inject it into the mould cavity and maintain the holding pressure during the cooling phase;

THE CLAMPING UNIT: it's role is to open and close the mould, and hold it tightly to avoid flash during the filling and the holding phases;

THE MOULD CAVITY: the mould is the central part of an injection moulding machine, its function is to distribute the melt into the cavities, shape the part and cooling it.

Through these parts the injection moulding process consists of the following phases:

1. Plasticizing: the rotating screw forces the pellets forward into the barrel which is heated to the desired melt temperature of the molten plastic. The melt is accumulated in front of the screw, ready to be injected;

2. Injection, Filling and Packing: the mould is close, the screw-plunger inject the molten polymer which fills the cavity. At the switchover point, the machine applies the packing pressure;

3. Cooling and Ejection: when the polymer in the cavity has solidified, the mould is opened and the ejectors demould the plastic part.

When downscaling to the micro injection moulding process for the production of smaller parts two kind of problems arises:

TECHNOLOGICAL: reduced dimension of the product requires a smaller shot-size, but this would lead to a thinner and so weaker screw's core. Sometimes pellet's weight is even bigger than that of the micro-moulded part. Thus it is impossible to reduce the screw-plunger size below a minimum value (12 mm) that ensures an

adequate resistance and a minimum stroke to accelerate and apply adequate injection speeds;

PROCESSING: when moulding micro-components with a reciprocating screw is not possible to control the metering accuracy and the homogeneity of the melt. Moreover, due to channel configuration and high injection pressure, required to fill micro-cavities, there is melt back-flow during injection.

For these reasons, when diminishing part volume and shot size, conventional injection moulding machines are no longer technically and economically viable solution. Therefore, in micro injection moulding machines the plasticizing and the injection units are decoupled: it is possible to obtain a precise injection (5-300 milligrams) with a small plunger, moved by an electric motor, supplied upstream by the rotating screw/extruder.

In other words, limitations of the conventional technology were overcome with the adoption of the plunger injection system, in which the plasticization and the injection phases are divided: the plasticization takes place in a dedicated functional part of the machine, which is separated from the injection unit. Injection plungers as small as 5 mm in diameter are used to produce polymer melt down to sub-gram levels; at the same time, a screw-extruder having sufficient channel depth to properly handle standard pellets and yet provide the required strength can be employed.

Consequently the μIM process consist of the following phases:

1. Plasticizing: the polymer is melted by the action of the rotating screw and accumulated into the metering chamber;
2. Metering: after the set volume has been achieved, the plunger in the dosage barrel delivers the shot volume to the injection barrel;
3. Injection, Filling and Packing: the melt is injected into the mould, once the plunger injection movement is completed, a holding pressure is applied;
4. Cooling and Ejection: when the polymer in the cavity has solidified, the mould is opened and the ejectors demould the plastic part.

Summarizing, the main difference between conventional and micro injection moulding machines lays in the decoupling of the plasticizing and injection units. The main benefits of having a dedicated injection module are the following [2]:

- all standard pellet sizes can be processed by the screw;
- stress free plasticization and dosing in a low pressure area are obtained;

- each shot is done with new raw material;
- shortest runners and gates and so control of process conditions near the cavity;
- injection of thermally homogeneous material;
- high processing security and excellent reproducibility results;
- minimum lost of pressure.

Moreover, in μIM applications, the need for micro-scale tolerances, fine details, and desired surface finish surpass those encountered in tool manufacturing for conventional injection moulding, where the cavity is usually machined directly on the mould plate. For micro injection moulding applications the procedure has instead undergone substantial alterations, as to obtain tailored tool inserts.

1.2.3 *Basic Mould Inserts Micro and Nano Fabrication Techniques*

The choice of the technique for the insert fabrication generally depends on three main factors: the insert material used, the dimensions of the micro-features and their aspect ratio. A number of techniques currently in use for micro-fabrication include: LIGA-process, photolithography, nano imprinting litography, micro-electrical discharge machining (μEDM) and mechanical micro-machining [3]. In general, direct structuring techniques (e.g., LIGA, photolithography) are far more attractive, due to their ease of application and lower costs, compared to conventional machining processes. In the following paragraphs the basic mould inserts fabrication techniques will be described, focusing on their challenging and limitations.

1.2.3.1 *LIGA*

LIGA is a high-aspect-ratio micromachining process that relies on X-ray lithography and electroplating (in German: *LIthographie Glvanoformung Abformung*) [4, 5]. With standard UV photolithography and photoresists, the maximum thickness achievable is on the order of a few tens of microns and the resulting metal structures show tapered walls. LIGA is a technology based on the same plating-through-mask idea, but can be used to fabricate metal structures of thicknesses ranging from a few microns to a few millimeters with almost vertical sidewalls. This is achieved using X-ray lithography and special photoresists. Due to their short wavelength, X-rays are capable of penetrating a thick photoresist layer with no scattering and defining features with lateral dimensions down to 0.2 μm (aspect ratio > 100 : 1).

The photoresists used in LIGA should comply with certain requirements, including sensitivity to X-rays, resistance to electroplating

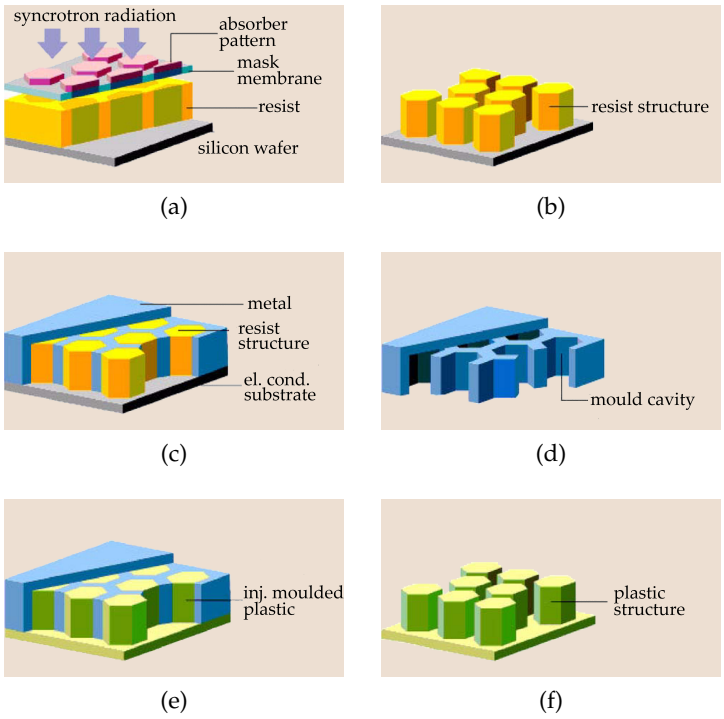

Figure 1.2: Schematic representation of LIGA process: (a) irradiation, (b) development , (c) electroforming, (d) mould insert, (e) mould filling, (f) mould separation.

chemicals, and good adhesion to the substrate. Based on such requirements Poly-(methylmethacrylate) (PMMA) is considered an optimal choice for the LIGA process.

The mask structure and materials for X-ray lithography must also comply with certain requirements. The traditional masks based on glass plates with a patterned chrome thin layer are not suitable, because X-rays are not absorbed in the chromium layer and the glass plate is not transparent enough. Instead, X-ray lithography uses a silicon nitride mask with gold as the absorber material.

Once the photoresist is exposed to the X-rays and developed, the process proceeds with the electroplating of the desired metal. Ni is the most common, although other metals and metallic compounds such as Cu, Au, NiFe, and NiW. Due to the high cost of the X-ray sources (synchrotron radiation), the LIGA technology is intended for the fabrication of moulds that could be used many times in hot embossing or injection moulding processes. The schematic illustration of LIGA process is represented in Figure 1.2.

1.2.3.2 *UV Litography*

Lithography is the technique used to transfer a computer generated pattern onto a substrate (silicon, glass,etc.). The starting point following the creation of the computer layout for a specific fabrication se-

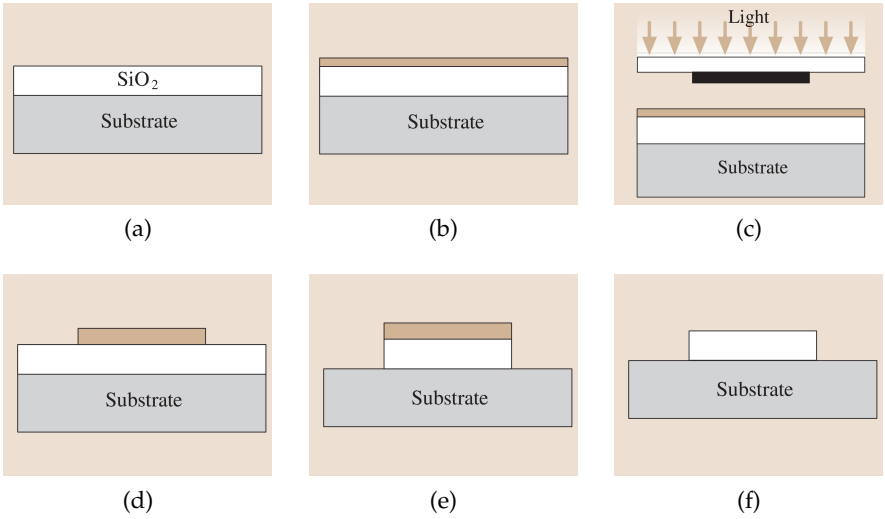

Figure 1.3: Schematic drawing of the photolithographic steps with a positive resist (PR): (a) oxidize the substrate, (b) spin the photoresist and soft bake, (c) expose the photoresist, (d) develop the photoresist and hard bake, (e) etch the oxide, (f) strip the photoresist.

quence is the generation of a photo mask. This involves a sequence of photographic processes (using optical or e-beam pattern generators) that results in a glass plate having the desired pattern in the form of a thin ($\sim$ 100 nm) chromium layer. Following the generation of photo mask, the lithography process can proceed as shown in Figure 1.3.

This sequence demonstrates the pattern transfer onto a substrate coated with silicon dioxide. However, the same technique is applicable to other materials. After depositing the desired material on the substrate, the photolithography process starts with spin coating the substrate with a photoresist. The spinning speed and photoresist viscosity will determine the final resist thickness, which is typically between 0.5–2.5 μm.

Two different kinds of photoresist are available: positive and negative. In the positive resist, the UV-exposed areas will be dissolved in the subsequent development stage, whereas in the negative photoresist, the exposed areas will remain intact after the development. After spinning the photoresist on the wafer, the substrate is soft baked in order to remove the solvents from the resist and improve the adhesion. Subsequently, the mask is aligned to the wafer and the photoresist is exposed to a UV source.

Depending on the separation between the mask and the wafer, three different exposure systems are available: 1) contact, 2) proximity, and 3) projection. Although contact printing gives better resolution compared to the proximity technique, the constant contact of the mask with photoresist reduces the process yield and can damage the mask. The exposure source for photolithography depends on the resolution. After exposure, the photoresist is developed in a process

similar to the development of photographic film. The resist is subsequently hard baked in order to further improve the adhesion. The hard bake step concludes the photolithography sequence by creating the desired pattern on the wafer. Next, the underlying thin film is etched, and the photoresist is stripped in acetone or other organic removal solvents.

The resolution limit in conventional UV litography is determined largely by the well-known Rayleigh's equation. The resolution (minimum resolvable feature) R and the corresponding depth o focus (DOF) are given by the following (Equation 1.1-Equation 1.2):

$$R = k_1 \lambda / NA \tag{1.1}$$

$$DOF = k_2 \lambda / NA^2 \tag{1.2}$$

Here λ is the exposure wave length, NA is the numerical aperture of the optical system, and k_1 and k_2 are costants that depend on the specific resist material, process technology and image-formation technique used.

To obtain higher resolutions, shorter wavelength light and lens systems with larger numerical apertures can be used. In general, the minimum feature size that can be obtained is almost the same as (or slightly smaller than) the wavelength of light used for the exposure, for which one needs a relatively large numerical aperture.

1.2.3.3 *Soft Litography*

Techniques that prepare a soft mould or stamp by casting a liquid polymer precursor against a topographically patterned master are commonly referred to as soft litography.

A number of polymers could be used for moulding. Elastomers are a versatile class of polymers for replication of a topographic master. The most widely implemented elastomer for nano fabrication is poly - (dimethylsiloxane) (PDMS) [6]. PDMS has a number of useful properties for nano fabrication. This material is durable, unreactive toward most materials being patterned or moulded and transparent above a wavelength of $\sim$ 280nm. Moreover, PDMS is chemically inert, an advantage for patterning many different types of materials. These materials include polymers, precursors to carbons and ceramics, sol-gel materials, organic and inorganic salts, colloids, biological macromolecules, and silanes. The sweeling of the PDMS both compromises dimensional stability and leads to unwanted adhesion after polymerization of monomers. The tensile modulus of PDMS is relatively low ($\sim$ 1.8 MPa) and limits the replication of nano-scale features [7]. High-resolution masters are reproduced accurately in composite stamps of hard PDMS or UV-curable PDMS, with tensile moduli of $\sim$8.2 and $\sim$3.4 MPa respectively.

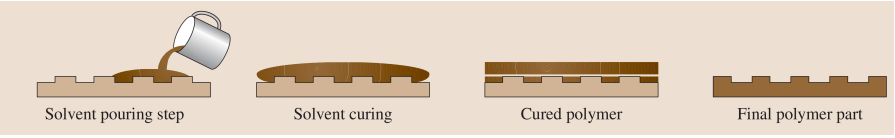

(a)

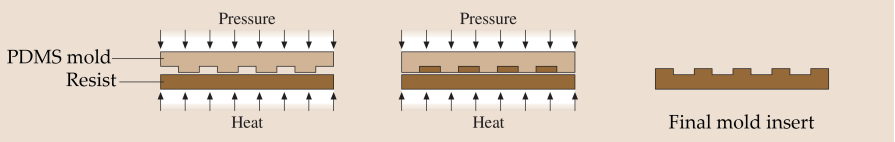

(b)

Figure 1.4: Schematic procedure for carrying out replica moulding against an elastomeric PDMS mould. (a) The PDMS mould is fabricated by casting against nano/micro-metre-sized relief structures fabricated using UV lithography or electron-beam writing; (b) the PDMS mould is used for the REM in order to obtain the final mould insert for the μIM process.

One of the soft-litography techniques is the replica moulding process (*REM*). This is commonly used for mass-produced, disposable plastic micro components, for example, micro fluidic chips, generally made of poly(dimethylsiloxane) (PDMS) and polymethyl methacrylate (PMMA). Replica moulding consists of three steps: (1) creating a topographically patterned master (usually by conventional techniques); (2) transferring the pattern of this master into PDMS by replica moulding (Figure 1.4a); and (3) fabricating a replica of the original master by solidifying a liquid precursor against the PDMS mould (Figure 1.4b). A benefit of moulding with PDMS is the ability to mould against non-planar, rigid and soft topographic surfaces.

Replica moulding can produce numerous moulds, replicas, and patterned surfaces from each master and provide capabilities for nano fabrication not commonly available in an academic setting. Replication of the high-cost, high-resolution masters reduces the financial burden of patterning nano structures and conveniently extends nano fabrication to a range of materials. Replica moulding has transferred $\sim$30 nm lateral features from a diffraction grating, a compressed PDMS stamp [8], but is still not clear what the ultimate limit to replication using PDMS (or other materials) is.

1.2.3.4 *Nano-Imprinting litography*

In previous sections, we discussed several important lithography techniques used commonly in micro and nano fabrication methods. However, these techniques are not suitable for nanometer-scale fabrication. E-beam lithography is an attractive alternative technique for fabricating nano structures [9]. It uses an electron beam to expose an electron-sensitive resist such as polymethyl methacrylate (PMMA) dissolved

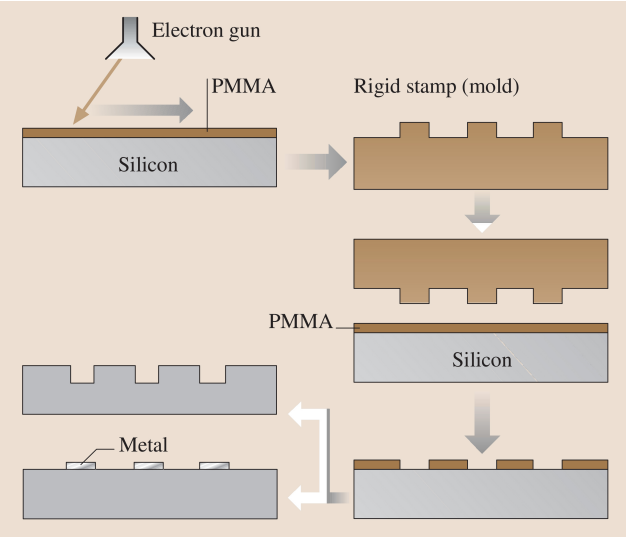

Figure 1.5: Schematic drawing of the nano imprinting lithography (NIL) steps.

in trichlorobenzene (positive) or poly chloromethylstyrene (negative) [10]. The e-beam gun is usually part of a scanning electron microscope (SEM), although transmission electron microscopes (TEM) can also be used. Although electron wavelengths on the order of $1\mathring{A}$ can be easily achieved, electron scattering in the resist limits the attainable resolutions to > 10 nm. An interesting technique that circumvents the serial and low throughput limitations of the e-beam lithography for fabricating nano structures is the nano-imprint technology [11]. This technique uses an e-beam fabricated hard material master (or mould) to stamp and deform a polymeric resist. This is usually followed by a reactive ion etching step to transfer the stamped pattern to the substrate. This technique is economically superior, since a single stamp can be used repeatedly to fabricate a large number of nano structures. Presently, nano-imprint moulds require replacement after $\sim$50 consecutive imprints [12].

Figure 1.5 shows a schematic illustration of nano-imprint fabrication. First, a hard material (e.g., silicon or SiO2) stamp is created using e-beam lithography and reactive ion etching. Then, a resist-coated substrate is stamped, and, finally, an anisotropic RIE is performed to remove the resist residue in the stamped area. The resist used in nano-imprint technology can be thermal plastic, UV-curable, or thermal-curable polymer. For a thermal plastic resist (e.g., PMMA), the substrate is heated to above the glass transition temperature (T_g) of the polymer before stamping and is cooled to below T_g before the stamp is removed. Similarly, the UV and thermal-curable resists are fully cured before the stamp is separated.

1.2.3.5 *Sol-Hybrid Resist*

The development of different new miniaturized devices increased the demand of materials with advanced functional and structural properties. An important class of advanced materials, sol-gel Hybrid Organic–Inorganic (*HOI*) systems, are well suited for such applications due to their high degree of flexibility to design their physical and chemical properties, directed to the application. These sol-gel hybrid materials combine the qualities of organic molecules or polymers (flexibility,versatility) and the physical properties of a glass (refractive index, transparency, thermal and mechanical resistance), which can be adjusted by incorporating other metal alkoxides (Ti, Zr, Al, etc.). In fact, among the many attractive features displayed by sol-gel route, the process versatility in terms of synthesis and final composition is very important, thanks to the wide range of available precursors on the market that allow to develop an incredible number of possible materials. Moreover, in addition to the high versatility in terms of chemical and physical properties and shaping, hybrid materials present the paramount advantage of facilitating both integration and miniaturization since they can be directly writable by different lithographic techniques, generally thanks to the engineered organic component. In this study, we explored the possibility of fabricating micro and nano injection moulding inserts by patterning both the developed hybrid organic-inorganic sol-gel systems on flat metallic surfaces.

The main advantages of using these materials for inserts fabrication are:

- the easier realization through the direct patterning of films with respect to conventionally used micro-machining of metallic bulk;
- the possibility of controlling the desired properties of the masters, such as superior mechanical resistance, chemical stability and low thermal dispersion that allows to maintain higher the temperature of the stamps during replication process with respect to metallic materials, thanks to the flexibility of hybrid materials;
- the possibility of realizing several structures with no grain size limitations to the final resolution and a better surface finishing, typical problems of metallic insert and of some micro machining tools.

2

THE REPLICATION OF MICRO- AND NANO-STRUCTURED SURFACES

Injection moulding has proven to be a feasible and efficient way to manufacture polymeric components with micro- and nano features on their surface. Mould surface topography is transcribed onto the plastic part through complex mechanisms (cfr. section 1.2.2). However this replication process is not perfect, and replication quality depends on material's properties, the topography itself and process conditions.

This chapter describes and discusses the state of the art of micro- and nano features injection moulding.

2.1 CONCEPT OF REPLICATION

Surface structuring based on replication allow for surface fictionalization by means of surface geometrical modification without back end processing such as coating or further treatments. Given a micro/ nano- pattern on a master, various tailored properties can be attributed to the replicated substrate, such as hydrodynamic, mechanical, biological, chemical, biomimetics properties. The potential of the so-called *functional surfaces* is highly dependent on replication technologies of micro- and nano-sized surface features.

Recent advances in micro- and nano- manufacturing processes have led to the development of various process chains for fabricating different surface structures. However, in most cases, the proposed manufacturing routes are limited to laboratory scale implementations and functional features can only be fabricated on planar surfaces, e.g. by applying wafer scale silicon based lithography processes that are cost intensive.

The utilization of replication processes for mass production, such as μIM, represents a major commercial opportunity for producing the so-called functional surface, i.e. surfaces possessing certain properties linked to surface topography and/or chemistry, that are economically viable.

Replication of work piece geometries is a well- established method which involves a mould geometry that is replicated by filling a material into it. As shown in Figure 2.1, in a replication process a master geometry is transferred to a substrate material in this way copying the master geometry. This transfer can be induced by means of heat, force, chemical activation or other energy input or activation; often it is a combination of effects which acts in the replication process.

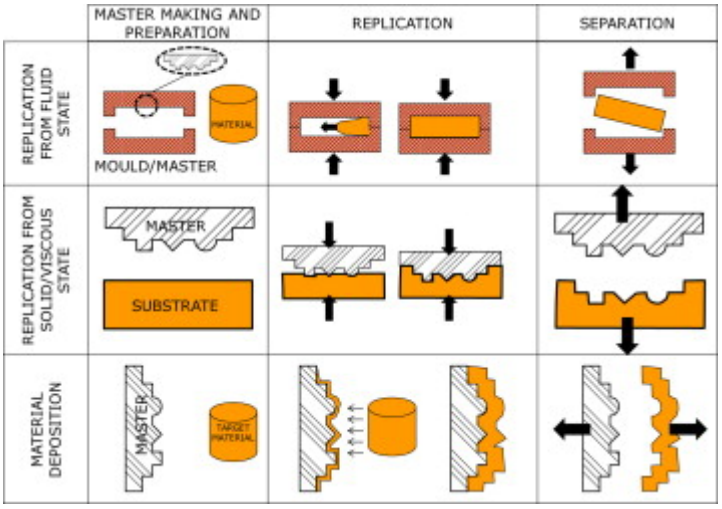

Figure 2.1: Concepts of replication [13].

As such, the method has been recognized over centuries as an effective technology for mass production, using both expendable and permanent moulds. The increased focus on precision manufacturing also is reflected in the demands for replication precision and quality. Depending on the material characteristics and process control, such a replication process can be more or less successful; usually the degree of resemblance between the mould geometry and the final work piece geometry is used as a measure of quality of the replication.

In case of a moulded surface, the topography of the surface is affected by the master topography and replication accuracy depends on process parameters.

2.2 MICRO INJECTION MOULDING FOR THE REPLICATION OF SURFACES

Micro injection moulding is the process of transferring micron or even sub-micron features from metallic moulds to polymeric products, and it refers to the production of parts that have one of the following characteristics: [14]:

- Weight in the range of milligrams, overall dimensions, functional features, and tolerance requirements that are expressed in terms of micrometers, as well as miniaturized gate and runner system;
- Overall dimensions in the macro-range, weight of the order of grams, and areas with micro-features. Such micro-structures have dimensions, functional features, and tolerance requirements that are expressed in terms of micrometers down to nanometres.

A typical micro-injection moulded part with micro-features could contain a substrate similar to standard injection moulded parts, on

which regions of micro-features are positioned, this substrate his usually called the "flow leader", "grounding plate" or "support" [15].

Micro features could have various geometries (e.g. micro-channels), their dimension are orders of magnitude smaller than the structured surface area.

The replication of micro features is a key issue determining the reliability of the selected manufacturing route. The success of the process greatly depends on feature's size, aspect ratio and surface area. The replication accuracy achievable in replicating micro features is one of the important characteristics of any micro fabrication process and determine the manufacturing constraints of a given process/material combination. The complete replication is still a challenge in μIM especially for features with a cross section in the order of few micrometers and high aspect ratio, or features with cross section in the order of few hundreds on nanometers poses over a large substrate.

The aspect ratio, achievable in replicating micro- and nano features is one of the most important characteristic of any micro-fabrication process and it constitutes a constraint in applying a given process/-material combination. High aspect ratio components can be found in many applications, therefore the trend towards miniaturization has to be accompanied by an accurate investigation of process limitations, in order to fully characterize it as a surface replication technology and to identify opportunities for further development.

Concerning the achievable aspect ratios, there is a limitation which is a function of geometry of the features, their position on the sample, the polymer type and the process parameters [16]. Although this has not been presented in a rigorous numerical relation, experiments have shown that the sub-micrometer scale can be reached for aspect ratios less than 1, for example in CD and DVD fabrication.

Polymeric melts can accurately fill micro-features in the order of hundreds of nanometres. Therefore, the minimum mouldable dimensions is determined by the tool-manufacturing capabilities. Micro injection moulding is under continuous development and it is not possible to specify a size limit below which features can no longer be successfully replicated. Nevertheless, it has been reported that it is possible to replicate structures of lateral dimensions smaller than 100 nm. However, reports on the smallest features have mostly explored the fabrication of low aspect ratio structures [17].

Over the last 10 years, impressive replication results have been reported for injection moulding of high aspect ratio micro/nano- features. Matschuk et al. replicated square arrays of 40 nm wide and 107 nm high pillars (aspect ratio > 2.5) [18]. Suzuki et al. [19] recently conducted injection moulding experiments to replicate microfeatures having a width of 5 μm and a depth of 15 μm. Liou et al. [20] studied the injection moulding characteristics of polymer micro-

Aspect ratio	Substrate thickness [mm]	Mould temperature	Ref.
0.1	1.2	$<T_g$	[21]
4	1	$>T_g$	[22]
1.6÷4	1.12÷2	$<T_g$	[23]
12	2.5	$>T_g$	[20]
1.6	0.65	$\sim T_g$	[24]
0.5	1.3	$\sim T_g$	[25]
~ 1	0.65	$>T_g$	[26]
0.3	0.2	$<T_g$	[27]
0.7	0.3	$<T_g$	[28]
1.2	1.2	$<T_g$	[17]

Table 2.1: Aspect ratios of replicated surface-features for published research in the field of micro-injection moulding.

and sub-micron structures using demonstration mould inserts with micro- and sub-micron channels with high-aspect ratios.

However the complete replication of high aspect ratio micro/nano-features placed over a large substrate has not yet been reported. In all these studies,the features where located on a small substrate, close to the gate and aligned along the melt flow direction. Table 2.1 compares different experiments performed at different temperatures, for different structural dimensions and materials.

2.3 OPEN ISSUES IN LITERATURE

Several research groups have conducted different injection moulding experiments on micro-featured parts to investigate their effects on replication quality. In particular, process optimization, development of new tooling technologies, material rheology, tool design and manufacture were considered.

Considering the variability of micro-parts design and purpose, their quality criteria are broadly diversified, including filling length [29], filling quality [17], part mass [30], weld-line formation [31], mould cavity pressure [32, 33], dimensional stability, surface finishing, pressure and temperature distribution using a three-dimensional simulation packages [34] and a range of mechanical properties of interest.

How important are the injection speed, mould temperature, and other processing parameters on mould filling and part quality? How does feature geometry affects the selection of processing conditions? What difficulties are encountered during micro-feature injection moulding operations? To answer these questions, several research group have conducted micro-feature injection moulding experiments with

well-defined simple geometries. From these studies very useful information concerning the whole micro-injection moulding process chain were provided, but results showed many discrepancies due to the fact that they were carried out under different experimental conditions. Furthermore, materials and geometric configurations of components showed different responses to changes of process factors.

Considering this studies, experimental analysis have been designed, aiming to face some open issues and to apply their indications to the optimization of the projects that are being considered in this work.

3

FACTORS AFFECTING REPLICATION QUALITY

Micro injection moulding of devices that have large overall dimension but incorporate micro-features is a critical task, especially when they are characterized by high aspect ratio or cross section in the order of few hundreds of nanometers.

When replicating micro-features, *surface quality* is one of the most important process characteristics and it constitutes a manufacturing constraint in applying this technology to a wider range of micro-engineering applications [13]. Consequently, the study of factors that affects the replication capabilities is very important in order to gain insight of the process and overcome technological limitations that still persists.

According to Bellantone et al., the factors that affect the quality of moulded parts can be classified into four categories [35]:

- processing conditions;
- mould design;
- performance of moulding machine;
- injected material.

Quality of micro-moulded parts is the result of a complex interaction of these factors. In order to achieve the desired replication accuracy, the factors that affects replication quality should be studied systematically.

Results from an extensive literature review showed significant effect of processing conditions on the flow of polymer melt in micro-cavities, which ultimately determine the replication capability of the process. A detailed review of factors, DoE methods, responses and main results recently obtained for micro injection moulding is further proposed. Moreover, the influence of the mould and of the injected material properties are here discussed.

3.1 MICRO-FILLING

Replication quality when injection moulding is strictly related to the flow of polymer melt into the cavity, which in its turn is influenced by process factors. Consequently, the understanding of the characteristics of the flow of polymer melt in narrow cavities, typical of micro injection moulded parts, is essential in order to in order to determine the quality of the moulded part.

Moulding micro-features is not an easy task, in particular when their width is small, causing faster temperature decrease than in regular-sized cavities. Micro-features may not be completely filled due to premature solidification. In the filling phase, a thin layer of solidified polymer grows rapidly from the cavity wall until the frozen layer covers the whole cross section of the micro-feature. Polymer is frozen when its temperature drops below the no-flow or solidification temperature.

Small features typically found in micro-moulding cavities can cause shear rates to be orders of magnitude higher than those experienced in conventional injection moulding [36, 37]. Indeed shear stress and shear rate are inversely proportional to cavity dimension:

$$\tau, \eta \propto \frac{1}{h} \tag{3.1}$$

The *shear heating* resulting from such high shear stresses may generate considerable heat as a result of viscous dissipation near cavity wall. This heat will lower the viscosity of the polymer melt near the wall. This effect is known as *shear thinning*. The decrease of η with the increase of $\dot{\gamma}$ is a factor that makes possible the filling of many thin walled parts with high aspect ratios.

Additionally, the filling resistance of the polymer in micro injection moulding is markedly higher than in the conventional process. Hence, more power would have to be provided by the injection moulding machine to ensure the success of the process. However, the power required to the machine is limited by the means of a reduction of resistance to deformation of the polymer melt. In this sense one of the most effective approach is to keep the filling polymer at a high temperature to obtain a relatively low viscosity of the polymer. This is achieved increasing barrel temperature of the injection moulding machine and mould temperature. The latter, which more rapidly and strongly affects the temperature of the polymer injected into narrow cavity, is particularly important in micro injection moulding.

3.1.1 *The Hesitation Effect*

When analysing the flow of polymer melt in a component with micro-feature on its surface, two different steps has to be distinguished:

- filling of the macro-cavity;
- filling of micro-cavities.

The filling of the macro-cavity is characterized by an essentially flat advancing melt front, and does not poses particular problems. On the other hand, the filling of micro-cavities involves more complexity. The filling mechanism that characterize the process is often underestimated and difficult to treat [38]. Even though the melt behavior with

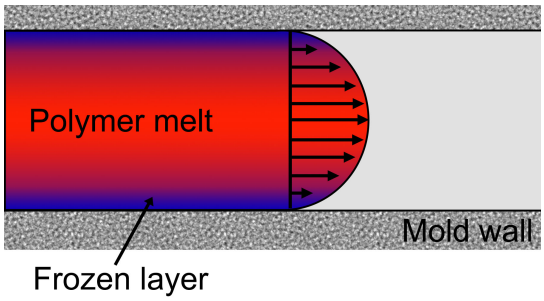

Figure 3.1: Fountain flow of polymer melt in mould cavity.

respect to the filling of micro-features is yet to be clarified, different authors proposed interpretations of the phenomenon.

Many researchers seems to agree in distinguishing two consecutive steps: a first step of filling the main cavity and a second phase of packing and filling of the micro-features [24]. According to Yoshii et al., the replication in the filling stage is negligible due to the low values of pressure [21]. The molten polymer initially flows into the ground plate where it encounters lower resistance to the flow, i.e. greater cross section, and stagnates at the entrance of micro-features, which are characterized by a cross section that is several orders of magnitude smaller. It is then the action of the holding pressure that promotes the filling of the micro-cavities [1].

This was reported also by Lin et al., and Liou et al., [20, 25]. According to them the polymer melt only fills a short distance into the micro-channel at the end of mould filling. While in the packing stage, the mould cavity is pressurized by a constant pressure at the sprue and the melt flow forward very fast into the micro-channels.

Shen at al., conducted numerical simulation of micro-lens arrays with a diameter of 150 μm and an aspect ratio of 0.08 [39]. Their results showed that the melt front firstly flows in the main cavity and then it fills into the micro-structure.

In the injection phase, when the polymer enters the cavity the outer skin in contact with the wall freezes. The core remains in a fluid state and it moves forward towards the melt front area and out to the wall surface (Figure 3.1). This is known as the *fountain flow*, and is characterized by a so called *skin-core* morphology. The skin formed along the surface of the main cavity opposes to the filling of micro-cavities placed on the surface, even reducing the effect of the packing pressure [40]. This filling behavior results in incomplete replication because the filling time of the substrate is usually greater than the freezing time of the micro-features. This is commonly known as the *hesitation effect* (Figure 3.2).

The hesitation effect is a physical phenomenon that can occur during the filling phase, and it is common when an injection moulded part contains different thicknesses [41]. It may also take place when

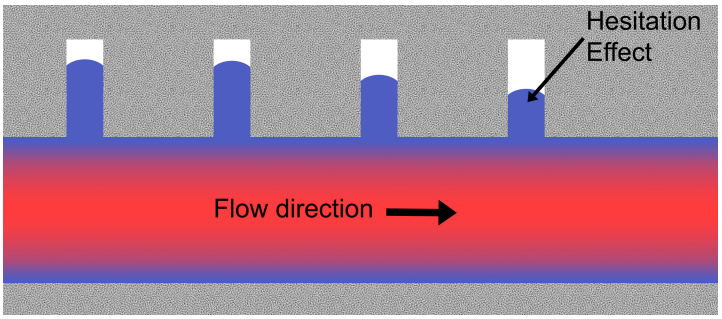

Figure 3.2: Hesitation effect of the melt flow in the proximity of micro channels.

high aspect ratio micro-features are placed on a relatively thick substrate, which is the case of micro-fluidic devices [30].

This behavior is confirmed also by the research of Yeong et al., which assumed that the polymer melt fill the substrate first and then the prism micro-pattern [42]. In fact, the melt has to gain enough pressure to flow into micro-features located on the mould surface. Therefore, the replication depends on how quickly the hot melt flows into the micro-cavities before losing its fluidity. This indicates the injection pressure at early stage is responsible for the replication of the surface micro-pattern.

Though many researchers agree with the "hesitation effect", Young et al., proposed a different model according to which the polymer melt fills the main cavity and the micro-features at the same time [43]. In this research a simplified analytical model to estimate the injection distance is developed, based on pressure built up at the entrance of micro-channels.

Also the work from Xu et al., gives some importance to the injection phase [44]. It is assumed that in the filling phase a layer of melt is quickly formed in the micro-channel when the main flow polymer melt passes through its entrance. Further filling depends on the packing stage. If the temperature of the melt polymer in the micro-channel is still higher than the no-flow temperature the fast increase of pressure in the packing phase can push the flow forward and a complete filling might be achieved. Otherwise, the polymer melt solidifies before the holding pressure can push it forward in the micro-cavity.

Compared to those considered so far, the research from Han and Yokoi, is more comprehensive [38]. The study of the behavior of the melt flowing over a tool with V-grooves was carried out. The melt at the flow front area flows by the means of a fountain flow, while near the surface it is an *extensional flow* (Figure 3.3). The melt fills the grooves due to the extensional flow and deformation of the flow itself as cavity pressure increases. Influence of the injection phase is reported, and it resulted affected by mould temperature and mould design. The contribution of the holding pressure is related to the injec-

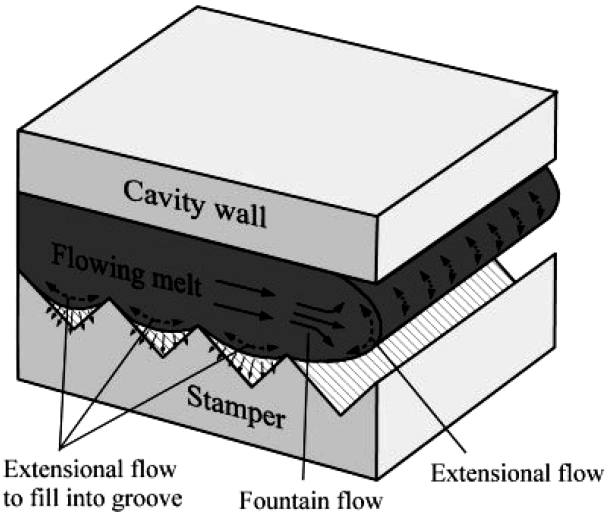

Figure 3.3: Schematic fundamentals of the filling process of the melt into V-grooves, [38].

tion phase. When the filling length achieved in the first phase is high further replication in a following stage is difficult. However, filling ratios are different when the mould temperature is sufficiently high to delay the freezing of the melt within or near the grooves, or when the holding pressure is sufficiently high to force the high-viscosity melt into the grooves by creep deformation. Cavity thickness is important too, because of its influence on cavity pressure. High thickness tends to limit the replication during the injection phase, due to low growth of cavity pressure. Hence, the replication in the holding phase become dominant. Likewise, too small thickness would not allow a complete transmission of the holding pressure along the cavity from the injection location to the end. In this sense, Rötting suggested that injection moulded parts with a sufficient quality of the microstructures need a minimum thickness of approximately 2 mm [45].

According to all the researches considered, the substrate is easily filled, while micro-features replication is tough and that often results in poor replication quality [46]. The key issue is the growth of the pressure at the entrance of micro-features, which depends on various factors, including melt and mould temperature, cavity thickness and geometry. All these factors and their interactions will be further analyzed, considering their influence on melt flow behavior.

3.1.2 *In-Cavity Pressure Profile*

One of the most important process function in micro injection moulding is the *in-cavity pressure history*. As explained the replication quality of micro-structures is greatly affected by the holding pressure. In-

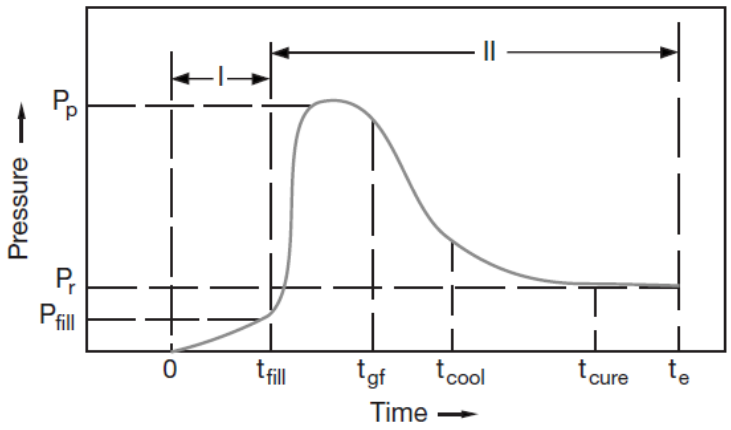

Figure 3.4: A schematic in-cavity pressure history.

deed, the melt flow behavior is strictly related to the profile of the in-cavity pressure.

In order to understand the role of the in-cavity pressure, it is useful to examine a typical pressure history as recorded inside a mould cavity during the injection moulding cycle (Figure 3.4).

The cycle can be divided into two phases: (I) filling phase and (II) post-filling phase. The former is governed by the hydrodynamics of the melt flowing in the cavity as it is injected under speed control. The latter starts as soon as the cavity is completely filled and is controlled by the heat transfer between the melt and the mould and by the compressibility of the solidifying melt.

The post-filling phase is usually characterized by large and abrupt changes in pressure and temperature inside the cavity. During the packing stage, the pressure grows rapidly, under nearly isothermal conditions. It reaches the value P_{p}, which is usually held for a short time and is controlled by the holding pressure applied by the machine. At the gate freeze-off time t_{gf} the material in the gate area solidifies, due its small cross section. The material that remains in the cavity is still in a fluid state. After t_{gf} the heat transfer to mould surfaces and the compressibility of the material lead to a monotonous decay in pressure until the termination of the cycle. Finally at t_{e} the mould opens and the solidified part is ejected.

t_{cool} and t_{cure} stand for two important events during the cooling stage. At t_{cool} the material in the innermost point in the cavity passes through the glass transition temperature and so the polymer in the cavity is fully vitrified, though not yet equilibrating to the mould temperature ($T_{\mathrm{mould}} < T \leq T_{\mathrm{g}}$). At t_{cure} the system approaches a thermal steady state, i.e. the temperature becomes evenly distributed throughout the cavity space ($T \approx T_{\mathrm{mould}}$), and the pressure approaches an asymptotic value, the residual pressure P_{r}.

If the cycle is terminated before the complete vitrification of the material ($t_e < t_{cool}$) or even before thermal equilibration ($t_e < t_{cure}$), the part is likely to distort and warp in the subsequent free-cooling stage, as a result of the following inhomogeneous shrinkage. Similarly, if P_p is too low, the pressure in the cavity will go to zero at $t < t_{cure}$ and the material will delaminate from the cavity walls before t_e, leading to inadequate replication of the cavity geometry.

3.2 PROCESSING PARAMETERS

The quality of a micro-moulded part can be largely modified by different selection of process parameters. The achievement of a complete replication is a challenging task. Indeed the higher the feature surface-to-volume ratio, the faster the polymer solidification. The injected material solidifies before it has reached the bottom of the grooves, thus producing sub-filled structures.

In order to reduce the appearance of the effect of hesitation many solution were proposed by different researchers. An increase in mould temperature, especially above the glass transition temperature of the material, could lessen the thermal gradient between the mould and the molten polymer [24, 30]. Otherwise, a high injection speed lead to a decrease of the time of contact between the polymer and the mould surface before the beginning of the filling phase [47].

In general the melt flow in micro-structures can be improved by applying high settings of process parameters [29]. However, when comparing the magnitude of their influence on the melt filling quality the reported results are not consistent.

3.2.1 *Mould Temperature*

Mould temperature is known to be the most important process factor affecting replication fidelity [38]. Kuhn et al. reported that mould temperature influences replication quality and morphology of the micro-features [48]. Compared to the conventional process, a high mould temperature is the most important condition for the achievement of the required replication. As cavities in micro injection moulding applications are long and narrow, the filling resistance to the flow of the polymer is markedly higher than in the conventional process. At a sufficiently high temperature of the mould, the power required to the moulding machine to overcome the filling resistance is greatly reduced. According to Ong et al., mould temperature not only determines the replication capability of the process, but also its efficiency and dimensional accuracy and part quality [49].

In micro injection moulding the polymer flow is characterized by a high surface-to-volume ratio, which leads to a high cooling speed of the polymer melt in the mould cavity. If mould temperature is

not sufficiently high the melt changes its state, from a fluid to a solid. The polymer melt near the wall of the cavity cool down to a solid skin, and reduce the cross section of the flow. Thus, premature material freezing precludes the complete filling of micro-features, not allowing the achievement of the required replication accuracy. This phenomenon can be countered by increasing the temperature of the mould, which improves the flow of the melt in the cavity. The higher the temperature of the mould the lower the thermal gradient between the mould and the melt, and so the thinner the thickness of the solidified layer along the surface of the cavity is. The cross section of the flow in the cavity is larger, and so the pressure drop is inferior.

The dominant factor for a successful replication is the strong dependence of the polymer melt viscosity on temperature, that will be further discussed in chapter 4.

In their work, Liou et al. studied the effect of mould temperature on the achievable aspect ratio for micro-walls [20]. They observed that the rate of increase of the achievable aspect ratio grows around the *glass transition temperature* T_g. In fact, to ensure a successful replication of micro- and sub-micron channels mould temperature must be above the no flow temperature of the selected material. This is indirectly confirmed by Attia which conducted moulding experiments below the glass transition temperature of the polymer and reported lack of significance of mould temperature [50]. Becker et al. assert that the selection of the mould temperature depends on the surface-to-volume ratio of the structures. The temperature of the mould needs to above the glass transition temperature of the material only in the case of small injection volumes and high aspect ratio structures [51].

The importance of moulding above the glass transition temperature means that the appropriate mould temperature changes with the type of polymer selected. However, it is worth noting that polymers respond differently to changes of mould temperature. Yu et al. conducted micro injection moulding experiments with different materials, POM, PP and ABS [26]. Their results indicates significant improvements of the melt flow and achievable aspect ratios when increasing mould temperature only for POM. The reason for this is that POM, PP and ABS have different thermal properties and so they demonstrate different sensitivity to variation of temperatures. Additionally, different polymers may yield different flow behaviors and moulding characteristics. According to this mould temperature should be carefully considered in relation to the injected material.

3.2.2 *Injection Speed*

The injection speed is a controlled parameter only during the filling stage of the injection moulding process. However as reported in many

researches, it is an important factor for improving the melt fill of micro cavities.

In micro injection moulding, with an increase of the injection speed the shear rate increases significantly. The relation between shear rate $\dot{\gamma}$ and injection velocity V_i can be approximated by the following:

$$\dot{\gamma} = \frac{4\dot{Q}}{\pi r^3} \tag{3.2}$$

where $\dot{Q}$ is the volume flow rate, and r is the radius of the flow path cross section. The flow rate is a function of the injection speed, so Equation 3.2 can be rewritten as:

$$\dot{\gamma} = \frac{4V_i R^2}{r^3} \tag{3.3}$$

where R is the radius of the injection plunger. From Equation 3.3, an increase of V_i leads to an increase of temperature due to shear heating, especially when flowing through thin-wall geometry [26]. Because of this, the polymer viscosity decreases resulting in a better filling of micro-features. Shear thinning behavior of the polymer melt allows moulding with less thermal degradation at lower barrel temperatures and/or residence times.

Chen et al. reported that a high-speed injection reduces the contact time between the cold mould and the hot melt [27]. Hence, the melt temperature drop is inferior and premature solidification of polymer may be reduced. A higher amount of material reaches the micro-features before the melt solidifies.

Xu et al. reported that a high injection speed both increases the cavity pressure, which drives the flow into the micro-features, and reduces the substrate filling time, contrasting the hesitation effect [44] . In fact, the filling of the micro features has to compete with the filling of the underlying thicker substrate and it begins when the maximum pressure is reached, i.e. at the end of filling of the substrate.

Sha et al. reported that a high injection speed improves the filling of micro-cavities, but it may also result in a poor surface quality and edge definition [52]. This negative effect on surface finishing was reported also by Griffiths et al. which noted that an increase in shear rate could also result in polymer degradation and cavity gassing. The presence of air in the cavity due to high injection speed could also damage the tool [29]. A good balance between injection speed and shear rate can prevent the reduction of bulk temperature prior to cavity filling and prevent polymer and tool damage.

3.2.3 *Holding Pressure*

After the filling phase that is conducted in speed control, in the packing phase a constant pressure is applied at the injection location and

kept constant for a certain time. During the holding stage, the flow speed of the melt is very low. The role of the holding pressure (P_h) is to prevent the melt from flowing back and also to compensate for any reduction of the volume due to the shrinkage of moulded parts.

The effect of the P_h has already been introduced, many authors consider it as the main driving force that pushes the polymer melt into the micro-channels, as it counteracts the hesitation effect. In this section the main effect of the P_h on replication quality is reported considering the literature.

Results from an extensive literature review confirms the positive effect on replication accuracy of an high packing pressure [27, 50]. High moulding pressure also improves replication accuracy by assisting the polymer melt flow in the micro-features and reduces the subsequent shrinkage during the cooling phase [53].

Oliveira et al., suggested that some difficulties related to the metering precision and process fluctuations can be attenuated by applying higher P_h [3]. Although the positive effect of the P_h has been widely reported, it seems uneasy to differentiate its single effect from its interaction with the mould temperature effect [20]. In fact, higher mould temperature could reduce cooling of the polymer during the filling stage, resulting in higher polymer temperature at the start of packing stage [25]. Yu et al., [26] found that if the packing pressure is increased, the replication can be completed with less time of application of their infrared heating system. However, they distinguish differences when moulding above and below the glass transition temperature of the injected material.

3.3 MOULD DESIGN

Another important category of factors affecting the injection process is the design of the mould. Indeed, the selectable processing conditions are limited by the physical capabilities of the moulding tools. Thus the definition of part geometry can be a factor that influences the melt filling and thus the quality of the replicated micro-features.

A micro-mould is a highly sophisticated device connected to the machine, which comprises many parts all requiring high quality. Different mould systems (gate and runner) should be used for good melt flow and cavity filling because, for different product design and polymers materials, whether a micro-part can be successfully moulded is dependent, to a large extent, on the design and fabrication of the tools.

Despite the fact that high settings of some process parameters can increase the melt fill in micro-cavities [54]. The influence of part geometry has been widely considered in literature, many researchers observed its significance for the determination of the replication quality. These studies provide very useful information for the design of

tools and components that incorporate micro-features on their surface, focusing on:

- the thickness of the main flow region;
- the flow direction;
- the distance from the injection location;
- micro-features dimensions;

3.3.1 *Thickness of the Main Flow Region*

The thickness of the main flow region is an important parameter that has to be considered for improving the behavior of the filling melt. The base plate is employed to support micro-structures and the thickness of the base plate will affect the balance of polymer melt and the quality of moulded results. Because the thickness of the base plate is much larger than the individual opening of the micro-mould cavity, the problem of hesitation occurs, which requires careful consideration to control the quality of the moulded parts [55].

The thickness of the main flow region influences the filling behavior in two opposite ways. Increasing the thickness of the main flow region improves the transmission of cavity pressure along the cavity. In this sense, Han et al., proved that the cavity thickness affects the replication process by changing the cavity pressure generated during the filling stage [38]. Surace et al., suggesting that ultra-thin wall plastic parts have great application potentialities for MEMS, indicated that part thickness is a decisive parameter because the filling capability of the melt declines rapidly with the reducing of part thickness [1]. Conversely, Young et al., reported that a decrease of the part thickness could enhance the filling in the micro-features by contrasting the rapid cooling [43]. In other words, a smaller thickness ensures a quick filling of the substrate, that allows time for the filling of micro-cavities before solidification starts. Indeed, the filling of the structures has to compete with the filling of the underlying substrate. Indeed Yoshii et al., found that substrate thickness is critical, as it determines the cavity filling time [21]. In general, the decision on the thickness of the main flow region should be balanced on both aspects of the problem.

3.3.2 *Flow Direction and Distance From the Injection Location*

In the design of the mould the position of the injection location should be selected in such a way that the melt flow throughout the cavities is well balanced, both in terms of uniformity of the in-cavity pressure and direction of the flow [29].

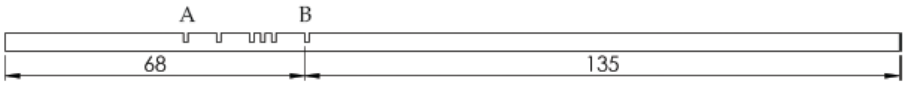

(a) *Long mould*.

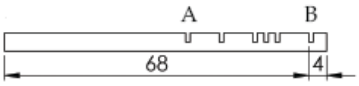

(b) *Short mould*.

Figure 3.5: Side views of the long and short moulds in the research from Xu et al., [44].

The influence on replication of the in-cavity pressure has been studied, reporting contrasting results. According to Schift el a., the replicated features are deeper near the injection point, due to an higher pressure in the proximity of the gate [56]. Conversely,Yu at al. and Sha at al., reported that the polymer can fill the downstream micro-channels more deeply than the upstream ones [23, 54].

Xu et al., proposed a more comprehensive study, that considered the effect of channel location using two mould with different lenght [44]. They observed that the filling lengths in channels A and B in the short mould are much longer than those in the long mould, and the filling length in channel B is much longer than in channel A in the short mould. On the other hand, there is not much difference between the filling lengths in channels A and B in the long mould. The difference in filling lengths between the long and short moulds is due to the fact that channel B is much closer to the end of the mould cavity in the short mould than in the long mould. The pressure profile is the same for both moulds before the main flow reaches the mould cavity end. After that, the pressure increases sharply in the short mould. Consequently, more melt can be packed into the channels, and the filling lengths in channels A and B in the short mould are longer than in the long mould. Since the polymer in channel B has undergone a shorter cooling time than in channel A, the melt in channel B can flow further. In the long mould, the polymer melt needs a much longer time to flow from channel B to the end of the mould, and the melt in both micro-channels may have frozen before the main flow reaches the mould cavity end. Consequently, the pressure increase does not affect the filling lengths, and the filling lengths are almost the same in different channel locations.

Concerning the direction of the flow, Monkkonen et al. observed that the features along the flow path fill much better than the perpendicular ones [17]. Thus when designing the mould, it has to be considered that the best results are achieved when the majority of the sub-micron features are not perpendicular to the flow.

3.3.3 *Micro Features Dimensions*

Considering the micro injection moulding process it is clear that the filling is more difficult to replicate micro features when the features size is smaller. In general terms, deeper and wider micro channels are more easily filled by the melt because of the reduction of the surface-to-volume ratio [54]. In particular the features width was reported to have a large effect on the melt filling distance [24]. It can be observed that the filling distance increases with the micro features width.

3.4 INJECTED MATERIAL

The researches that have so far been considered revealed that in general, increasing the barrel temperature, mould temperature and the injection speed improves the polymer melt fill in micro-cavities. However, the effects of these factors on the process replication capabilities are not consistent for different polymer materials, and could be adverse in specific conditions [52]. The interaction between the used polymer and the quality of the moulded part is a challenging task for the definition of materials useful for each application without testing them under different conditions.

Chen at al., compared the replication accuracy of the micro-channels for four different polymer resins (PS, PC, PMMA, COC) revealing different results [27]. They reported that the influence of the injected material is increasingly significant for higher aspect ratios. Moreover, due to the importance of moulding above the glass transition temperature it is clear that the appropriate mould temperature changes with the selected type of polymer. Indeed, longer molecules have more difficulties in sliding past each other and thus higher temperatures are necessary in order to fill the micro-structures [57].

3.5 AUXILIARY TECHNOLOGIES

In previous chapter we have seen that the large surface-to-volume ratio that characterizes micro injection moulding applications, promote the quick decrease of polymer melt temperature from the moment at which it enters the cavity. Moreover, the pressure generated by the air not evacuated from the cavity can increase the resistance to the flow, thus not allowing the achievement of a complete replication.

Two modifications have been identified to improve the process. First, the mould temperature must remain higher than the transition temperature of the polymer to reduce the viscosity during the filling stage. In this situation, no solidified layer will be generated and longer filling time and lower injection pressure can be employed to reduce residual stress. Secondly, vacuum venting is applied to avoid possible air traps. These auxiliary technologies have been widely in-

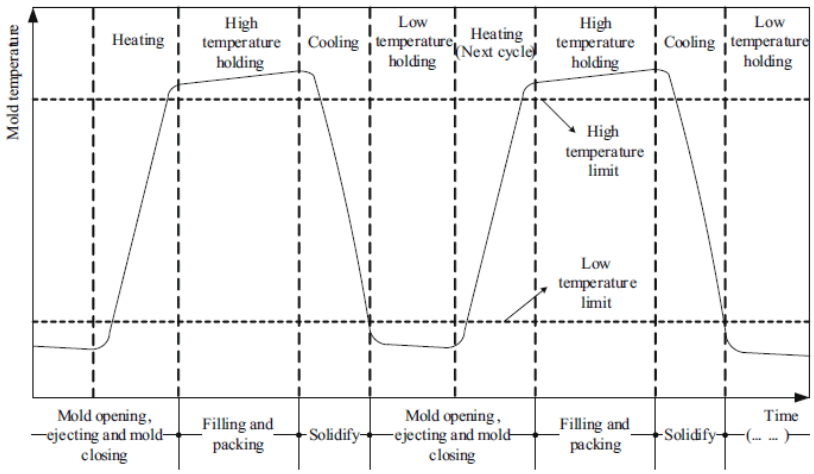

Figure 3.6: Schematic of mould temperature changes during the RHCM processes.

vestigated by many researchers; in this section the results from some significant works are reported.

3.5.1 *Rapid Heat Cycle Moulding*

As the mould temperature has been identified as the most critical process parameter to ensure high accuracy of replication, the conventional injection moulding process has been modified to the so called *vario-therm process* or *rapid heat cycle moulding (RHCM)*. The conventional isothermal process employs a constant temperature mould to shape the molten polymer and then cool the moulded article for ejection. Conversely, in micro injection moulding applications the ideal condition for improving the replication is to have a hot mould during the filling stage and a cold mould during the cooling stage. The hot mould during the filling stage, with the mould temperature above the polymer softening temperature, prohibits the polymer from freezing, while the cold mould during the cooling stage maintains a short cycle time. However, the use of higher temperatures lengthens the heating and cooling cycle of the mould, resulting in considerably longer cycling time for the total process. Typical cycle times for a cold-cavity process are of the order of $0.5 \div 2$ min, while a vario-therm process can take up to 5 min [51].

A RHCM process can be divided into four stages: heating, high temperature holding, cooling and low temperature holding. Figure 3.6 gives the schematic of mould temperature changes during the process. In order to reduce the moulding cycle time, the heating stage can start at the same time of part ejection. In the heating stage, the mould is heated up to a preset high temperature, usually higher than the glass transition temperature of the polymer. When the mould tem-

perature reaches the preset value, the heating stage is completed and the process goes into the high temperature holding stage, in which the polymer melt is injected into the cavity. After filling and packing, the high temperature holding stage is finished and the moulding process switches to the cooling stage. In this stage, the mould is quickly cooled down by the cooling water. As the polymer temperature reduces to the ejection temperature, the cooling stage is completed and the low temperature holding stage starts. During the second holding stage, the mould is opened and the part is ejected. After that, the mould will be heated again for the next cycle.

The approach to rapidly heating and cooling only the mould has been a continuous research topic in the plastics industry for more than fifty years. Among all available heat generation technologies, electrical resistive heating is the most widely used mechanism for mould rapid heating [58]. Other techniques are induction heating and proximity heating [59, 60]. Infrared radiation has been also applied for heating the cavity surface [26]. Another approach to thermally cycle the cavity surface temperature consists in circulating a hot and a cool fluid in alternate sequence in the mould cooling channels [61]. In particular, an efficient and uniform heating can be achieved using either superheated steam or pressurized hot water circulating in conformal cooling channels [62].

3.5.2 *Cavity Air Evacuation*

The application of vacuum venting for the evacuation of air from the cavity has been introduced in injection moulding with the intent to further enhance feature replication and definition (sharpness of edges) by removing air pockets trapped in the micro-features, which can resist the melt filling flow [53, 63].

At macroscale, air entrapment inside the moulds is usually avoided by venting the air through slots, that are machined on the interior surfaces of the two mould platens, in the parting line, and the air is expelled as the melt fills up the mould. In other cases, the clearance gaps around the ejector pins provide sufficient volume to vent the mould. In micro injection moulding the venting of the mould prior to injection is a critical task [64].

According to Menges et al., *passive venting* should be adopted for micro injection moulding applications [65]. This type of venting is used when micro-structures are present, since conventional venting gaps are too large compared to the dimensions of the cavities. Thus, the cavity is evacuated by the means of an evacuation system, and the resistance from compressed air in micro-cavities is reduced [38]. Additionally, the evacuation of air from the cavity can prevent the gasification of the polymer, because of the residual gases that are present in the cavity at the beginning of the filling phase [20].

Feature size		Injected	ΔDR	Ref.
Width (μm)	Aspect Ratio	Material	%	
100	1	ABS	> 0	[66]
2÷20	12	PMMA,PP,HDPE	/	[20]
8	0.5	PMMA	< 1	[25]
60	4	PP	/	[67]
80	10	POM	$4.6 \div 5.4$	[49]
110	0.5	PMMA	0	[68]

Table 3.1: Evaluation of cavity air evacuation efficiency for micro injection moulding, results from different research groups

Sha at al., observed a negative effect that could possibly arises from the application of vacuum venting [54]. In fact, air evacuation could lead to a decrease of the surface temperature in microfeatures as a result of taking away warm air from the cavity. Hence, with the increase of the surface-to-volume ratio in micro-cavities air evacuation could have a detrimental effect on the melt fill for polymers that are sensitive to changes of the mould temperature.

Although incomplete filling of micro-scale features has often been attributed to poor venting, the limited research examining the application of vacuum venting has produced mixed results. Table 3.1 summarize the results of some researches. In general, the impact of vacuum venting may depend on feature size, processing conditions and the injected material.

Part II

MATERIALS AND METHODS

4 MATERIALS CHARACTERIZATION

The materials for the experimental analysis were chosen according to each project specifications and requirements. For the CellDiaSP project, it was required a material with the following characteristics:

- Low birefringence;
- Extremely low water absorption;
- Excellent water vapor barrier properties;
- High rigidity, strength and hardness;
- Very good blood compatibility;
- Excellent biocompatibility;
- Very good electrical insulating properties;
- Very good melt processability/flowability.

In this case, a commercial polystyrene resin (*Total, PS Crystal* 1540) and a cyclic olefin copolymer (*Topas, COC* 5013 *L*-10) were chosen. In order to identify which of these two materials has the best characteristics for the microinjection moulding process, both rheological and wettability analysis were performed. Concerning the Nanobones project, it was required a biodegradable material with certain optical and biodegradable properties. Together with the project partners, a specific poly-lactic acid was selected (*Purac, PLA Purasorb PL* 10). The main properties of the three materials are summarized in Table 4.1.

Property	Units	PS 1540	COC 5013	PL 10
Density	g/cm^3	1.00	1.02	$1.21 \div 1.43$
Tg (10 °C/min)	°C	100	134	$60 \div 65$
Melting Range	°C	$210 \div 240$	$300 \div 320$	$180 \div 190$
Price	€/kg	~ 2	~ 14	~ 2700

Table 4.1: Comparison of the main properties of the tested materials.

4.1 RHEOLOGICAL CHARACTERIZATION

As approaching the processing of polymers it is clearly important to investigate the way viscosity depends on shear rate, temperature and pressure (cf. Equation 4.1).

$$\eta = f(T, p, \dot{\gamma}) \tag{4.1}$$

Rheometers are instruments used to characterize the rheological properties of materials, typically fluids that are melts or solution. These instruments impose a specific stress field or deformation to the fluid and monitor the resultant deformation or stress. The rheological properties of both the polystyrene and the cyclic olefin copolymers were characterized by means of a rotational and a capillary rheometer, as to evaluate the whole flow curve.

4.1.1 *Rotational Rheometer*

A rotational rheometer (ARES, TA Instruments, New Castle, USA) was used to characterize the *newtonian region* of the flow curve. A cone-plate geometry has been used. The angle between the surface of the cone and the plate is of the order of 1 degree. Typically the plate is rotated and the force on the cone measured. The known response of the torsion bar and the degree of twist give the shear stress, while the rotational speed and cone dimensions give the shear rate. The viscosity is calculated as:

$$\eta = \frac{\tau}{\dot{\gamma}} = \frac{3M\alpha}{2\pi R^3 \omega} \tag{4.2}$$

The rheometer was used in dynamic oscillatory mode to determine the linear viscoelastic properties at an imposed strain. Measurements were performed in a frequency sweep mode (0.1 to 100 s^{-1}), for temperatures around the melt temperature of the polymers.

4.1.2 *Capillary Rheometer*

The *pseudoplastic region* of the flow curve was characterized using a capillary rheometer. In this work, the capillary rheometer (Rheo 250, Ceast, Pianezza, Italy) was used with two different dies with a diameter (D) of 1 mm and length to diameter ratios (L/D) of 5 and 20, as to apply the *Bagley* correction. The imposed shear rate ranged from 50 to 5000 s^{-1}.

The data collected with the capillary rheometer were collected considering the following hypothesis:

1. the fluid is newtonian;
2. the pressure drops at the entrance and at the exit of the capillary are neglected.

The collected data were corrected with the *Rabinowitch* and *Bagley* corrections, as to consider the polymer melt as a non-Newtonian fluid and to introduce the pressure drops that were neglected. To do so the following assumptions were made:

- the flow is incompressible, isothermal and established;
- the melt sticks to the wall;
- the viscosity is not pressure dependent.

4.1.3 *The Cross-WLF Model*

The *Cross model* was used to describe the shear rate dependence of polymer melt viscosity on the whole range of variation of the shear rate:

$$\eta(\dot{\gamma}) = \frac{\eta_0}{1 + \left(\frac{\eta_0}{\tau^*}\dot{\gamma}\right)^{1-n}} \tag{4.3}$$

where $\eta(\dot{\gamma})$ is the the viscosity as a function of the shear rate, and η_0, τ^*, n are coefficients.

The data were fitted to the Cross model by minimizing the sum of squares between experimental and Cross points. The variables that were changed by the solver are τ^*, n.

The effects of temperature on viscosity was accounted by means of the *William-Landel-Ferry (WLF)* model:

$$\eta_0 = D_1 \exp\left(\frac{-A_1(T - T^*)}{A_2 + (T - T^*)}\right) \tag{4.4}$$

$$T^* = D_2 + D_3 \cdot P \tag{4.5}$$

$$A_2 = \tilde{A}_2 + D_3 \cdot P \tag{4.6}$$

where D_1, D_2, D_3, A_1 and $\tilde{A}_2$ are constants to be determined, while T^* is a reference temperature.

4.1.4 *Glass Transition Temperature Characterization*

One of the most fundamental measurements made on polymeric materials is the measurement of the glass transition, T_g. Although there are several thermal techniques available to make T_g measurements, by far the most sensitive technique is dynamic mechanical analysis, DMA. DMA measures the viscoelastic moduli, storage and loss modulus, damping properties, and tan delta, of materials as they are deformed under a period (sinusoidal) deformation (stress or strain). After scanning the sample under test, any of these three viscoelastic parameters can be used to define the glass transition temperature:

- *g' Onset*: occurs at the lowest temperature and relates to mechanical failure.
- *g" Peak*: occurs at the middle temperature and is more closely related to the physical property changes attributed to the glass transition in plastics. It reflects molecular processes and agrees with the idea of T_g as the temperature at the onset of segmental motion.

- *Tan Delta Peak*: occurs at the highest temperature and is used historically in literature. It is a good measure of the "leather like" midpoint between the glassy and rubbery states of a polymer. The height and shape of the tan delta peak change systematically with amorphous content.

For this study, the glass transition temperature was measured by evaluating the peak of the tangent of the phase angle.

4.2 TOTAL PS CRYSTAL 1540

Polistyrene crystal 1540 is an easy flowing crystal polystirene designed for extrusion or injection molding applications. In injection molding, PS crystal 1540 possesses low viscosity at high shear rate and it does combine excellent fluidity with high softening point. Table 4.2 reports the processing conditions suggested by the manufacturer.

The material was characterized using both the rotational rheometer and the capillary rheometer for the newtonian and pseudoplastic region respectively.

The rotational rheometer was used in dynamic oscillatory mode at an imposed strain. Measurements were performed in a frequency sweep mode (0.1 to 100 s^{-1}), for temperatures between 220 and 260 . The capillary rheometer was used with two different dies (L/D of 5 and 20) and an imposed shear rate ranged from 50 to 5000 s^{-1}.

The data were fitted to the Cross model by minimizing the sum of squares between experimental and Cross points. The variables that were changed by the solver are τ^*, n. The minimum distance between the experimental and cross data was found for:

$$\begin{cases} n = 0.231 \\ \tau^* = 23548 Pa \end{cases} \tag{4.7}$$

Figure 4.1a compares the experimental flow curve and the fitted Cross model at temperatures of 220 - 240 - 260 °C.

Suggested processing conditions	
Melt temperature (°C)	$180 \div 240$
Mould temperature (°C)	$30 \div 50$
Max. residence time	< 25 min
Injection pressure (bar)	$105 \div 145$
Hold on pressure (bar)	$400 \div 600$
Back pressure (bar)	180
Screw speed (rpm)	$50 \div 200$
Injection speed (mm/s)	$50 \div 150$

Table 4.2: Total PS processing conditions for injection moulding.

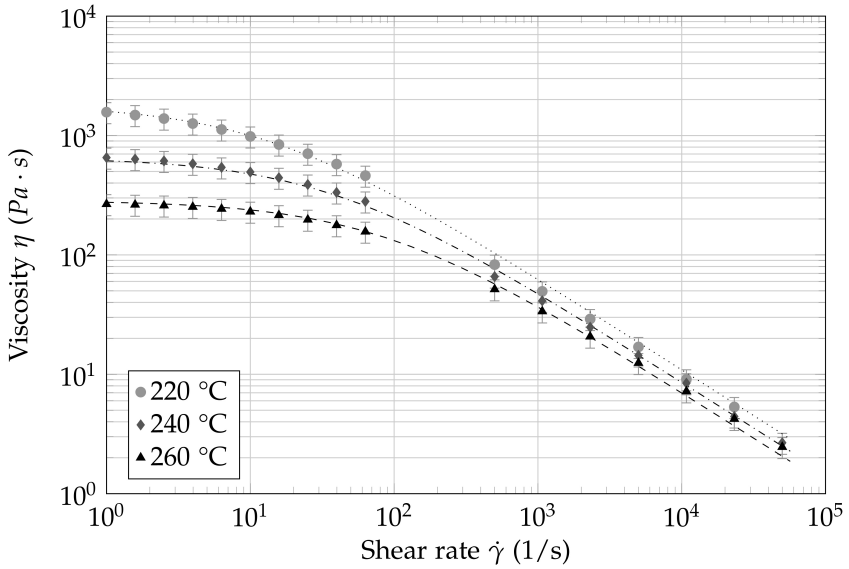

(a) *Viscosity plots for the PS Crystal* 1540.

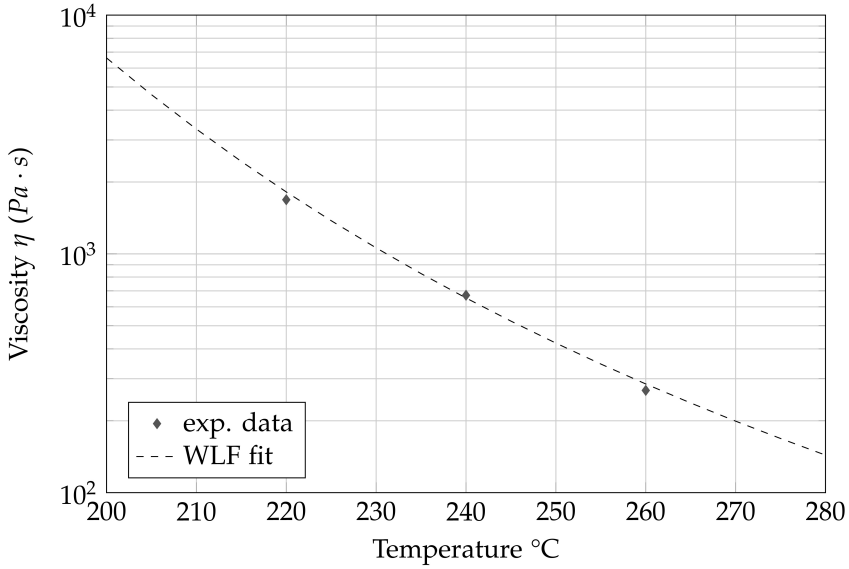

(b) *WLF model for the effect of temperature on viscosity - PS*1540.

Figure 4.1: Total PS crystal 1540 rheological characterization.

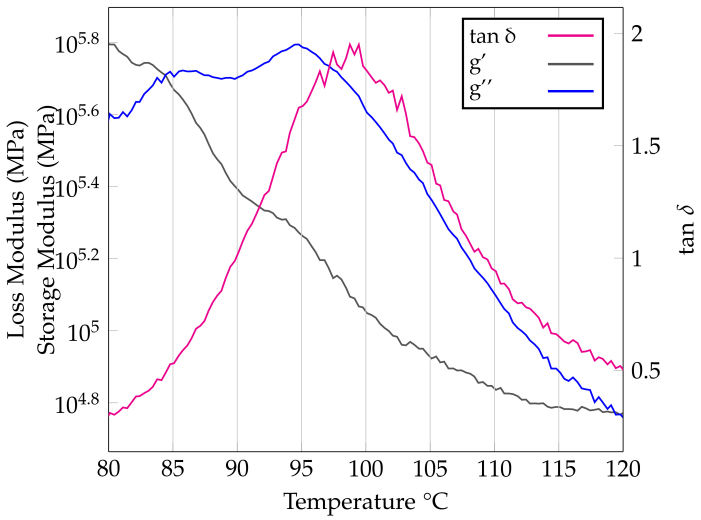

Figure 4.2: Measurements of the glass transition temperature of the PS 1540 using DMA test.

The effects of temperature on viscosity was accounted by means of the *William-Landel-Ferry (WLF)* model (Figure 4.1b).

The constants of the WLF model for the tested material were fixed to the following values:

- T^*=100 °C;
- D_1=32.58;
- D_2=451.6;
- D_3=0;

The glass transition temperature value was measured using a temperature - sweeping dynamic mechanical analysis (DMA). A rotational rheometer in a parallel plate configuration was used with plates diameter of 25 mm and sample initial thickness of 2 mm. A dynamic strain sweep test was firstly conducted to evaluate the linear visco-elastic region. The tests were performed sweeping the strain from 0.015% to 150%, with a frequency of 6.28 rad/s at 40 °C. A constant strain in the linear visco-elastic region was applied (0.10%), associated to a temperature sweep from 80 °C to 120 °C with an increment step of 2 °C, and a frequency of 6.28 rad/s. Figure 4.2 reports the

Parameters	T_g values
g′ Onset	75.13 °C
g″ Peak	94.78 °C
tanδ Peak	98.76 °C

Table 4.3: Glass transition temperature measurements for the PS.

Suggested processing conditions	
Melt temperature (°C)	$240 \div 300$
Mould temperature (°C)	$95 \div 125$
Max. residence time	< 15 min
Injection pressure (bar)	$95 \div 125$
Hold on pressure (bar)	$300 \div 600$
Back pressure (bar)	150
Screw speed (rpm)	$50 \div 200$
Injection speed (mm/s)	$50 \div 150$

Table 4.4: Topas COC processing conditions for injection moulding.

experimental curves obtained with the DMA tests. The values of the glass trasition temperaure considering *g' Onset*, *g" Peak* and *tan δ Peak* are summarized in Table 4.3.

4.3 TOPAS COC 5013 L-10

The COC 5013L-10 was chosen because of its low viscosity. The replication capability of these material will be compared with that of the polystyrene, focusing on the interaction of the material with some processing parameters. Cyclic olefin copolymers are a new class of polymeric materials with property profiles which can be varied over a wide range during polymerization. This type of materials are suitable for the production of transparent mouldings for use in optical data storage, optics, e.g. lenses, sensors, and industrial products e. g. in the construction and lighting sectors. For instance, they are increasingly popular as substrate material for micro-fluidics. This is due to their promising properties, such as high chemical resistance, low water absorption, good optical transparency in the near UV range and ease of fabrication. Table 4.4 reports the processing conditions suggested by the manufacturer.

The COC needs to go through desiccant drying and a dehumidifying cycles before the trials, in order to remove surface or absorbed moisture. The manufacturer suggests that for special applications imposing high surface quality requirements, the material should be predried in a dehumidifying oven at temperatures > 100 °C for a period of $4 \div 6$ hours.

The material was characterized using both the rotational rheometer and the capillary rheometer for the newtonian and pseusoplastic region respectivelly.

The rotational rheometer was used in dynamic oscillatory mode at an imposed strain. Measurements were performed in a frequency sweep mode (0.1 to 100 s^{-1}), for temperatures between 280 and 320.

Parameters	T_g values
g' Onset	126.12 °C
g'' Peak	131.43 °C
tanδ Peak	137.02 °C

Table 4.5: Glass transition temperature measurements for the COC.

The capillary rheometer was used with two different dies (L/D of 5 and 20) and an imposed shear rate ranged from 50 to 5000 s^{-1}.

The data were fitted to the Cross model by minimizing the sum of squares between experimental and Cross points. The variables that were changed by the solver are τ^*, n. The minimum distance between the experimental and cross data was found for:

$$\begin{cases} n = 0.329 \\ \tau^* = 50948 Pa \end{cases} \tag{4.8}$$

Figure 4.3a compares the experimental flow curve and the fitted Cross model at temperatures of 280 - 300 - 320 °C.

The effects of temperature on viscosity was accounted by means of the *William-Landel-Ferry (WLF)* model (Figure 4.3b).

The constants of the WLF model for the tested material were fixed to the following values:

- T^*=100 °C;
- D_1=28.96;
- D_2=51.6;
- D_3=0;

The same procedure used for the PS, was applyed for the measurement of the glass transition temperature of COC. In this case, a constant strain in the linear visco-elastic region was applied (0.29%), associated to a temperature sweep from 120 °C to 160 °C with an increment step of 2 °C, and a frequency of 6.28 rad/s. Figure 4.4 reports the experimental curves obtained with the DMA tests. The values of the glass trasition temperaure considering *g' Onset*, *g'' Peak* and *tan δ Peak* are summarized in Table 4.5.

4.4 WETTABILITY ANALYSIS

In order to completely describe the material properties that affect the replication at a micro scale, the wettability of both the PS andCOC was analyzed by monitoring the evolution of the contact angle over time, at a fixed temperature. As suggested by Lee et al., the analysis of the wettability characteristics of the polymer to the mold surface,

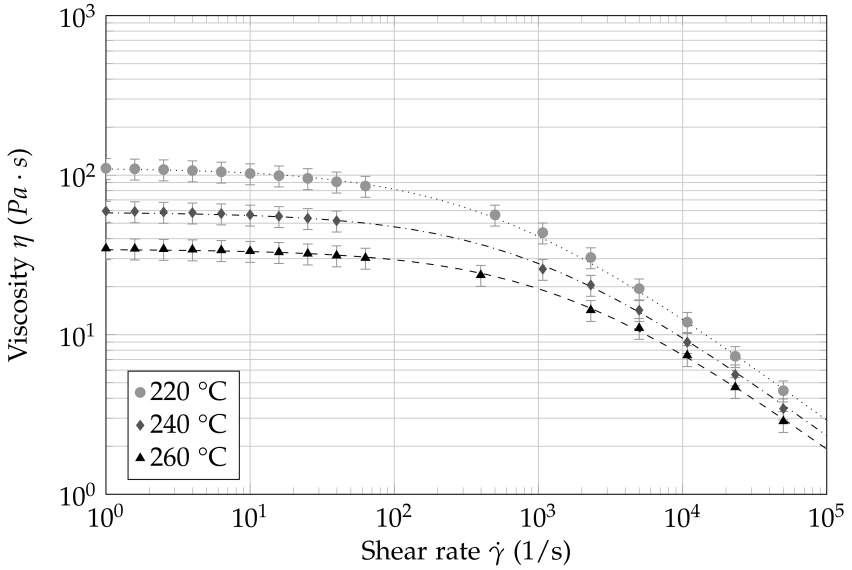

(a) *Viscosity plots for the COC* 5013 *L*-10.

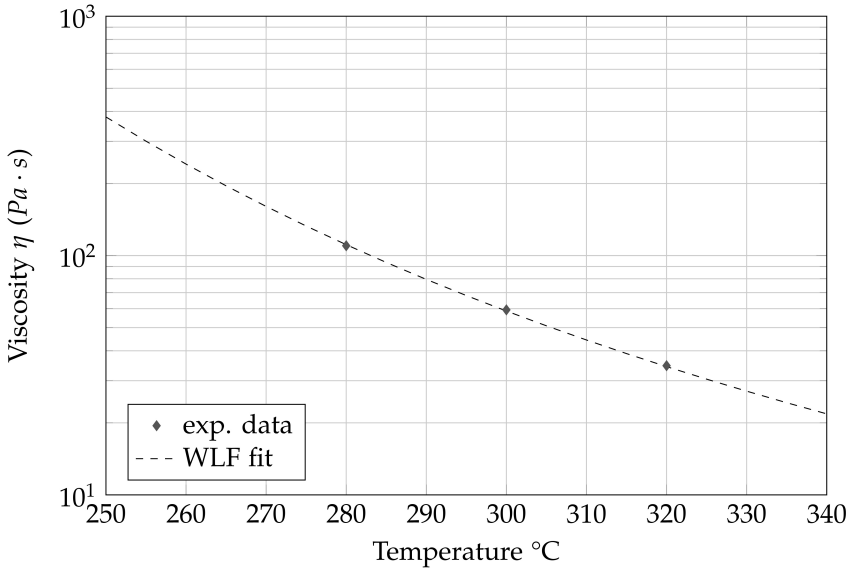

(b) *WLF model for the effect of temperature on viscosity - COC* 5013 *L*-10.

Figure 4.3: Topas COC 5013 L-10 rheological characterization.

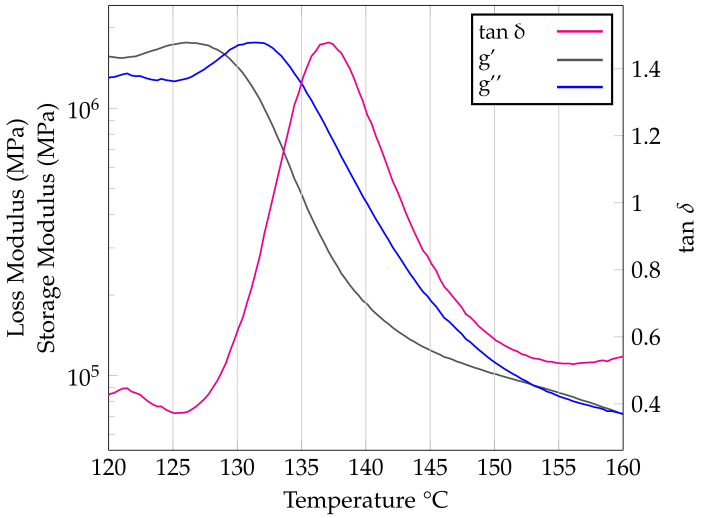

Figure 4.4: Measurements of the glass transition temperature of the COC 5013 L-10 using DMA test.

should consider the contact angle at the actual molding temperature [69].

The samples used for the wetting analysis were microinjection-molded cylinders, with a diameter of 1.5 mm and a length of 1.65 mm. The cylindrical shape was preferred to standard pellets, in order to guarantee mass homogeneity. Fifty pellets were molded and three of them were selected for each material. In particular, PS pellets had an average weight of 3.04 ± 0.02 g, while COC pellets had an average weight of $2.97 \pm 0.02g$.

The wettability analysis was experimentally performed by measuring the contact angle between the melting polymer and a flat nickel plate [70]. The melting polymer was assumed to have a hemispherical shape, so that the measurement can focus on the elaboration of a 2D image. This hypothesis was then verified by comparing the measured left and right contact angles.

Figure 4.5 shows the schematics of the experimental setup. The system includes an electrical thermal chamber, a light source, a high-speed camera and an image analyzer. The tests were conducted by: (i) heating the chamber up to the test temperature, (ii) inserting the cylindrical sample on the nickel plate and (iii) recording the wetting behavior of the melting polymer for 10 minutes [71]. The measurements of the contact angles, both left and right, were repeated three times for each material. The temperature inside the chamber was monitored by thermocouple, which was connected to a temperature controller. The set temperatures were 300 °C for COC and 240 °C for PS, which correspond to the melt temperature used in the μIM experiments for the two polymers respectively. A soaking time of ten minutes was waited before inserting the sample into the chamber, in

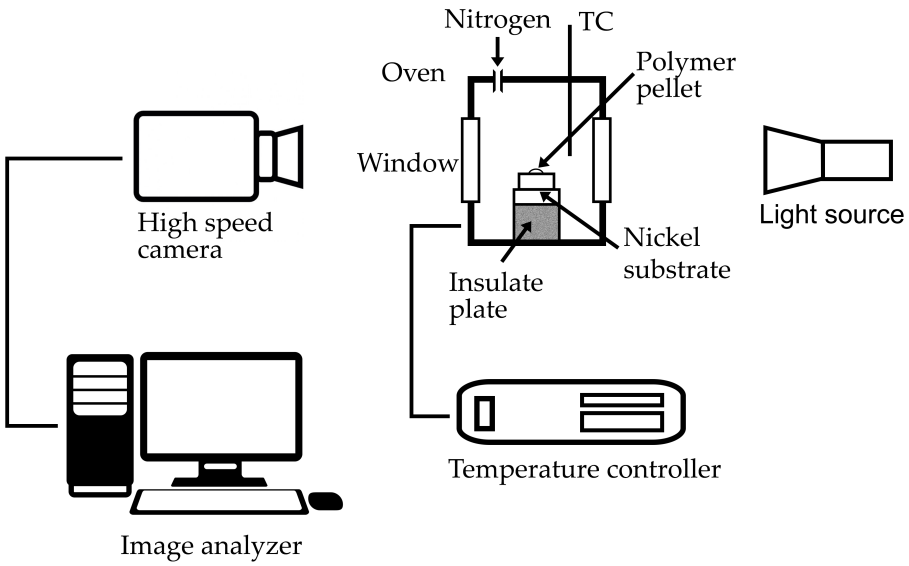

Figure 4.5: Experimental setup for contact angle measurements and analysis.

order to thermally stabilize the setup. A nitrogen atmosphere was used in order to avoid thermal degradation of the polymers.

The evolution of the sample was recorded using a 25X magnification high-speed camera. An image of the polymer sample placed over the nickel plate was collected every 1.5 minutes. The images were then processed using the 'Canny - Edge Detection Method' in Matlab. The contour of the samples was obtained by fitting the base line with a straight line and the curved profile with an ellipse. The left and right contact angles were calculated at intersection points.

4.5 COMPARISON BETWEEN PS AND COC

As it is clear from the Cross-WLF models, the PS and the COC have different properties. Figure 10.2 displays the different sensitivity of the two polymers in different ranges of temperature. In particular, temperature dependence of viscosity is higher for COC than for PS, especially around T_g.

The results of the wettability analysis, reported in Table 4.6, show that the differences between right and left contact angles are negligible, validating the hemispherical shape hypothesis. Comparing the measurements for the two polymers, it can be observed that the contact angle is smaller for COC than for PS (Figure 10.3).

The different behavior of the two material will be one of the objectives of the subsequent experimental investigation.

Figure 4.6: Different sensitivity of PS1540 and COC 5013L-10 to mould temperature variations.

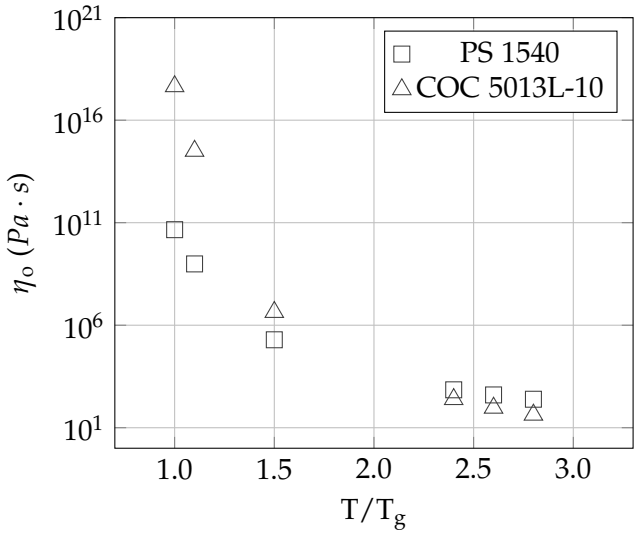

Material	Time [min]	θ sx [deg]	Std.Dev. [deg]	θ dx [deg]	Std.Dev. [deg]
COC	10	49.1	0.6	50.0	1.5
PS	10	68.6	1.2	67.6	0.7

Table 4.6: Results of the wettability analysis.

4.6 PURAC PLA PURASORB P-10

The choice of this polymer has been driven by the need to use a biocompatible and bioresorbable material within the NanoBones project. The aim of this project, as reported in section , is to realize bone fixation devices using a biodegradable material since the metallic fixations have several disadvantages.

The development of biomaterials (biodegradable and bioabsorbable) with the required characteristics to aid in the recovery of tissues damaged by accident or human disease is one of the greatest re-

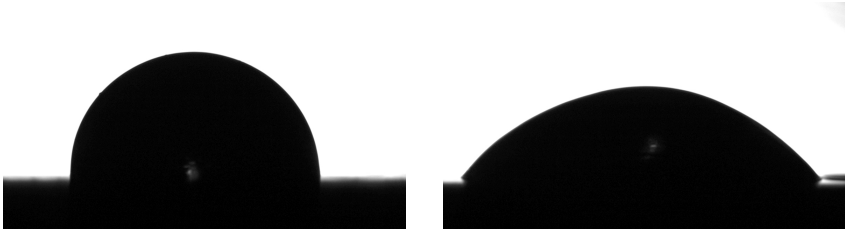

(a) (b)

Figure 4.7: Image of PS drop (a) and COC drop (b) after 10 minutes.

Suggested processing conditions	
Melt temperature (°C)	$170 \div 200$
Mould temperature (°C)	$10 \div 15$
Max. residence time	< 10 min
Injection pressure (bar)	$95 \div 125$
Hold on pressure (bar)	$250 \div 450$
Back pressure (bar)	120
Screw speed (rpm)	$50 \div 200$
Injection speed (mm/s)	$50 \div 150$

Table 4.7: Purac PLA processing conditions for injection moulding.

search challenges involving areas such as medicine and engineering. Biopolymers offer an alternative to traditional biocompatible materials (metallic and ceramic) and non-biodegradable polymers for a large number of applications. Synthetic biodegradable poly-lactones such as poly-lactic acid (PLA), poly-glycolic acid (PGA), and poly-caprolactone (PCL) as well as their copolymers are now commonly used in biomedical devices because of their excellent biocompatibility. These polymers are degraded by simple hydrolysis of the ester bonds, which does not require the presence of enzymes and in turn prevents inflammatory reactions. The hydrolytic products fromsuch degradation process are then transformed into nontoxic subproducts that are eliminated through normal cellular activity and urine. On the other hand, synthetic degradable polyesters have been used in surgery as suturematerials and bone fixation devices for about three decades. Regarding PLA, it has an extensivemechanical property profile and it is thermoplastic with high biocompatibility and biodegradability properties. PLA is obtained fromlactic acid and converted back to the latter onewhen hydrolytically degraded. Purasorb PL 10 is a GMP grade homopolymer of L-lactide with an inherent viscosity midpoint of 1.05 dl/g, primarily used for mediacal device applications and is suitable for all commonly used polymer processing techniques. Due to its high cost, in this works, the PLA was not characterized. Its processing conditions suggested by the manufacturer are summarized in Table 4.7.

5

EXPERIMENTAL SETUP

This chapter describes the experimental setup that was employed during the experimental analysis. For micro injection moulding applications, due to the reduced dimensions of the micro-features, it is important to be accurate when designing the experimental apparatus.

The evolution of micro-moulding to produce components with ever smaller dimensions imposes technological challenges in many areas. One of the most important is the manufacturing of the mould cavity, for the production of components with dimensions that meet the required specifications.

Furthermore, technological challenges are required on the processing equipment. The production of sub-standard components must be minimized by ensuring acceptable process repeatability, which is dependent on homogeneous melting, high precision dosing and a tightly controlled injection dynamic.

In this work a state-of-the-art micro injection injection moulding machine was used, and it was integrated with a variotherm system and a vacuum unit. Particular attention was given to the mould design and mould insert fabrication, which comprises a fixed and a moving parts. The extraction system was designed accurately.

5.1 THE INJECTION MOULDING MACHINE

In this work, a state-of-the-art micro injection moulding machine (*MicroPower* 15 from *Wittmann-Battenfeld*) was used for the moulding experiments. The machine is characterized by a maximum clamping force of 150 kN and a maximum injection speed of 750 mm/s. The plasticizing screw has a diameter of 14 mm and the injection plunger has a diameter of 5 mm. All the main characteristics of the machine are reported in technical data sheet in Table 5.1.

5.2 THE MOULD

Moulds made for micro injection moulding are similar to moulds made for conventional injection moulding. They usually consist of a fixed part and one or more moving parts, depending on the design. Finished parts are demoulded with ejector pins that are usually controlled hydraulically and electrically.

The mould that has been used for this study is composed of a fixed and a rotating moving plate. The main cavity was machined on the moving plate, while the tooling insert was placed on the fixed one.

Properties	Unit	Value
Clamping unit		
Clamping force	kN	150
Opening stroke / Opening force	mm/kN	100/15
Ejector stroke / Ejector force	mm/kN	40/5
Injection unit		
Dosing screw diameter	mm	14
Dosing screw stroke	mm	26
Screw L/D ratio		20
Injection plunger diameter	mm	8
Injection plunger diameter	cm^3	4
Specific injection pressure	bar	2,500
Max. screw speed	min^{-1}	200
Max.plasticizing rate	g/s	1.7
Max. screw torque	Nm	90
Nozzle stroke b / Contact force	mm/kN	230/40
Injection speed	mm/s	750
Injection rate into air	cm^3/s	38
Barrel heating power, nozzle inc.	kW	2.45
Drive		
Electrical power supply	kVA	9

Table 5.1: Wittmann Battenfeld Micropower 15t technical data sheet.

The two parts of the mould are characterized by a contact area of 156x156 mm^2.

The main structure of the mould was used for both the ErytroChip and the NanoBones project. To switch from a project to the other it was just necessary to change the main cavity, the tooling insert and the extraction system. Mould design concepts with removable inserts can be adopted as a key enabling technology to answer the demand for the rapid development of new components. In fact, the replaceable inserts have the aim of minimizing mould manufacturing cost and of increasing the mould versatility.

The main cavity of the ErytroChip mould is characterized by overall dimensions of 19.7 mm x 47.5 mm x 1 mm, and was placed on the movable plate at the end of a trapezoidal cold runner 13 mm long, 3 to 2.10 mm wide and 1.50 mm thick (Fig. 5.1a).

The cylindrical cavity for the MicroBones, was placed on the movable plate too, at the end of a rectangular cold runner (14 mm long, 2 mm wide and 1.5 mm thick). Two different versions of this cavity were used, one with a thickness of 1 mm and the other with 2 mm. However both were cylindrical with a diameter of 5.9 mm (Fig. 5.1b).

The cavity on the moving plate is important, because this the part of the mould that shapes the plastic part. Thus when machining

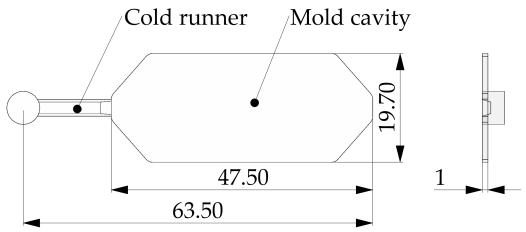

(a) *CellDiaSP project*.

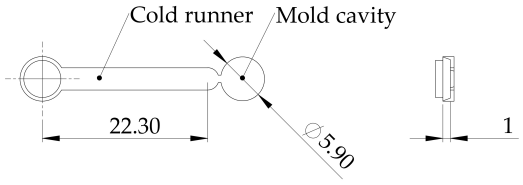

(b) *Nanobones project*.

Figure 5.1: Schematic top view of the part design.

it a proper finishing must be achieved. The main cavities for both projects were machined by the means of a 5 axis micro-milling machine (Kugler Micromaster 5X), that allowed the achievement of a good finishing.

5.2.1 *Ejection System*

In replication of features with high aspect ratio, demoulding is a critical stage. In the ErytroChip project, a particular extraction system was designed to ensure a correct demoulding of the chip. The large contact surface between the mould and the high aspect ratio microstructures lead to an elevated frictional resistance during ejection. In addition, in order to preserve the geometrical structure and functionality of the device, there were no possibilities no place the ejector pins inside the mould cavity. To overcome this, 8 ejector pins were placed around the cavity and undercuts were machined on the top of each via wire micro WEDM Sarix, SX 200 (Figure 5.2).This was not necessary for the NanoBones, where cylindrical extractors were sufficient.

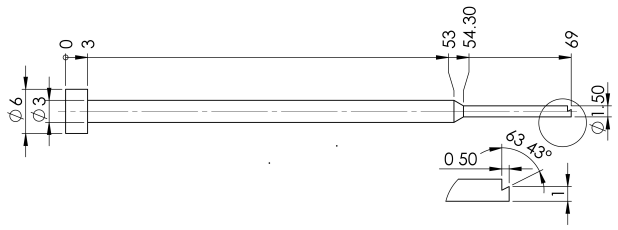

Figure 5.2: Erytrochip ejector pin.

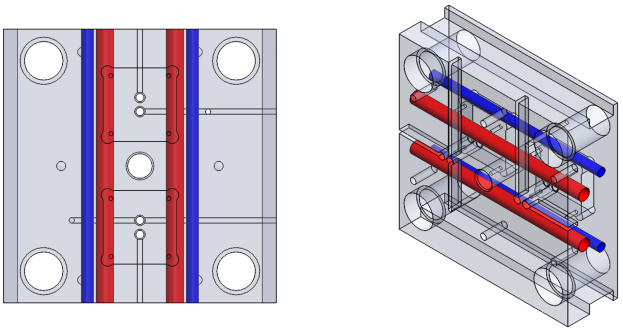

(a) *Fixed plate.*

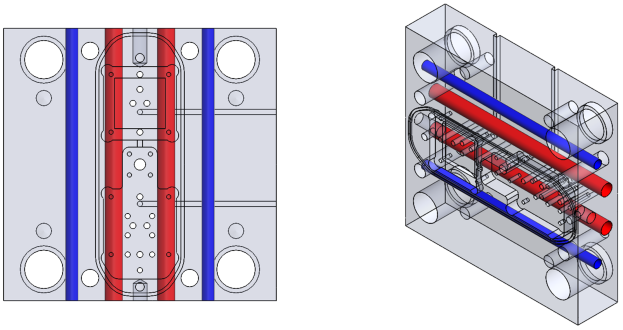

(b) *Movable plate.*

Figure 5.3: The schematic representation of the variotherm system for the (a) fixed plate and (b) movable plate.

5.2.2 *The Vario-Therm System*

In section 3.5.1, the importance of a *vario-therm process* was explained through the analysis of the literature review.

In this work, the electrical heating of the mould was combined with water cooling. A total of 8 heating cartridges were installed in the mould, 4 in the fixed plate and 4 in the moving one. The cooling was realized with cold water (5 °C) circulating in the mould.

Figures 5.3a and 5.3b displays the configuration of the vario-therm system for both the fixed and the movable plate respectively. In red are indicated the heating cartridges, while in blue, the channels where the water was made flowing.

The vario-therm system control was realized with the B6 *control unit* integrated in the μIM machine . Two *thermocouples* were placed in the two plates, just behind the tooling inserts. The control unit heated the mould up to the set temperature, when the value got stabilized the moulding cycle was started. At the end of the injection phase the heating system was turned off and the cooling water was made circulating into the mould.

This system permitted the rapid control of the mould surface temperature during the process. Despite this, not particular attention was given to the optimization of the cycle time. Heating the mould

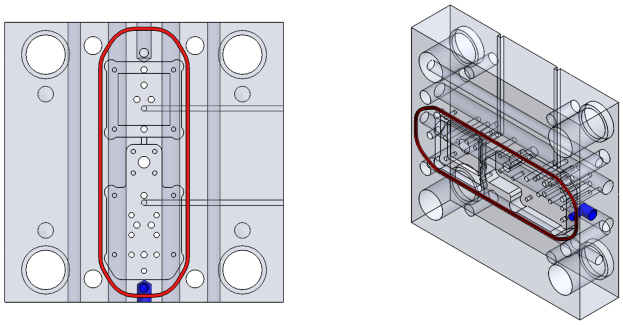

Figure 5.4: The schematic representation of the vacuum system.

at temperature greater than $\sim$ 120 °C required approximately 10 minutes. Conversely the cooling was much faster, the cooling time was decided to be of 180 s, as to reach a temperature lower than 70 °C and to hold it for the necessary time.

5.2.3 *The Vacuum Venting Unit*

In addition to the vario-therm system, a *vacuum pump* was connected to the mould as to evacuate the air from the cavity before the injection phase.

As explained in the literature review (cfr. section 3.5.2), in micro injection moulding the evacuation of air from the cavity can improve the filling distance in micro-features. Conventional vent slots are too big compared to the dimensions of micro-features. Hence, they can not be machined on mould with micro-features.

The evacuation of air from the cavity obtained with the vacuum pump, allowed the achievement of pressures inside of the cavity lower than 6 mbar before the injection. The evacuation of the air from the cavity was applied for 10 s before the injection and for all its time, as suggested by Yokoi et al.[72].

A channel was machined on the moving plate of the mould, as to accommodate an O-ring, which surrounds the cavity and seals the mould parting plane. The pump was connected to the mould with a vent that was machined at the opposite side of the gate, and placed inside the sealed area (Figure 5.4). This experimental setup permits the investigation of the influence of cavity air evacuation on the replication of high aspect ratio micro-features.

5.3 CELLDIASP PROJECT MOULD INSERT REALIZATION

The mould insert for the CellDiaSP project, was manufactured via the UV LIGA process (cfr. section 1.2.3) . A silicon-based SU-8 photoresist was firstly prepared on a silicon wafer, followed by electroforming with nickel. The LIGA process for the realization of the micro-

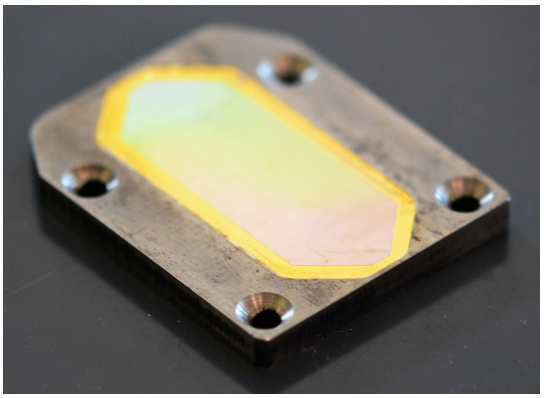

Figure 5.5: The final insert for the CellDiaSP project.

structured mould insert, was performed by *Mildendo Gesellschaft für mikrofluidische Systeme mbH - Germany*, as one of the collaborators of the CellDiaSP project. The insert is characterized by more than 5700 micro-channels, that have a width of 5 μm and an height of 15 μm (aspect ratio: 3). These micro-features are oriented perpendicular to the flow direction and located at an increasing distance from the injection location.

5.4 NANOBONES PROJECT MOULD INSERT REALIZATION

For the NanoBones project, different mould insert with different micro and nano structures geometries were realized. In particular, a first micro structured insert was manufactured by using direct UV lithography on HOI reist in order to carry out some preliminary injection moulding tests. Then, four nano structured inserts were realized by nano imprinting lithography on HOI resist for the optimization of the micro injection moulding process and the subsequent realization of the polymer supports for the in vitro preliminary cells culture (for the basic mould inserts fabrication techniques cfr. section 1.2.3).

The realization of the tooling inserts started from a rectangular pieces of steel 39NiCrMo3, which were lapped in order to obtain a surface with Ra $\leq$ 0.050 μm. Infact, for both the direct UV litography and NIL, the surface of the substrate must be flat and with a very low rughness.

The idea of using directly patternable hybrid materials for micro injection moulding realization arose from the need for easily obtainable inserts to be used for replicating microand nano- structured surfaces.

5.4.1 *HOI Resist Selection*

Different HOI systems have been experimentally tested in order to identify which ones has the better structures resolution and the higher resistance to the μIM process. For this purpose, four mould inserts

were realized by REM technique using four different type of resist. This techniques was adopted since the micro pattern was the same for all four inserts and it was characterized by micro holes with a diameter of 4 μm and inter spacing of 10 μm. This micro structure was selected in order to facilitate the metrological characterization of both the mould insert and the injection moulded polymeric parts.

The tested HOI were:

- ELO: thermal-curable epoxy resins synthetized with a bio-based epoxy resin from epoxidized linseed oil, crosslinked with a hexa idrophtalic anhydride EH;
- GBGDE: thermal-curable epoxy resins synthetized with an epoxy monomer (glyceroldiglycidylether),crosslinked with a hexa idrophtalic anhydride GH;
- TMSPM: hybrid Zr-based systems, organically modified with 3-(Trimethoxysilyl)propyl methacrylate;
- GZ: hybrid Zr-based systems, organically modified with 3-glycidoxy propyltrimethoxysilane.

As describe in section 1.2.3, the REM process is characterized by a two-steps replication process. The master was produced by UV Litography of a commercial PMMA resist spin coated on a silicon wafer following these steps:

- spin coating of PMMA resist on silicon wafer at 1000 rpm for 30 sec;
- soft bake at 150 °C for 3 minutes;
- UV exposure for 90 sec;
- develop of the photoresist for 90 sec.

The PMMA pattern was tranfered into PDMS (Stylgard 184) by replica moulding and then a replica of the original master was obtained by solidifying the different types of HOI against the PDMS mould. A series of tests were performed for each HOI in order to identify a standard procedure for the realization of the final mould insert:

- Procedure for ELO resist:
  1. spin coating of ELO resist at 2000 rpm;
  2. REM of the PDMS mould and degassing for 2 min;
  3. UV exposure for 3 min;
  4. soft bake at 100 °C for 2 min.
- Procedure for GBGDE resist:

1. spin coating of GBGDE resist at 3000 rpm;
2. REM of the PDMS mould and degassing for 2 min;
3. UV exposure for 2 min;
4. soft bake at 100 °C for 3 min.

- Procedure for TMSPM-Zr resist:
  1. spin coating of TMSPM-Zr resist at 2000 rpm;
  2. REM of the PDMS mould and degassing for 2 min;
  3. UV exposure for 1 min;
  4. soft bake at 100 °C for 2 min.
- Procedure for Gz resist:
  1. spin coating of Gz resist at 2000 rpm;
  2. REM of the PDMS mould and degassing for 2 min;
  3. hard bake at 120 °C for 20 min.

To analyze the effect of high temperature on the dimensional accuracy of the micro pattern, two mould inserts were realized for each HOI resist and one on them was hardly backed at 200 °C for 10 min.

Starting from the PMMA master, each replica was measured by using a 3D optical profiler (Sensofar, PLu Neox) in 3 different positions. Figure 5.6 shows the REM steps and the metrological characterization of the micro feature for the production of the ELO-based mould insert. The average height and diameter of five micro holes were selected as indicator of the goodness of the REM process (Table 5.2).

Figure Figure 5.7 shows the comparison between the average diameter of the measured micro holes along the REM process for each reist. It is evident that replica moulding against PDMS mould faithfully replicates the original master.

To test the resistance of the different HOI resist at μIM process, an experimental campaing was carryed out. Each mould insert was used for produce 300 injection moulded samples in polistyrene (PS, Total crystal 1540) using the following process parameters:

- barrel temperature: ((240-230-220-200)$\pm$10) °C;
- mould temperature: 80 °C
- clamping force: 150 kN
- injection speed: 750 mm/s
- pressure switch over: 80% of the maximum injection pressure;
- holding pressire: 400 bar for 8sec;
- cooling time: 2 sec.

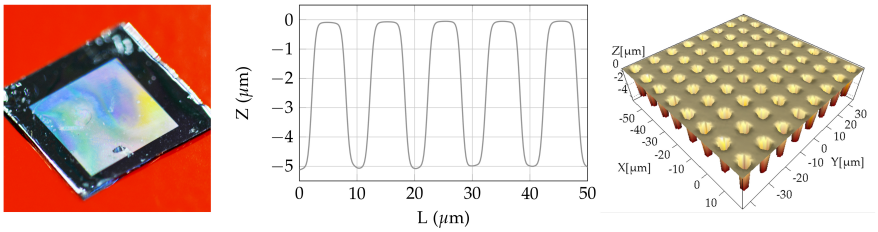

(a) *PMMA resist on silicon wafer*

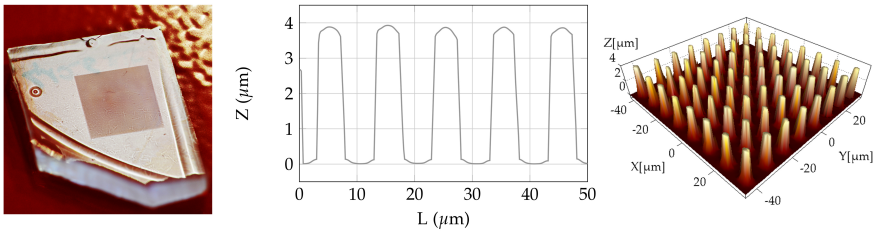

(b) *PDMS replica*

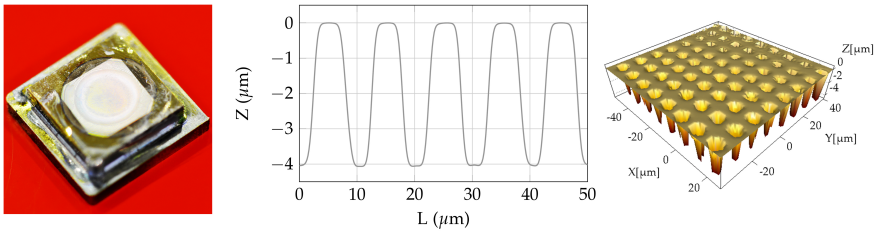

(c) *ELO based mould insert soft baked*

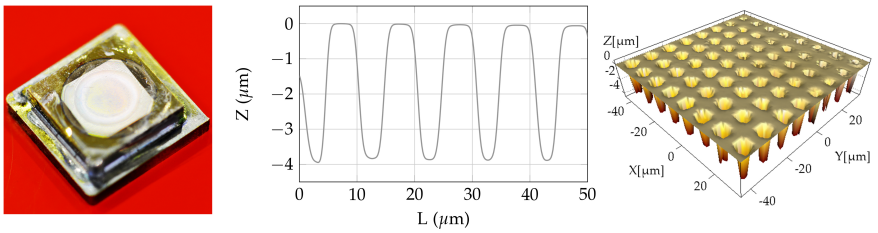

(d) *ELO based mould insert hard baked*

Figure 5.6: Steps of replica moulding process for the realization of ELO-based mould insert. The first step is the realization of the micropattern by direct UV litography on PMMA resist spin coated on a silicon wafer (a), followed by castng of PDMS (b) and soft litography of the PDMS mould on the ELO resist spin coated on the metallic insert (c),(d).

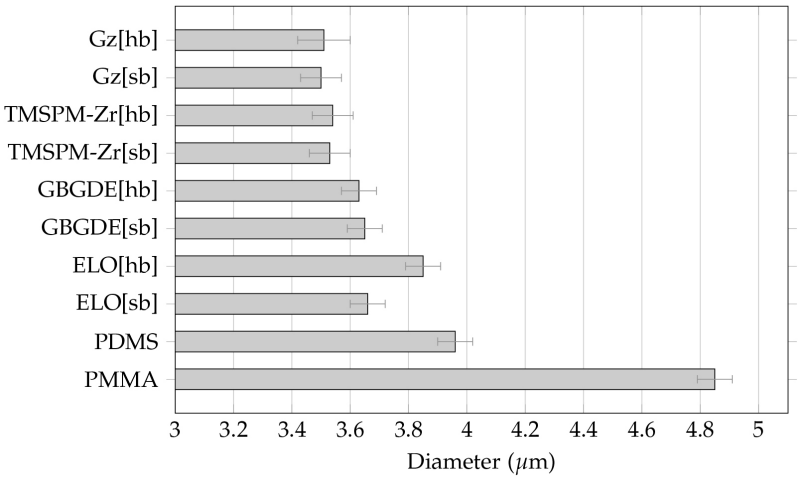

Figure 5.7: Average diameter of the micro holes during the REM process for the selection of the resist.

Replica	**Diameter** (μm)	**Height** (μm)	**Aspect ratio**
PMMA on silicon	4.72 ± 0.23	4.85 ± 0.06	1.03
PDMS	4.32 ± 0.16	3.96 ± 0.06	0.917
ELO			
soft bake	4.66 ± 0.13	3.66 ± 0.06	0.785
hard bake	4.56 ± 0.09	3.85 ± 0.06	0.844
GBGDE			
soft bake	4.79 ± 0.16	3.65 ± 0.06	0.762
hard bake	4.94 ± 0.37	3.63 ± 0.06	0.735
TMSPM-Zr			
soft bake	4.35 ± 0.24	3.53 ± 0.07	0.811
hard bake	4.87 ± 0.31	3.54 ± 0.07	0.727
Gz			
soft bake	4.03 ± 0.57	3.50 ± 0.07	0.868
hard bake	4.53 ± 0.32	3.51 ± 0.09	0.775

Table 5.2: Average values for holes depth and diameter.

These process settings were selected to yield complete filling of the cavity. During injection, an automatic execution of the process was performed. During the experiments a moulded sample was collected every 50 cycles for the metrological characterization.

Some resist yield before the achievement of 300 cycles due to adhesive failure, thermal cycling and compression. In particular, the ELO resist and the GBGDE resist, withstood for 30 cycles, after that it was observed a delamination on the mould insert surface probably due to the compression cycles (Fig. 5.8a and Fig. 5.8b). The best results have been obtained with Zirconia based systems, TMSPM-Zr and Gz, which resisted for 300 cycles without showing signs of failure (Fig. 5.8c and Fig. 5.8d).

In first analysis, zirconia-based systems better behave during the μIM process. However, to verify the integrity of the micro structures, the height of the micropillars on the moulded samples were analyzed.

Three measurements point were selected for each collected sample (cfr. section 6.3). The first measurement area was at 0.5mm far from the injection location (A), the second area in the center of the cavity at 3.0mm from the injection location (B) and the last area at the opposite site of the gate at 5.5mm from the gate (C). The results for both the TMSPM-Zr and Gz systems are reported in Table 5.3.

Sample n.	TMSPM-Zr (μm)	Gz (μm)
1	0.76 ± 0.05	1.22 ± 0.25
50	0.75 ± 0.04	1.22 ± 0.23
100	0.76 ± 0.02	1.17 ± 0.23
150	0.74 ± 0.04	1.24 ± 0.25
200	0.75 ± 0.04	1.21 ± 0.18
250	0.75 ± 0.05	1.21 ± 0.26
300	0.75 ± 0.05	1.22 ± 0.18

Table 5.3: Average height of moulded PS samples for both TMSPM and Gz systems.

As shown in Table 5.3, the replication degree is about 20% for TMSPM-Zr and 30% fro Gz systems. This is due beacause the μIM process parameters were not optimized for the complete replication of the miro features, since the main objective of this analysis was to determine the life of the mould inserts.

The results shown that both the Zr-based systems withstand for 300 cycles without compromising the quality of the micro-structuerd surface. According to this, the UV-curable TMSPM-Zr resist was choosen for the realization of the micro structured insert with direct UV litography process, while the thermally curable Gz resist was selected for the realization fo the nano structured mould insert via NIL (cfr.section 1.2.3).

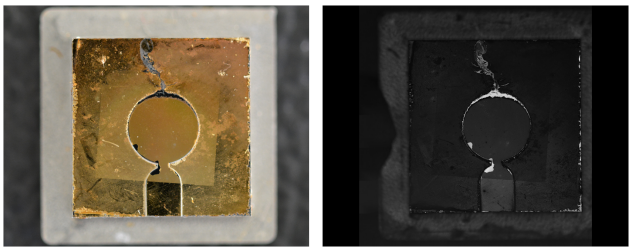

(a) *ELO resist*

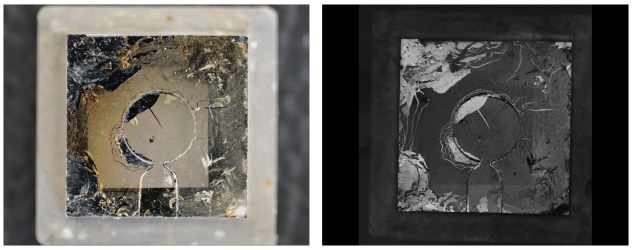

(b) *GBGDE resist*

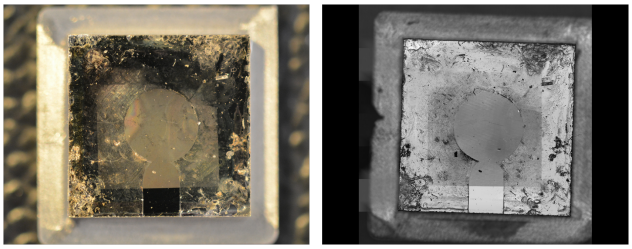

(c) *TMSPM-Zr resist*

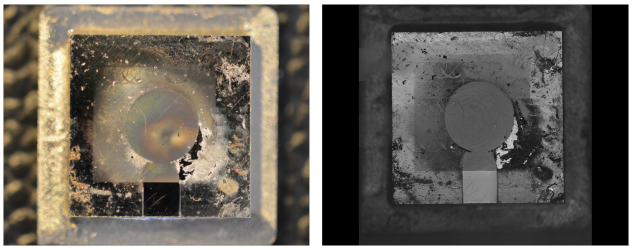

(d) *GZ resist*

Figure 5.8: Inserts surface after μIM capmaing. (a) ELO and (b) GBGDE resist withstood for 30 cycles, while Zr-based resist, (c) TMSPM-Zr and (d) Gz, resisted for 300 cycles without showing signs of failure.

5.4.2 *Micro-Structured Insert Realization*

According to the results obtained in section 5.4.1, the UV-curable TMSPM-Zr resist was choosen for the realization of the micro structured insert.

TMSPM-Zr is a negative resist: the exposed areas undergo polymerization and crosslinking. Since the*Hamamatsu Lightningcure LC5* lamp used for film exposure and patterning was not collimated and no mask aligner was available, some problems of exposure of the films were detected, even under the covered structures (smaller the structures more difficult was to develop the films up to the substrate). In order to reduce this setup issue and lower the exposure time, three expedients were adopted: (1) the resist was exposed a shorter time to UV in combination with a milder development (a mixture of Acetone and Ethanol) compared with Acetone; (2) TMSPM-Zr 110 g/l solution was added with 1%mol of *IRGACURE 369* photoinitiator in order to compensate the shorter UV exposure; (3) the lamp fibre was approached to the sample up to 2 cm distance. TMSPM-Zr films were spin coated at 700 rpm for 30s (thickness around 3 μm) on lapped steel substrate. After spin coating, the insert was exposed to a 4 J/cm² ultraviolet dose through a mask, which contains the desired pattern. The obtained mould insert surface was characterized by a pattern of cylindrical micro holes with a diameter of 4μm interspaced by 10μm. The insert, was then characterized by means of an optical profiler, as will be discussed in section 6.2.

5.4.3 *Nano-Structured Inserts Realization*

According to the results obtained in section 5.4.1, the thermally curable Gz resist was selected for the realization fo the nano structured mould insert. The thermally curable GZ system was used as NIL resist in order to realize the nanostructured inserts. Nanoimprint lithography was conducted by applying a pressure of 100 bar for 5 min at RT and 10 min at 120 °C between the 8x8 mm2 Si master and the spin coated (1000 rpm for 5s) GZ film. A sidewall angle of around 2 ° from the vertical was realized in order to favor the NIL process and reduce friction during demoulding. The patterned films were then treated at 100 °C for 1h in order to further condense the structures before using the insert as stamp for micro injection moulding. The nanometer scale silicon master needed for nanoimprint lithography were produced by *Laboratory for nanofabrication of nanodevices - LANN*. Four different pattern were realized:

- Pattern 200-300: 200 nm diameter holes interspaced by 300 nm;
- Pattern 200-400: 200 nm diameter holes interspaced by 400 nm;
- Pattern 400-600: 400 nm diameter holes interspaced by 600 nm;

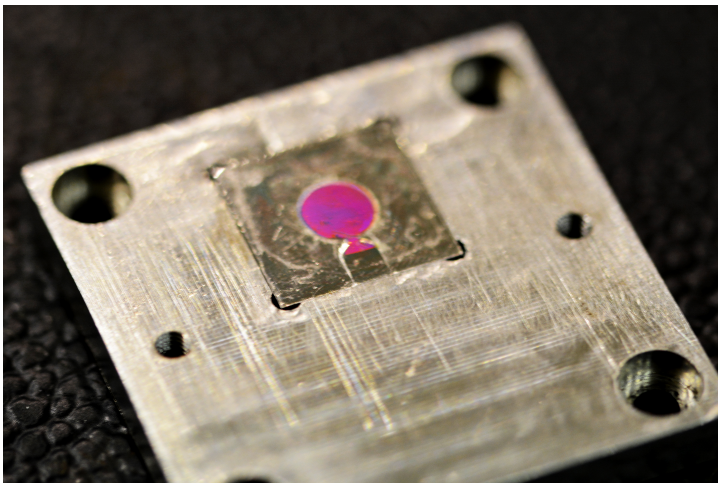

Figure 5.9: The final insert for the NanoBones project.

- Pattern 400-800: 400 nm diameter holes interspaced by 800 nm;

The choice of the dimensions and the shape of the nano structures derived from literature, according to the work of Kolind et al. that shows how the pillars diameter and pitch influence the cells growth rather than the single pillar shape [73].

Every inserts, was then characterized by means of an Atomic Force Microscopy (*AFM*), as will be discussed in section 6.2. Figure 5.9 shows the nano-structured final insert for the μIM process.

6

METROLOGICAL CHARACTERIZATION

Quality control is an issue regarding any kind of production. When investigating the micro injection moulding process, the importance of metrology refers to all the steps of the product and process development chain. The use of effective and reliable instruments for quality control of micro-moulded parts is fundamental for the accuracy of the analysis.

In micro/nano-technology the critical dimension is to be read as that interesting dimension of a specimen that is important for its function, and not necessarily restricted to very small-sized samples. One of the critical tasks in micro and nano-metrology, is the measurements of features with high aspect ratio. The *aspect ratio* of a geometry is defined as the ratio of its longer dimension to its shorter. It may be applied to two characteristic dimensions of a three-dimensional shape, such as the ratio of the longest and shortest axis.

Moreover, the level of miniaturization and the geometrical complexity must be taken into account when measuring micro/nano features.

Figure 6.1 shows a proposed illustration of selected measurements tasks based on the classification made in chapter 1. Figure 6.1 is based on the principles of a typical *Stedman diagram*, and therefore it holds no information about geometrical complexity.

6.1 BASIC OF DIMENSIONAL MICRO AND NANO METROLOGY

The description of the technologies used in this study, will follow in this section. The technologies will be described summarizing working principle, range and resolution.

6.1.1 *Imaging Confocal Microscopy*

Imaging confocal microscopy is a well-known technology for the 3D measurement of surface topography. A confocal microscope is used for the acquisition of a sequence of confocal images through the depth of focus of the objective. The highest signal within the images of the sequence for each pixel correlates with the height position of the topography. Confocal microscopy has many advantages over other optical techniques such as having a high numerical aperture, meaning a high lateral resolution and a high measurable local slope [74].

The basic principle of confocal profiling relies on storing a sequence of confocal images in the memory of a computer taken from different z axis planes along the depth of focus of the microscope's objective.

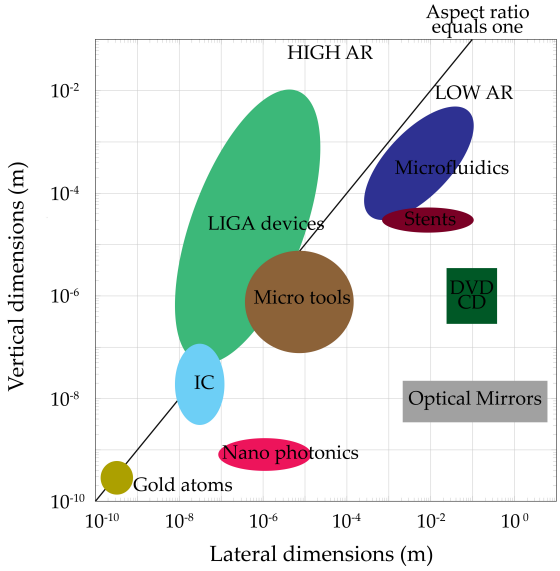

Figure 6.1: Selected components for dimensional micro and nano metrology.

	20X	100X
Numerical aperture	0.45	0.90
Maximum slope (deg.)	21	51
Field of view (μm)	636 x 477	127 x 95
Spatial sampling (μm)	0.83	0.17
Optical resolution (μm)	0.31	0.15
Vertical resolution (nm)	< 20	< 2

Table 6.1: Main characteristics of the 3D optical profiler used in this work.

An optically sectioned image shows bright gray pixel levels for those regions of the surface that lie within the depth of focus of the objective, and dark grey pixel levels for the rest of the parts of the surface that are out-of-focus. Each pixel of the image contains a signal along the z direction called the axial response similar. Different pixels will have the axial response maximum located on different z axis positions according to the 3D surface shape. By locating the z axis position of the maximum of the axial response for each pixel, the 3D surface is reconstructed. A confocal image is built up by scanning in plane (on the x and/or the y direction) the illumination and detection patterns.

In this work the replication accuracy of the polymeric micro-features (both micro-channels and micro-pillars) has been evaluated with a state-of-the-art 3D optical profiler (*Sensofar Plu Neox optical profiler*. The instrument was used in confocal mode with 20X and 100X objectives. The main characteristics of the instrument are reported in Table 6.1. Vertical calibration was performed using silicon depth standards type A1 (ISO 5436-1).

Electron optics	
Accelerating voltage	200 V to 30 kV
Probe current	$\leq$ 200 nA, continuously adj.
Max. horizontal field width	6.5mm at 10 mm WD
	24.3mm at 25 mm WD
Magnification	6 to 1000000 x
Chamber	
Dimension	284 mm left to right
Number of ports	8
Stage	
X-Y	100 mm
Z	60 mm
T	-5 to +70 deg
R	360 deg
Repeatability	2 μm
Electron Beam resolution	
at 30 kV (SE)	3 nm
at 30 kV (BSE)	4 nm
at 3 kV (SE)	8 nm

Table 6.2: SEM FEI, Quanta 250 specifications.

6.1.2 *Scanning Electron Microscopy*

Scanning electron microscopy (SEM) is a microscopy method existing for several decades. It is based on scanning an electron beam on the specimen. The interaction between the beam and the specimen surface leads to several emissions, which can be detected and used to characterize physical and chemical properties of the sample under investigation. Among others, it is possible with the SEM, to obtain topography images. As regards topography, SEM has some unique properties that, combined together, are not matched by any other microscopy technique. These include: magnification levels (100x to 100.000x), resolution down to 2 nm (for highest magnification), large depth of field, long working distance (allowing multiple positioning measurement strategies), elemental analysis capability and minimum diffraction effects [9]. Some disadvantages compared to optical microscopy include usually high vacuum requirement, relatively low throughput, potential for sample charging, electron beam/sample interaction etc..

Scanning electron microscopy (SEM) can also be used for qualitative surface topography analysis, primarily based on the fact that SEM allows an excellent visualization achieved through the very high depth of focus of this technique. However, SEM photographs are still inherently 2D, and no height information can be extracted directly

	scanning by sample	Scanning by probe
Sample size	up to 40 x 10 mm	Up to 100 x 20 mm
Scanners	3 x 3 x 2.6 μm	50 x 50 x 5 μm
	10 x 10 x 4 μm	100 x 100 x 7 μm
	50 x 50 x 5 μm	100 x 100 x 10 μm
Min. scan step (DAC)	0.0004 nm	0.006 nm
	0.0011 nm	0.012 nm
	0.006 nm	0.012 nm
Optical viewing system	Res. 1 μm	Res. 3 μm
	Num. aperture 0.28	Num. aperture 0.1
XY sample positioning	5 x 5 mm	
Positioning resolution	5 μm	

Table 6.3: AFM NT-MDT Solver pro-M specifications

from the images. Furthermore calibration of scales and uncertainty estimation is a prerequisite for the use of SEM pictures for quantitative evaluations.

The use of SEM for highly accurate dimensional measurements is reliant upon the interpretation of the electronic representation of the sample. This means that all distortions of the image directly influence the measurement accuracy.

SEM images are purely two-dimensional as they are built up of intensity variations displayed in an array of pixels obtained as the electron beam is scanned rectilinearly over the specimen surface. The sample could be tilted of a certain angle inside the vacuum chamber and, using the *tilt correction* algorithm, is it possible to obtain a measurement of the third dimension z.

In this work the SEM *FEI Quanta 250*, was used to characterized the nano structered inserts. The SEM was also employed to evaluate the *in vitro* mesenchemical stem cells culture for the NanoBones project. The main characteristics of the instrument are reported in Table 6.2.

6.1.3 *Scanning Probe Microscopy*

The atomic force microscope (*AFM*) relies on a scanning technique to produce very high resolution, 3D images of sample surfaces. The AFM measures ultrasmall forces (less than 1 nN) present between the AFM tip surface and a sample surface. These small forces are measured by measuring the motion of a very flexible cantilever beam having an ultrasmall mass.

In an AFM, the force between the sample and tip is detected, rather than the tunneling current, to sense the proximity of the tip to the sample. The AFM can be used either in a static or dynamic mode. In the static mode, also referred to as repulsive mode or contact mode, a sharp tip at the end of a cantilever is brought in contact with a

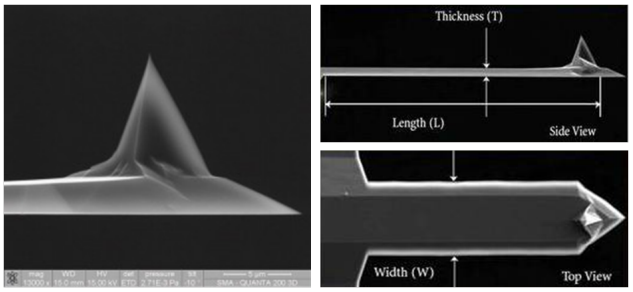

Material			Single crystal Silicon
Chip size			3.4 x 1.6 x 0.3 mm
Reflective side			Au
Cantilever number			1 rectangular
Tip curvature radius			6nm
Cantilever legth (L)			125 $\pm$ 5 μm
Cantilever width (W)			30 $\pm$ 3 μm
Cantilever thickness (T)			2 $\pm$ 0.5 μm
	min	typical	max
Resonant frequency	87	150	230
Force costant	1.45	5.1	15.1

Table 6.4: NSG01 tip series specification.

sample surface. During initial contact, the atoms at the end of the tip experience a very weak repulsive force due to electronic orbital overlap with the atoms in the sample surface. The force acting on the tip causes a cantilever deflection which is measured by tunneling, capacitive, or optical detectors. The deflection can be measured to within 0.02 nm, so for typical cantilever spring constant of 10 N/m a force as low as 0.2 nN can be detected. In the dynamic mode of operation for the AFM, also referred to as attractive force imaging or non contact imaging mode, the tip is brought in close proximity (within a few nm) to, and not in contact with the sample. Although in this technique, the normal pressure exerted at the interface is zero (desirable to avoid any surface deformation), it is slow, and is difficult to use, and is rarely used outside research environments.

In the two modes, surface topography is measured by laterally scanning the sample under the tip while simultaneously measuring the separation dependent force or force gradient between the tip and the surface. In the contact (static) mode, the interaction force between tip and sample is measured by measuring the cantilever deflection. In the non contact (or dynamic) mode, the force gradient is obtained by vibrating the cantilever and measuring the shift of resonant frequency of the cantilever. With an AFM operated in the contact mode, topographic images with a vertical resolution of less than 0.1 nm (as

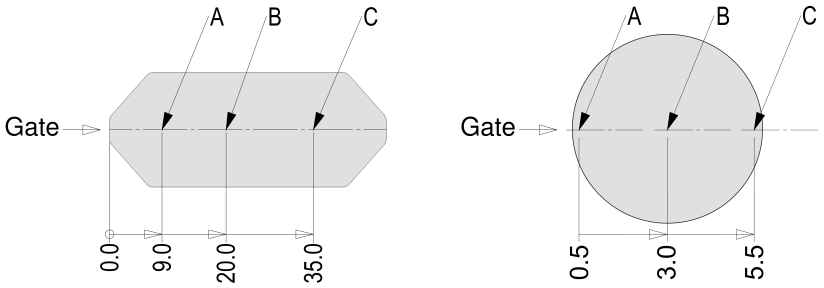

(a) *CellDiaSP project*. (b) *NanoBones project*.

Figure 6.2: Measured areas for the characterization of both the (a) microchannels, (b) micro and nanopillars.

low as 0.01 nm) and a lateral resolution of about 0.2 nm have been obtained.

In this work the AFM *NT-MDT Solver Pro-M*, with *NSG01 Golden* tip, was used for measuring the height of the replicated nano pillars. The main characteristics of the system are reported in Table 6.3 (AFM) and Table 6.4 (Tip).

6.2 MOULD INSERT CHARACTERIZATION

Before the μIM experimental campaign, the mould inserts for both the CellDiaSP and NanoBones projects were metrologically characterized in three different positions (Figure 6.2). The moulds inserts characterization is required in order to evaluate the goodness of the replication during the micro injection moulding tests. As described in section 5.3 and 5.4, the considered mould inserts are characterized by different types of micro and nano features and this required the use of different metrological techniques.

6.2.1 *CelldiaSP Project*

The mould insert surface for the CellDiaSP project is characterized by more than 5700 micro channels, which have a width of 5 μm and a height of 20 μm (aspect ratio:4).

As discussed before (section , the characterization of micro features with high aspect ratio is a critical task in metrology. In this work, the characterization of the mould insert was carried out using both the SEM and the optical profiler (crf. section 6.1.2 and 6.1.1).

In first analysis the micro channels were characterized using the SEM. The pitch between the channels and their width were measured from the top of the mould insert with a magnification of 2000x with the ETD detector (Figure 6.3a). SEM photographs are still inherently 2D, and no height information can be extracted directly from the images. For this reason, the sample was 45 deg tilted and the measure-

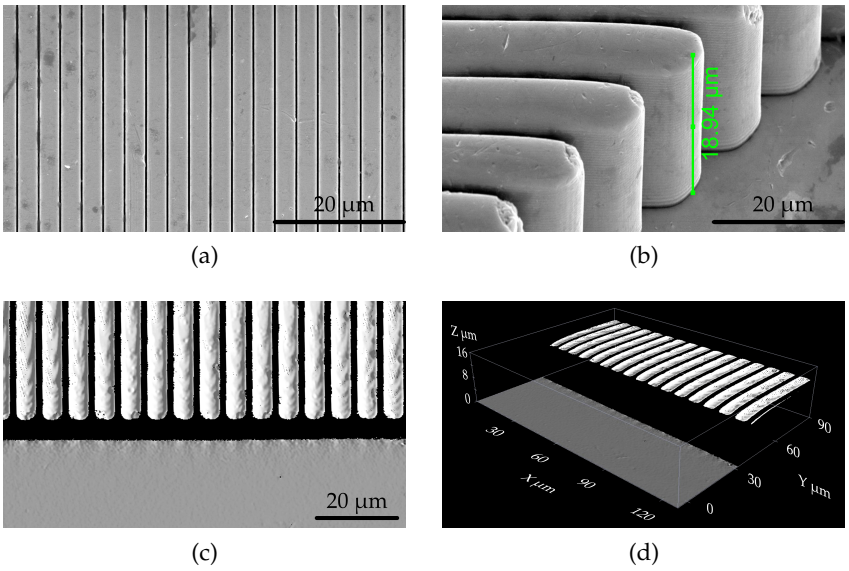

(a) (b)

(c) (d)

Figure 6.3: Metrological characterization of the nickel insert using both the (a,b) optical profiler and (c,d) the SEM.

ment was carried out on the border of the micro structured area, as shown in Figure 6.3b. Due to the high aspect ratio of the micro channels and being the SEM dimensional measurements dependent to the interpretation of the electronic representation of the sample, the use of this instruments for measuring these type of micro features was not appropriate.

The use of optical profiler for the mould insert characterization has provided better results. The pitch and the width of the micro channels were measured in confocal mode, using a 100x objective (Figure 6.3c). The depth of the micro channels was measured also in this case on the border of the micro structured area, as shown in Figure 6.3d.

The data acquired with the optical profiler were elaborated using the *SensoSCAN* software. A section of the scanned area topography was extracted in order to measure the dept of the microchanlles (Figure 6.4a), the pitch and the width (Figure 6.4b).

The mould insert was measured in different areas as reported in Figure 6.2a and three measurements at each position were carried put. TableTable 6.5 reports the average dimensions for the metrological characterization of the CellDiaSP mould insert.

Depth (μm)	20.556 ± 1.02
Pitch (μm)	8.1489 ± 0.86
Width (μm)	3.2913 ± 0.63

Table 6.5: Main dimensions the CellDiaSP mould insert (cfr. Figure 6.7).

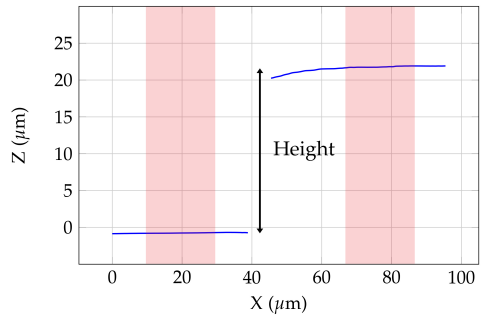

(a)

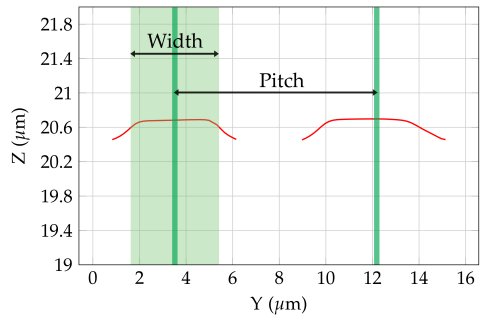

(b)

Figure 6.4: Elaborated image from optical profiler for the measurements of the (a) depth, (b) the pitch and the width of the micro channels.

6.2.2 *NanoBones Project*

The NanoBones inserts were realized by UV-Lithography and NIL techniques (depending on features sizes) on directly patternable hybrid resist. As described in section 1.2.3, the sol-gel hybrid materials combine the qualities of organic molecules or polymers and the physical properties of glass such as: refractive index, transparency, thermal and mechanical resistance. Hence, the combination of the physical properties of the mould insert surface and the dimensions of both micro and nano structures, required the use of AFM for the metrological characterization of the mould insert. In fact, due to the refractive index and the transparency of the mould surface, the use of optical profiler was not allowed.

The micro structured mould insert was measured in three areas along the diameter of the moulded part (Figure 6.2b) for a total of 15 measurements. For each measurements both the topography and the profile of the scanned areas were analyzed in order to calculate the average values for the holes depth (Figure 6.8), which correspond to $5.00 \pm 0.09 \mu$m. Hence, the micro holes are characterized by an aspect ratio of 1.25.

The nano structured inserts were realized by using nano imprinting lithography technique. As described in section 1.2.3.4, this techniques

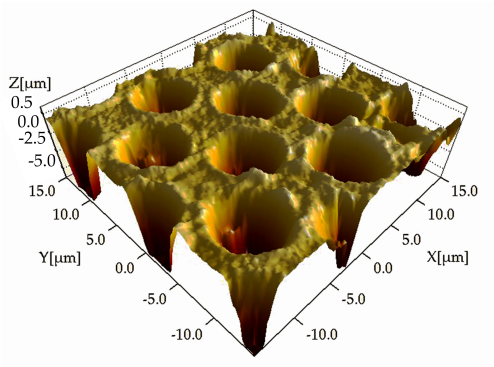

(a)

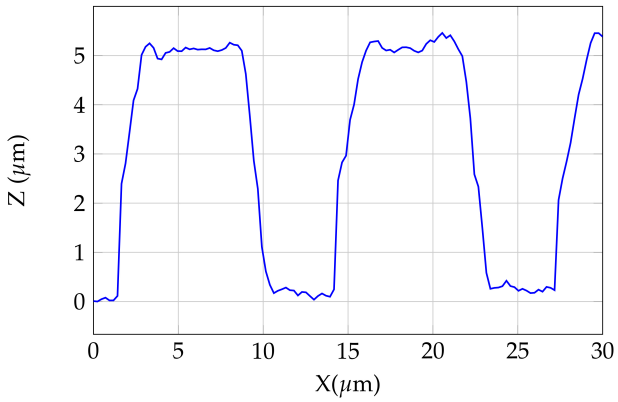

(b)

Figure 6.5: AFM measurements for the micro structured mould insert, (a) topography, (b) height profile.

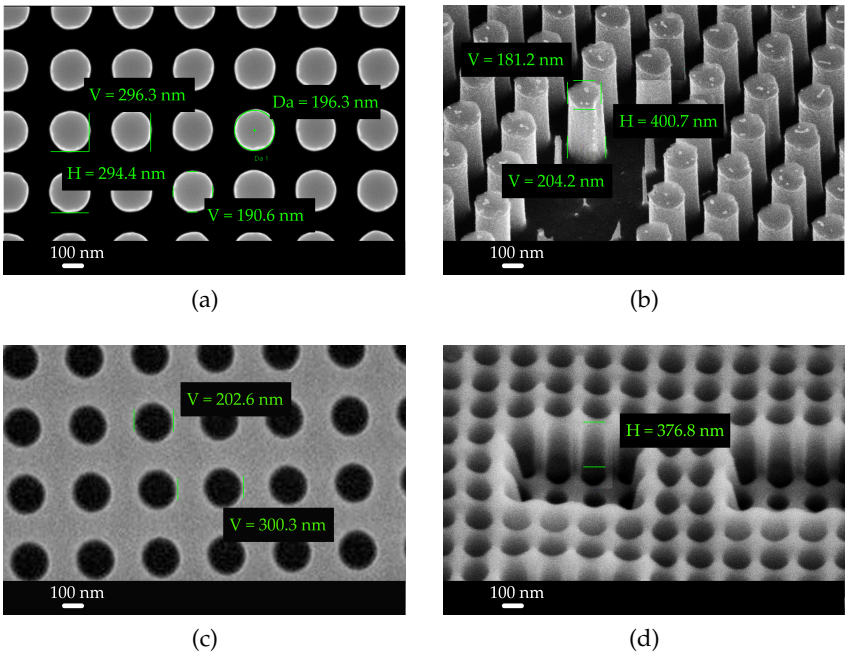

Figure 6.6: Metrological characterization of the (a) diameter, interspace and (b) height of the nano structured master and metrological characterization of the (c) diameter, inter space and (d) height of the final mould insert.

is based on the transfer of a nano structured hard material stamp (in this case obtained by *EBL*) into a resist coated substrate.

To fully characterized the entire process chain for the realization of polymeric nano structured substrate for cell differentiation studies, both the "hard material" stamp obtained by EBL (from now *master*) and the final mould insert obtained by NIL, were characterized. Also in this case, due to the physical properties of the spin coated resist, and the dimensions of the nanostructures, the use of optical instruments were not allowed. Moreover, due to the shape of the nano holes (min. diameter of 200 nm, min. inter space of 300 nm and aspect ratio of 2), the SEM was selected instead of the AFM to metrologically characterize both the master and the final mould insert.

The measurements of the diameters and the inter spaces of the nano features were done from the top of the measured sample for both the masters and the mould inserts (Figure 6.6a and 6.6c). The height of the nanopillars obtained by EBL, was measured by tilting the samples of 45deg and selecting as measurements areas some zones in which the pattern was not complete as shown in Figure 6.6b. For measure of the depth of the nano holes, a focused ion beam technique (*FIB*) was adopted in order to dissect the pattern and reach the bottom of the holes as shown in Figure 6.6d. A focused ion beam system is a relatively new tool that has a high degree of analogy with a focused electron beam system such as a scanning electron microscope.

Insert	Depth (nm)	Interspace (nm)	Aspect ratio
200 - 300	382 ± 4	300 ± 3	1.91
200 - 400	393 ± 6	401 ± 3	1.97
400 - 600	789 ± 6	600 ± 3	1.97
400 - 800	784 ± 6	800 ± 3	1.96

Table 6.6: Average values for holes depth and interspace for the nanostructured mould inserts.

In these systems, the electron beam is directed towards the sample, and upon interaction it generates signals that are used to create high magnification images of the sample. As the beam is well controlled in size and position and the signal are strong enough to be detected without excessive noise, these kinds of tools are very powerful to analyze samples in great detail over a wide range of magnifications [75]. The measurements for all the inserts are summarized in Table 6.6.

6.3 REPLICATED MICRO AND NANO FEATURES CHARACTERIZATION

To quantitatively characterize the replication quality of the micro and nano features, the collected polymeric samples were examined in few positions either for the NanoBones and for the CellDiaSP projects (Figure 6.2b and Figure 6.2a). Three measurements at each position were carried out on the moulded samples, the same as those were used for the mould inserts characterization.

The replicated micro channels were measured using the optical profiler operating in confocal mode, with the 100x objective. Contrary to the case of the mould insert characterization, the pitch between the replicated channels was enough for using the optical profiler. The topography and the profile of the replicated micro channels are reported in Figure 6.7.

For the NanoBones project, the replicated micropillars were charaterized by using the optical profiler. The topography and the profile of the replicated micropillars are reported in Figure 6.8.

The optical profiler allowed the reconstruction of surface topography, and so the quantitative measurement of the replicated micro features height. The use of this measurement technology did not permitted the characterization of the shape of both the micro channels and the micro pillars, as the maximum measurable slope is of 51 degrees.

The replicated nanopillars were measured by using atomic force microscope. The topography and the profile of the replicated nanopillars are reported in Figure 6.9. Also in this case, the characterization

of the shape of the nanopillars is not possible, due to the inherent limitations of the applied measurement technology.

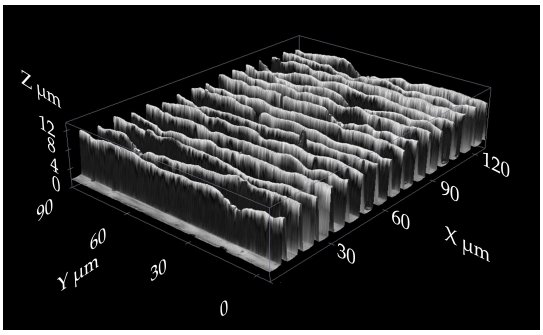

(a)

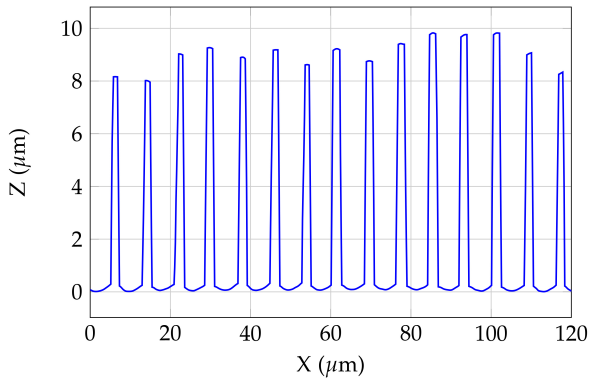

(b)

Figure 6.7: Measurements of the replicated microchannels: (a) topography and (b) height profile.

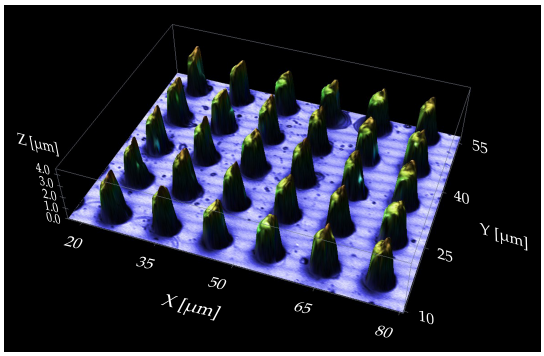

(a)

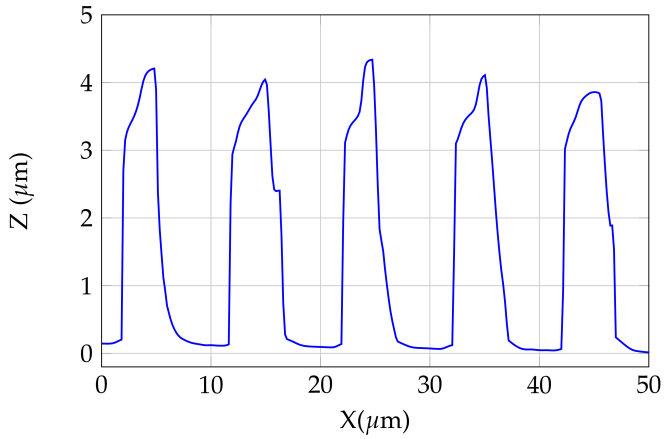

(b)

Figure 6.8: Measurements of the replicated micropillars (conf. 4-10): (a) topography and (b) height profile.

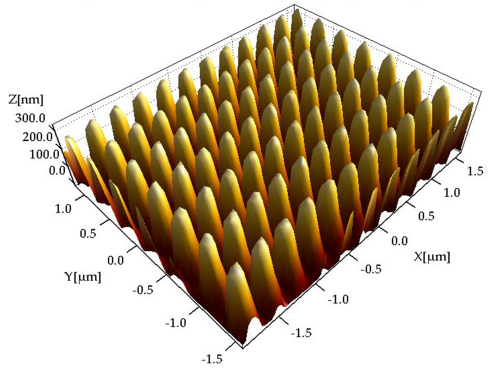

(a)

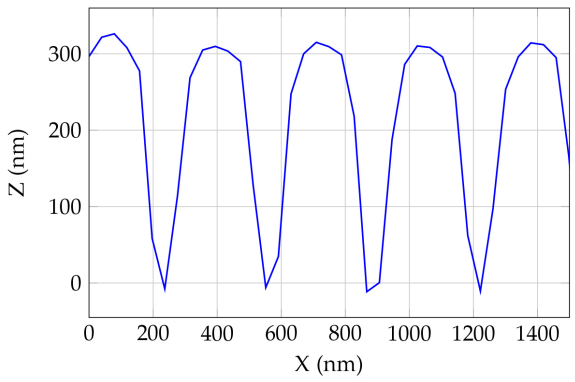

(b)

Figure 6.9: Measurements of the replicated nanopillars (conf. 200-300): (a) topography and (b) height profile.

Part III

EXPERIMENTAL ANALYSIS

7

APPROACH TO THE EXPERIMENTAL ANALYSIS

An *experiment* can be defined as a test or series of tests in which purposeful changes are made to the input variables of a process or system so that we may observe and identify the reasons for changes that may be observed in the output response. In any experiment, the results and conclusions that can be drawn depend to a large extent on the manner in which data are collected. The general approach to planning and conducting the experiments is called the *strategy of experimentation*. There are several strategies that an experimenter could use. In this work we adopted the factorial experiments approach.

Experimental design methods have found broad application in many disciplines. In fact, we may view experimentation as part of the scientific process and as one of the ways we learn about how systems or processes work. Experimental design is a critically important tool in the engineering world for improving the performance of a manufacturing process. It also has extensive application in the development of new processes.

The use of experimental design in these areas can result in products that are easier to manufacture, products that have enhanced field performance and reliability, lower product cost, and shorter product design and development time. The objectives of a factorial experiment are usually the following:

CHARACTERIZING A PROCESS: determine which factors (both controllable and uncontrollable) affect the response. To accomplish this, the experimenter can design an experiment that will enable him to estimate the magnitude and direction of the factor effects. How much does the response variable change when each factor is changed, and does changing the factors together produce different results than are obtained from individual factor adjustments, that is do the factors interact? This is usually referred to as the *screening phase*. The information from this screening experiment will be used to identify the critical process factors and to determine the direction of adjustment for these factors.

OPTIMIZING A PROCESS: after the characterization of the process, the next step is to optimize it, that is, to determine the region in the significant factors that leads to the best possible response. For example, if the response is yield, we would look for a region of maximum yield, whereas if the response is variability in a critical product dimension, we would seek a region of minimum variability. Once we have found the region of the

optimum, a second experiment would typically be performed. The objective of this second experiment is to develop an empirical model of the process and to obtain a more precise estimate of the optimum operating conditions for time and temperature. This approach to process optimization is called *response surface methodology*.

7.1 PRINCIPLES OF THE DOE

The three basic principles of experimental design are *replication*, *randomization* and *blocking*, cf. [76]. By replication we mean a repetition of the basic experiment. Replication reflects sources of variability both between runs and (potentially) within runs and it has two important properties. First, it allows the experimenter to obtain an estimate of the experimental error, second, if the sample mean $\overline{y}$ is used to estimate the effect of a factor in the experiment, replication permits the experimenter to obtain a more precise estimate of this effect. Randomization is the cornerstone underlying the use of statistical methods in experimental design. By randomization we mean that both the allocation of the experimental material and the order in which the individual runs or trials of the experiment are to be performed are randomly determined. Statistical methods require that the observations (or errors) be independently distributed random variables. Randomization usually makes this assumption valid. Blocking is a design technique used to improve the precision with which comparisons among the factors of interest are made. Often blocking is used to reduce or eliminate the variability transmitted from *nuisance factors*; that is, factors that may influence the experimental response but in which we are not directly interested. Generally, a block is a set of relatively homogeneous experimental conditions.

7.2 THE CHOICE OF THE LEVELS

Once the experimenter has selected the design factors, the ranges over which these factors will be varied, and the specific levels at which runs will be made, must be chosen. A region of interest for each variable (that is, the range over which each factor will be varied) and on how many levels of each variable to use, should be selected. Process knowledge is required to do this. This is usually a combination of practical experience and theoretical understanding. It is important to investigate all factors that may be of importance and to not be overly influenced by past experience, particularly when we are in the early stages of experimentation or when the process is not very mature.

When the objective of the experiment is factor screening or process characterization, it is usually best to keep the number of factor levels low. Generally, two levels work very well in factor screening studies.

Choosing the region of interest is also important. In factor screening, the region of interest should be relatively large–that is, the range over which the factors are varied should be broad. As we learn more about which variables are important and which levels produce the best results, the region of interest will usually become narrower.

7.3 SELECTION OF THE RESPONSE VARIABLE

In selecting the response variable, the experimenter should be certain that this variable really provides useful information about the process under study. Most often, the average or standard deviation (or both) of the measured characteristic will be the response variable. Multiple responses are not unusual. Gauge capability (or measurement error) is also an important factor. If gauge capability is inadequate, only relatively large factor effects will be detected by the experiment or perhaps additional replication will be required. In some situations where gauge capability is poor, the experimenter may decide to measure each experimental unit several times and use the average of the repeated measurements as the observed response. It is usually critically important to identify issues related to defining the responses of interest and how they are to be measured before conducting the experiment.

The primary advantage of statistical methods is that they add objectivity to the decision-making process. Statistical techniques coupled with good engineering or process knowledge and common sense will usually lead to sound conclusions. Statistical methods should be used to analyze the data so that results and conclusions are objective rather than judgmental in nature. If the experiment has been designed correctly and if it has been performed according to the design, the statistical methods required are not elaborate.

In statistics, a result is considered significant not because it is important or meaningful, but because it has been predicted as unlikely to have occurred by chance alone. The statistical analysis of the data is applied in the design of the experiments by the means of the *Analysis of Variance - Anova*. This is a collection of statistical models used to analyze the differences between group means and their associated procedures, which in the DoE means the "variation" among and between treatments.

The present-day concept of statistical significance originated from Ronald Fisher when he developed *statistical hypothesis testing*. These tests are used to determine which outcomes of a study would lead to a rejection of the *null hypothesis* based on a pre-specified low probability threshold called *p-values*, which can help an investigator to decide if a result contains sufficient information to cast doubt on the null hypothesis. P-values are often coupled to a significance or alpha α level, which is also set ahead of time, usually at 0.05 (5%). Thus,

if a p-value is found to be less than 0.05, then the result would be considered statistically significant and the null hypothesis would be rejected.

There are many excellent software packages designed to assist in data analysis (cf. Minitab 16.2.3), and many of the programs used to select the design provide a seamless, direct interface to the statistical analysis. Often we find that simple graphical methods play an important role in data analysis and interpretation. Because many of the questions that the experimenter wants to answer can be cast into an hypothesis-testing framework, hypothesis testing and confidence interval estimation procedures are very useful in analyzing data from a designed experiment.

8

CELLDIASP PROJECT. THE EXPERIMENTAL INVESTIGATION

For the CellDiaSP project, a first preliminary analysis was conducted with the aim to investigate the influence of injected material and its interaction with process parameters on the replication quality of high aspect ratio micro channels. A low-viscosity polystyrene and a cyclic olefin copolymer were selected and their rheological and wetting properties were evaluated in order to select which material has better properties for the replication of high AR micro features. Subsequently, an optimization study was carried out analyzing the main process parameters that could affect the replication quality in μIM process.

8.1 PRELIMINARY ANALYSIS. MATERIAL SELECTION

The interaction between the used polymer and the quality of the moulded part is a challenging task in micro injection moulding process. For this reason, the selection of a proper thermoplastic material must be done with particular attention. Regarding the CellDiaSP project specifications, it was required a material with certain characteristics (cfr. chapter refcap:matchar) according to which a commercial polystyrene (*Total, PS Crystal* 1540) and a cyclic olefin copolymer (*Topas, COC* 5013 *L*-10) have been selected and characterized.

This preliminary analysis aim to investigate the influence of injected material and its interaction with process parameters on the replication quality of high aspect ratio micro features.

A design of experiments (DoE) approach was applied to the design and analysis of the experimental campaign. A two-level, three-factor, full factorial plan was designed. This is characterized by a full resolution, consequently the interactions are not aliased but they can be evaluated.

For each run, the parts produced in the first 10 cycles were discarded in order to stabilize the process, then the following part was collected for a successive metrological characterization. Each treatment of the designed experiments was repeated three times in a completely randomized order for a total of 24 produced samples, with the aim of minimizing the interference of external variability sources. The mould was used during all experiments without dismounting and the material was taken from a single batch.

Level	T_m/T_g	E_a	Material
(-1)	0.95	off	PS
$(+1)$	1.10	on	COC

Table 8.1: Factors and levels for the design of the factorial plan of the CellDiaSP project preliminary analysis.

8.1.1 *Analyzed Factors*

The factors investigated were the ratio between the mould temperature normalized on the glass transition temperature of the injected material (T_m/T_g), the presence of cavity air evacuation (E_a) and the injected material, as their influence on replication quality has been repeatedly reported in the literature. The choices of the upper and lower levels for the factors derived from a literature review, recommendations of the material supplier and technological limits of the available experimental setup. The range values for each factor are summarized in Table 8.1.

The parameters that were not considered as design factors were fixed at the highest possible value as allowed by the experimental setup. In particular, the injection speed was fixed at 750mm/s and the holding pressure at 400bar for 6sec. The melt temperatures for the materials were set at the maximum values in the range recommended by their suppliers (240 °C for PS, 300 °C for COC). The response variable for this analysis was chosen to be the replicated height of micro features (cfr. section6.3).

8.1.2 *Analysis of the Factorial Plan*

The analysis of variance (ANOVA) results (Table 8.2) indicate, as expected, that among the main factors, the normalized mould temperature markedly affects the replication degree, as reported in the literature.

Factors	SS	MS	F	P
T_m/T_g	3652155	3652155	178.97	0.000
Mat.	219173	219173	10.74	0.004
E_a	56982	56982	2.79	0.113
$T_m/T_g \cdot$ Mat.	945991	945991	46.36	0.000
Mat. $\cdot E_a$	20673	20673	1.01	0.052
$T_m/T_g \cdot E_a$	82958	82958	4.07	0.060
Error	346902	20406		

Table 8.2: ANOVA results for the factorial plan of the CellDiaSP preliminary analysis.

Figure 8.1: Influence of the main factors on the replicated height of micro-channels.

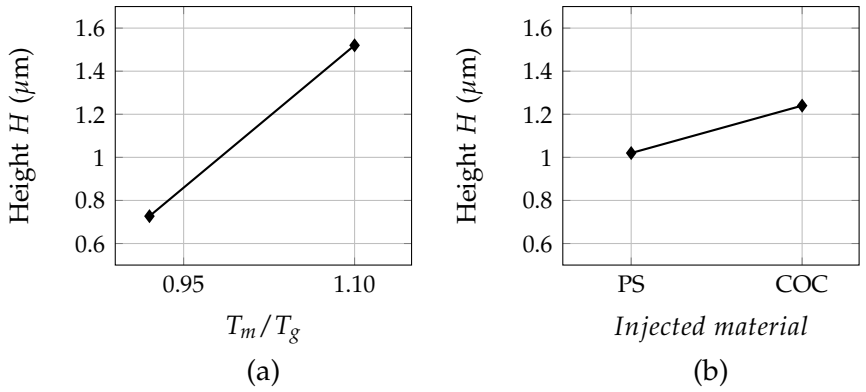

By varying T_m/T_g from 0.95 to 1.10, the average height increased from 0.73 to 1.51μm (Figure 8.1a). Moreover, the lack of fit test for the temperature ratio highlighted that the average height increases more than linearly when varying this parameter.

mould temperature is important due to its influence on the thermal gradient between the cavity surface and the injected polymer at temperatures close to T_g. The viscosity of the polymer melt is highly dependent on temperature, therefore it is crucial to keep the material flowing at high temperature during the filling phase. This was achieved by maintaining the highest possible value of the barrel temperature according to the material data sheets and by implementing a RHCM, allowing the polymer to fill in micro features from the very beginning of the process.

Using COC instead of PS, the average height of the micro features increases from 1.02 to 1.25 μm (Figure 8.1b). The different effect of the materials is due to their rheological properties. Indeed, PS 1540 is more viscous than COC 5013L-10 at melt temperature which is at least two times higher than T_g for both the materials. The effect of the low viscosity is markedly higher close to the gate, where the injection pressure is higher. The main effect of air evacuation is not significant (p-value of 0.113) however E_a has significant interaction with others factors.

The influence of first order interactions is important for a complete understanding of the process. The interactions are:

1. *Interaction between T_m/T_g and Material*:Figure 8.2a shows that the two materials yield different responses to variation of T_m/T_g. In particular, COC is more sensitive to mould temperature varying from below to above T_g. In fact, the height of micro features increases by +188.4% when changing T_m/T_g from 0.95 to 1.10. With PS the percentage increase for the same variation of T_m/T_g is +46% as its viscosity is less sensitive to temperature variation around T_g.

Figure 8.2: Influence of the first order interactions on the replicated height of micro-channels.

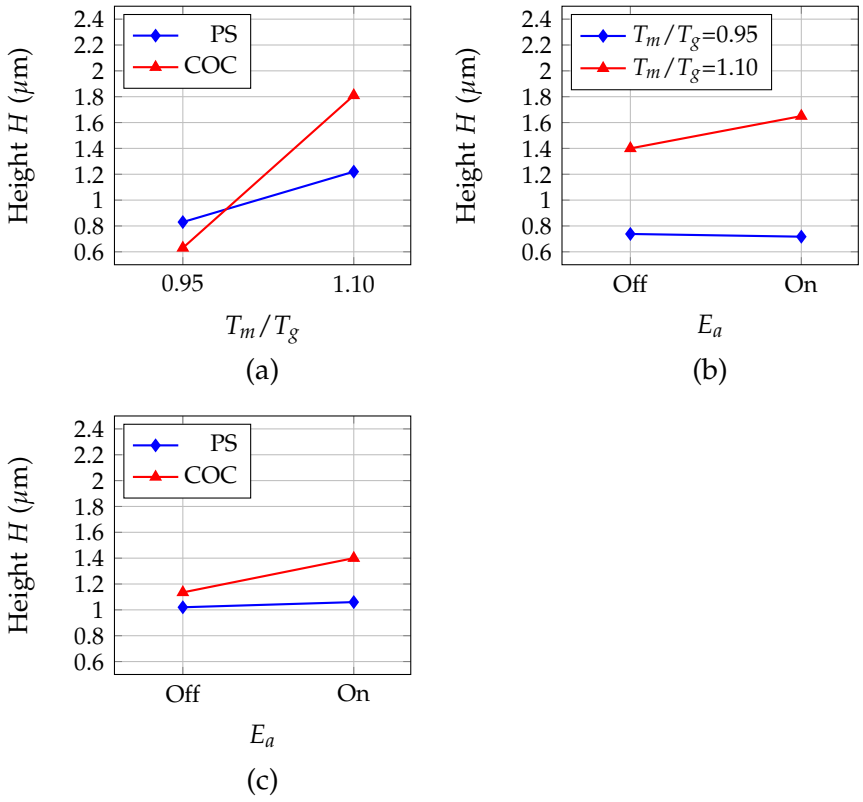

2. *Interaction between T_m/T_g and E_a*: Figure 8.2b reports the different results of the application of vacuum venting when moulding with different T_m/T_g. With a T_m lower than T_g the cavity air evacuation has no significant effect. In fact, due to its higher viscosity the polymer melt is not sensitive to the application of cavity air evacuation. Conversely for $T_m/T_g > 1$ the application of cavity air evacuation leads to better replication results. This behavior is related to the reduction of viscosity that accompanies an increase of the mould temperature: a combination of a lower viscosity and vacuum venting can facilitate the filling of the micro cavities.

3. *Interaction between E_a and Material*: Figure 8.2c indicates that COC has a greater sensitivity to cavity air evacuation than PS. In particular, when applying the evacuation of air from the cavity the replication increases by +13.6% for COC, while for PS the variation is not significant. The different responses that the two materials yield to the application of vacuum venting are due to different viscosity and wettability properties.

The results of the μIM experiments and of the characterization of material properties indicate an interesting relation between materials properties and process parameters.

The better replication obtained moulding COC with RHCM and vacuum venting is related to

- the higher sensitivity of COC viscosity to temperature values around T_g;
- its higher wettability behavior on nickel moulds, correlated to lower values of the contact angle.

In general, the combination of higher temperature dependence of viscosity and higher wetting properties in the COC facilitate the replication and allow vacuum venting to significantly enhance the filling ratio.

Conversely, the interfacial effects between the nickel mould surface and the polymer are less significant with PS than COC. PS has a simpler molecular structure than COC, thus it yields a higher surface tension and consequently a lower wettability.

Moreover, the interaction between T_m/T_g and E_a , emphasizes that different materials have different sensitivity and thus yield different responses to the application of vacuum venting. PS is not sensitive to the application of cavity air evacuation due to its higher viscosity and lower wettability.

8.1.3 *Concluding Remarks*

From this preliminary analysis, some interesting considerations can be done. Firstly, the results of the experimental tests not only showed that among design factors, mould temperature is confirmed to be the most important parameter influencing the replication accuracy, but they also indicated that RHCM effect can be further enhanced by using a polymer characterized by a higher temperature dependence of viscosity around T_g. Moreover, at high mould temperature air evacuation can be effectively exploited to maximize the average height of the micro features, especially for a combination of polymer and mould material characterized by high interfacial effects. A combination of low viscosity and high wetting properties is an ideal condition to improve the replication of micro features. As emerged from the replication of nickel micro features on COC parts, the combination of higher temperature dependence of viscosity and higher wetting properties facilitate the replication and allow vacuum venting to significantly enhance the filling ratio. For this reason the COC (*Topas, COC* 5013 *L*-10) was selected for the subsequent optimization analysis.

8.2 OPTIMIZATION ANALYSIS FOR THE REPLICATION OF HIGH AR MICRO FEATURES.

Considering the results obtained in the previous analysis, a new experimental investigation was designed, in order to further investigate this case of study.

According to project's specifications, the objective that have to be pursued are:

1. an high degree of replication and so an high average height of the channels;

2. a reduced standard deviation and consequently an uniform distribution of the height of micro-channels along the chip;

These objectives can be attained by following the indications on process parameters suggested by the results of the preliminary studies, i.e. increasing mould temperature and using a material with low viscosity and high wetting properties. Despite this, other process parameters were considered in the analysis, as suggested by the literature (cfr. section 3.2).

The investigation was designed according to a two-levels, four-factors, 1/2 fractional plan. A full-factorial design would have required 16 experiments if all parameters combinations are considered. To reduce this number, a fractional design was applied, scheduling 8 treatments that were carried out in a randomized sequence. This fractional experimental design has of resolution *IV* and provided sufficient information about both single-factor effect and two-factor interaction effects that are not confounded each other. This allowed for a relatively reduced number of experiments to be undertaken without compromising the accuracy of results. Also in this case, for each run, the parts produced in the first 10 cycles were discarded in order to stabilize the process, then the following part was collected for a successive metrological characterization. Each treatment of the designed experiments was repeated three times in a completely randomized order for a total of 24 produced samples, with the aim to minimize interference from external variability sources.

8.2.1 *Analyzed Factors*

The parameters considered for the experimental investigation are:

- Ratio between mould temperature and glass transition temperature T_m/T_g;

- Injection Speed V_{inj};

- Holding Pressure P_{hold};

Factor	Selection Criteria	
	Lower Level	Higher Level
T_{mould}	The minimum was selected as the temperature recommended by the material supplier.	The high level was selected above the T_g of the material, and below the technological limit.
P_{hold}	The minimum value was obtained from the literature [77].	The higher value was selected not to cause the material to flash.
V_{inj}	This value was selected based on experimentation.	This value was selected according to machine maximum limitation.

Table 8.3: Criteria for selecting the upper and the lower levels of the experimental plan.

- Air Cavity Evacuation E_a.

These parameters were considered to be the ones affecting the capabilities of the process in optimizing replication quality, as resulting from literature and the preliminary study.

The criteria used for selecting the upper and lower values were the recommendation of the material supplier, the literature and the experimentation. The criteria adopted for the selection of the process parameters are summarized in Table 8.3. The range values for each factor are summarized in Table 8.4.

During the realization of this experiments, the following parameters were fixed at a level suggested from technological consideration on the specific project and literature:

- *Holding Pressure Time*: 15 s;
- *Barrel Temperature (Tollerance* $\pm$ 10 °C*)*: 300-290-280-270 °C;
- *Metering Size - Injection Plunger Stroke*: 8.7 mm;
- *Pre Drying*: 100 °C/ 6 hour;
- *Vacuum-Valve*:
  - *On, with Time Monitoring*;
  - *After Build Up Clamping Force*;
  - *Time Evacuate Before Injection*: 15 s;
  - *Time Evacuate After Start Injection*: 7 s;

Level	T_m/T_g (°C)	V_{inj} (mm/s)	P_h (bar)	E_a
(-1)	0.95	450	250	off
(+1)	1.10	750	400	on

Table 8.4: Process parameter settings for the optimization analysis.

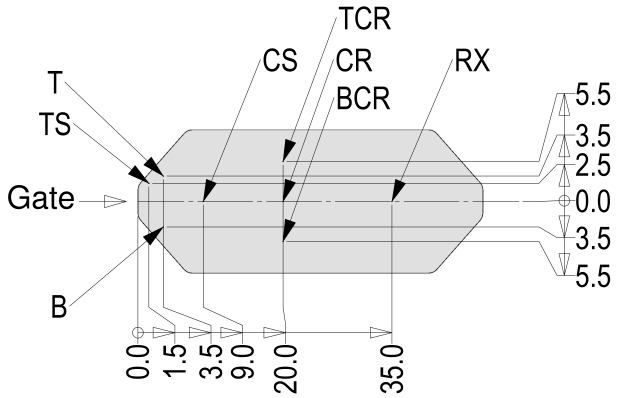

Figure 8.3: Measured areas for the characterization of the height of microchannels. All quotes are expressed in (mm).

– *In Cavity Pressure After Air Evacuation*: $\sim 3 \div 5$ millibar.

The response variable for this analysis was chosen to be the replicated height of micro-channels. As the project required a high degree of replication, as well as an uniform distribution of the height of micro-channels along the chip, the measurements were performed in eight different areas distributed on the surface of the moulded part as shown in Figure 8.3.

8.2.2 *Experimental Data*

The measurement from this set of experiment are reported in Table 8.6, where only the calculated average value and the standard deviation are given. Table 8.5 reports the codification used to uniquely identify each replication. For instance the code *BDFS*-3 stands for the third (3) replication obtained at higher value of mould temperature (B), 400 bar of holding pressure (D), 750 mm/s of injection speed (F) and with the evacuation of air from the cavity on (S).

Parameter	Code	Value
T_m/T_g	A	0.95
	B	1.10
P_{hold} [bar]	C	250
	D	400
V_{inj} [mm/s]	E	450
	F	750
E_a	S	on
	N	off

Table 8.5: Codification of the treatments - CellDiaSP project.

Code	Replication	Average Value (μm)	Standard deviation (μm)
BDFS	1	2.05	0.37
	2	1.52	0.19
	3	2.29	0.38
BCES	1	1.79	0.45
	2	1.87	0.33
	3	2.11	0.47
ADES	1	0.66	0.13
	2	0.61	0.16
	3	0.65	0.13
ACFS	1	0.61	0.13
	2	0.65	0.10
	3	0.61	0.10
BDEN	1	1.73	0.30
	2	1.61	0.33
	3	1.67	0.30
BCFN	1	1.21	0.19
	2	1.59	0.21
	3	1.75	0.22
ADFN	1	0.61	0.10
	2	0.59	0.10
	3	0.65	0.10
ACEN	1	0.23	0.10
	2	0.45	0.10
	3	0.38	0.10

Table 8.6: Average value and standard deviation for the replication of the designed experiment - CellDiaSP project.

8.2.3 *Analysis of the Factorial Plan*

The 1/2 fraction factorial design has been analyzed in order to comprehend which factors and interactions are significant for the replication of micro-channels. A *General Linear Model* was used to perform an univariate analysis of variance for the design factorial plan. The terms included in the model are all the main factors selected.

The analysis of variance (*ANOVA*) results indicate that the mould temperature markedly affects the replication degree, as reported in literature. By varying the ratio T_m/T_g from 0.95 to 1.10, the average height increased from 0.56 to 1.78 μm (Figure 8.4a).

Moreover, the lack of fit tests for this factor highlighted that the replication degree increases more than linearly with higher values of T_m/T_g. The effect of both injection speed and holding pressure is far less important as shown in Figure 8.4b and Figure 8.4c. The main effect of the air evacuation it to increment the average height of the micro features by 24% (Figure 8.4d). As discussed in section 8.1, a combination between a material with high wetting properties and the cavity air evacuation lead to a better replication degree.

The experimentation has been conducted according to a two-levels, four-factors, 1/2 fractional plan. An important property of a fractional design is its resolution or ability to separate main effects and low-order interactions from one another.

The considered plan is characterized by resolution IV. In these designs the main effects are not confused with each other, but first order interactions may be aliased with one another. Consequently, this design reduced the number of treatments but can not include 2-factor interactions in the general linear model and so in the analysis of variance.

The analysis of variance was not able to evaluate the statistical significance of first order interactions. Their influence on the response variable has been investigated only graphically, by the means of the interaction plots. The concept of interaction is graphically represented in the *Interaction Plot*. Where the levels of one variable are reported on the *X* axis, the means of each level of the other variable

Factors	SS	MS	F	P
T_m/T_g	86337552	86337552	245.61	0.000
V_{inj}	6404	6404	0.18	0.674
P_h	66028	66028	1.88	0.187
E_a	353876	353876	10.06	0.005
Error	668184	668184		

Table 8.7: Anova table for the designed experiment.

Figure 8.4: Influence of the main factors on the average height of the replicated micro-channels for the CellDiaSP optimization analysis.

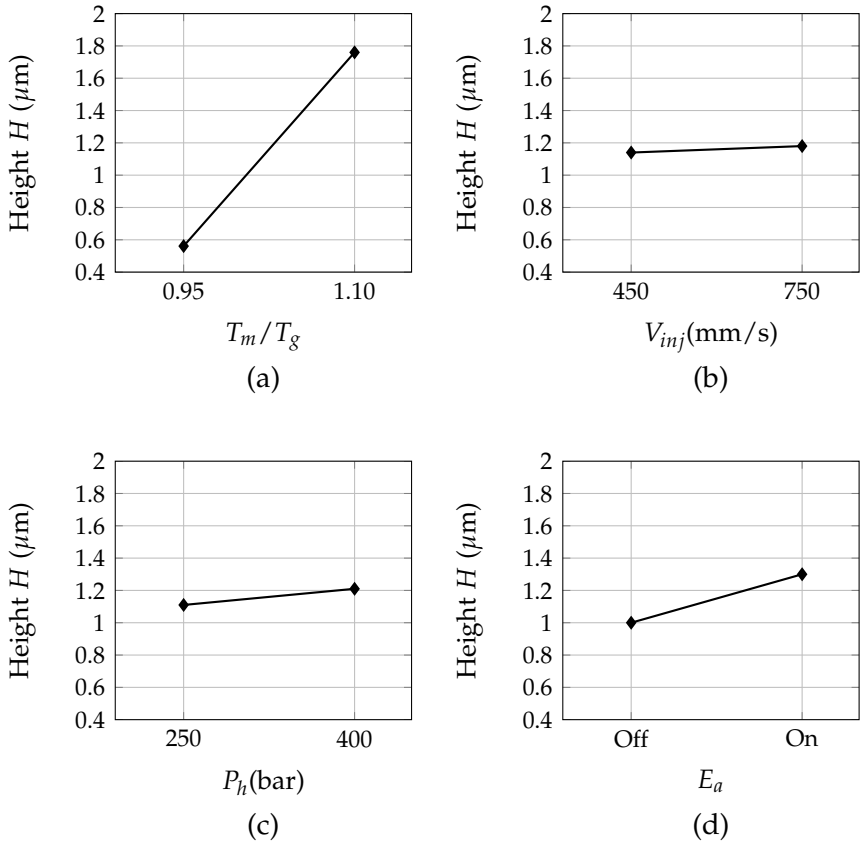

Figure 8.5: Influence of the interactions between cavity air avacuation and other factors on the average height of the replicated micro-channels for the CellDiaSP optimization analysis.

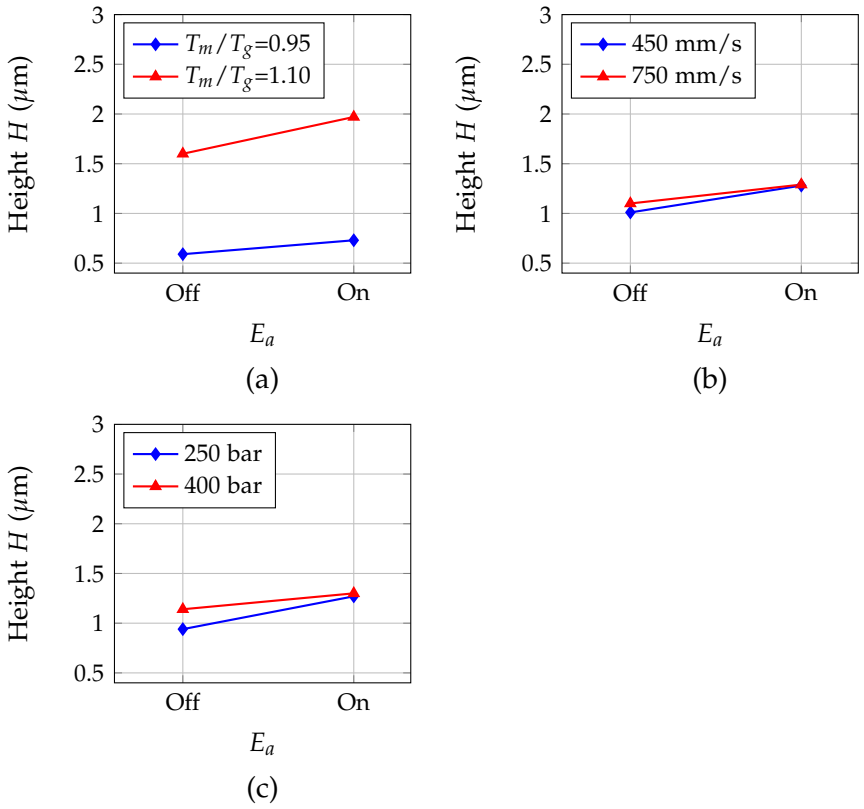

are introduced by a separate line. The Y axis is the dependent variable, the response variable.

For the designed experiment the interactions that resulted significant are the following:

- Vacuum·T_m/T_g;
- Vacuum·V_{inj};
- Vacuum·P_h;
- P_{hold}·V_{inj};

Figure 8.5 shows the significant interactions between vacuum venting and other factors. In particular, its interactions with the holding pressure is marked, while the interactions with the mould temperature and the injection speed are evident but of little importance.

The significant interaction between V_{inj} and P_h , shown in Figure 8.6 shows that the effect of the holding pressure increases for high values of V_{inj}. In fact, a rapid filling of the substrate both increase the cavity pressure, that drives the melt into micro-cavities, and allows a quick filling of the main cavity, counteracting the hesitation effect.

Figure 8.6: Influence of the interactions between the holding pressure and the injection speed on the average height of the replicated microchannels for the CellDiaSP optimization analysis.

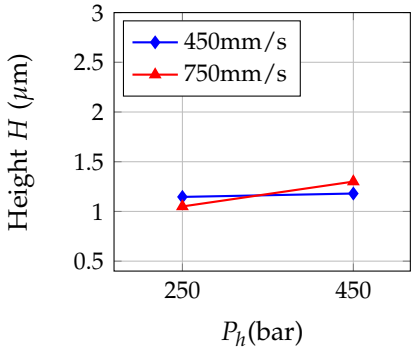

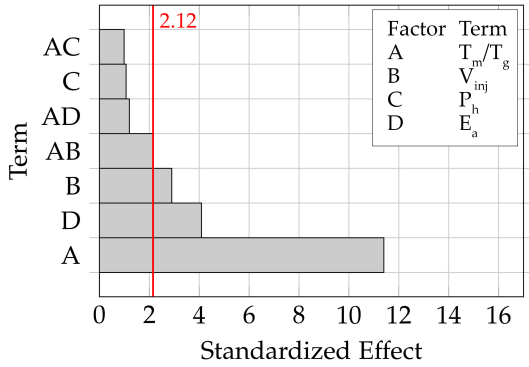

Figure 8.7: Pareto chart of the standardized effect. The response is the standard deviation of the replicated micropillars. (Alpha=0.05).

Moreover, the interaction between the holding pressure and the injection speed points out that with an high injection speed the effect of the holding pressure is greater. In fact, a rapid filling of the substrate makes the polymer melt more fluid at the beginning of the holding stage, due to a shorter cooling time. Conversely with a low injection speed, an increase of the holding pressure is insignificant, due to the heat loss of the polymer melt during the slower filling phase.

The replication quality of a micro structured surface has to be also evaluated in terms of uniformity of the replication. To maximize the height uniformity of the micro features, the standard deviation (σ_H) of the 8 height values was calculated for each combination of the optimization experimental plan. Figure 8.7 reports the Pareto charts for the standard deviation of the replicated microchannels.

These graphs allow the comparison of the relative magnitude of the effects and the evaluation of their statistical significance. The effect of the ratio between mould temperature and glass transition temperature, is the most influent parameter. At high value of T_m/T_g, the standard deviation of the replicated micro channels increased from 0.12 to 0.31μm. Moulding at high value of injection speed, reduced

Figure 8.8: Influence of the main factors on the standard deviation of the average height of the replicated micro-channels for the CellDiaSP optimization analysis.

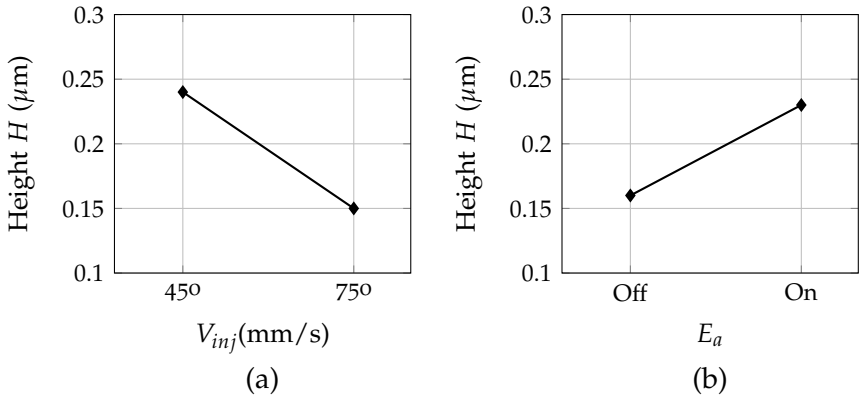

Code	Response variable	Fit	SE Fit	Residual	St Resid
BCFN1	1213.42	1603.29	85.60	−389.86	−2.34 R
BDFS2	1517.63	1951.04	85.61	−433.42	−2.60 R
BDFS3	2288.35	1951.05	85.62	337.31	2.02 R

Table 8.8: Unusual observation in the DoE - ErytroChip project.

σ_H by 32%. Moreover, Air evacuation has a detrimental effect on the channels height distributions, increasing σ_H by 35%.

8.2.3.1 *Residue Analysis*

The residuals are here analyzed to determine the adequacy of the model. Figure 8.9 reports the residual plots for the variable response. The residue analysis did not reveal particular deviations from normality for all the replications. However, some unusual observation were reported (cf. Table 8.8), where R denotes an observation with a large standardized residual. All these observation refers to replication of treatments at high mould temperature. This may indicate some mistake in the experimental procedure that has been followed. However, due to the screening view followed in this analysis, the results are considered acceptable.

8.2.4 *Concluding remarks*

From the analysis of the replicated microchannles, emerged that the distribution of the micro features height values along the cavity is extremely uneven as shown in Figure 8.10. The replication is much better for micro features closer to the gate (Figure 8.10a), as in this region the holding pressure is higher, but it quickly worsens within

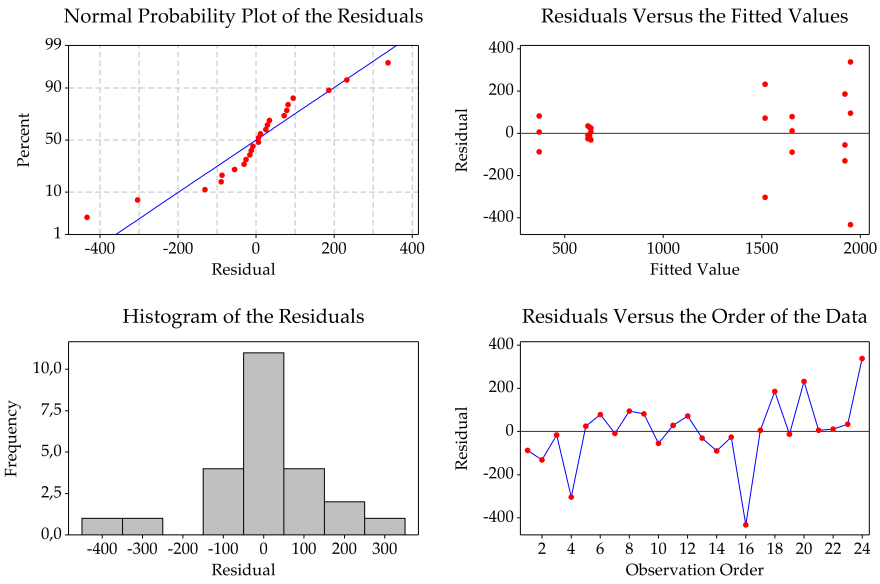

Figure 8.9: Residual plots for the DoE - CellDiaSP project.

the first 10 mm (Figure 8.10b). This is probably due to the reduced thickness of the substrate, which rapidly solidifies attenuating the effect of the holding pressure. The replication profile is mainly a result of pressure distribution along the cavity. In fact, it monotonously decays as the cavity pressure distribution at the end of filling, which was calculated using a calibrated numerical simulation (Figure 10.1). The non-linearity of the replication profile,which is more evident in the gate region, is due to the combined effect of holding pressure and mould temperature.

Comparing the results obtained for the average height and the standard distribution, it can be noticed that the optimum process parameters are a good compromise solution between the factors that maximize h and minimize σ_H. This solution can be determined by aggregating the max(H) and min(σ_H) goals into the single objective function of max(H-σ_H), which has an optimal solution for V_{inj} of 750 mm/s (Figure 8.8a), P_h of 377 bar and the presence of cavity air evacuation (autoreffig:maineffestdb). This result clearly indicates that to better replicate large surfaces with high aspect ratio micro features the μIM process has to be performed at a low injection speed and a high holding pressure. With this combination of process parameters mould micro features are filled in only during the holding phase. However, to contrast the hesitation effect at low values of injection speed, mould temperature needs to be further increased.

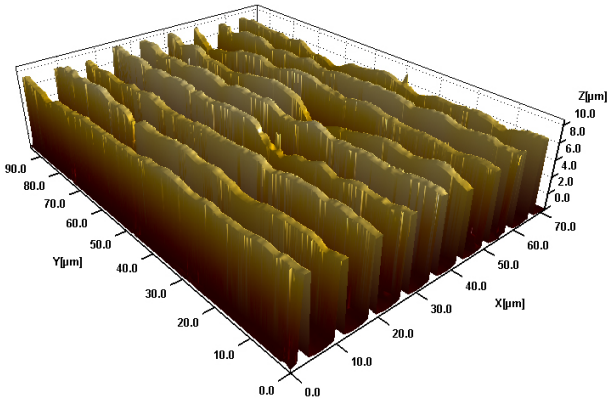

(a)

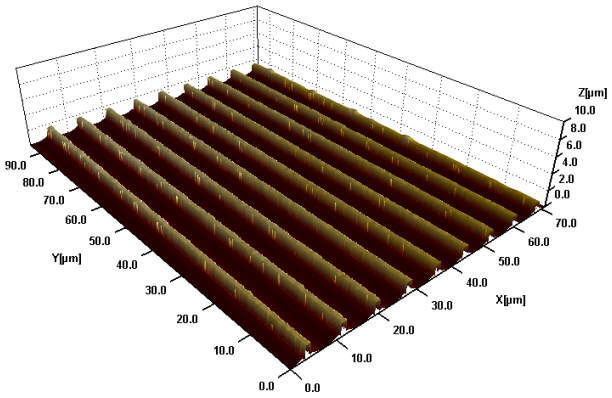

(b)

Figure 8.10: Replicated micro features located at (a) 1.5 mm and (b) 35 mm from the gate.

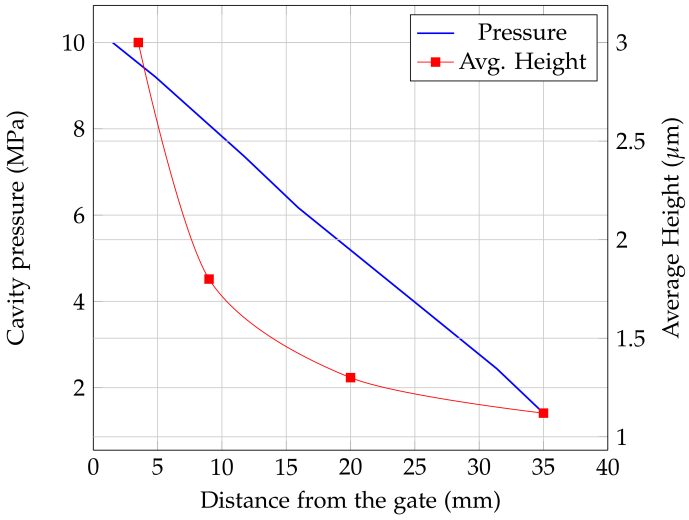

Figure 8.11: Comparison between micro features height and pressure distribution along the cavity.

9

NANOBONES PROJECT. THE EXPERIMENTAL INVESTIGATION

The NanoBones project experimental investigation is composed by two different analysis. The first one aim to investigate the influence of cavity thickness on replication quality, analyzing the replication of micro pillars distributed over a large surface.

In the second analysis, nano-structured surfaces were manufactured by injection moulding to obtain osteoinductive materials for bone replacement applications. A polylactic acid was selected as injected material, due to its biocompatibility and biodegradability. A design of experiments approach was applied to the optimization of the process in order to maximize the replicated height of the nano pillars. The effects of mould temperature, injection speed, holding pressure and cavity air evacuation were investigated.

9.1 PRELIMINARY ANALYSIS. EFFECT OF THE THICKNESS OF THE MAIN FLOW REGION.

As discussed in chapter 3, high values of process parameters, such as mould temperature and injection speed can improve the flow in the cavity. The geometry of the moulded part can influence the melt filling by directly affecting the pressure profile in the macro cavity. In particular, the thickness of the substrate, which is much larger compared to the micro features, affects the replication quality by changing the evolution of the cavity pressure generated during the injection phase. Moreover, substrate thickness is critical because it determines the cavity filling time for a given injection speed. The influence of cavity thickness on replication quality is not consistent among different researches reported in the literature. Thus, a careful consideration of part geometry is required to control the quality of the moulded parts.

The relation between the replicated height of micro features and the thickness of the main flow region needs to be further investigated, especially in combination with state-of-the-art micro injection moulding technologies, such as rapid heat cycle moulding (RHCM) and cavity air evacuation. In this analysis, the influence of cavity thickness on replication quality was studied analyzing the replication of micro pillars distributed over a large surface. The evacuation of air from the cavity and RHCM were used in order to enhance the degree of replication in combination with the geometry of the cavity. The results provides interesting informations about the effect of the main flow region thickness on the replicated micro features, which will be taken

into account for the optimization analysis. As described in previous sections, the moulded part is a cylindrical support having a diameter of 5.9mm and a micro-pillared surface topography. The micro pillars are characterized by a diameter of 4μm and an interspace of 10μm. Two different versions of the cavity were used, with thicknesses of 1 and 2 mm, respectively.

9.1.1 *Analyzed Factors*

The investigation was designed according to a two-level, five-factor, 1/4 fractional plan. This fractional design is of resolution III, hence providing sufficient information about the main effect of the factors. However, two-factor interactions are aliased. This plan allowed for a relatively reduced number of experiments to be carried out with an acceptable compromise in terms of results accuracy, only regarding the effects of main factors. For each run, the parts produced in the first 10 cycles were discarded in order to stabilize the process, and then the following part was collected for the metrological characterization. Each run was repeated 3 times in a completely randomized order for a total of 24 produced samples. In order to minimize interference from external variability sources, the polymer was taken from a single batch. The material used for this preliminary analysis was polystyrene (*Total PS Crystal* 1540).

The analyzed factors were:

- The mould temperature normalized on the glass transition temperature of the injected material (T_m/T_g);
- Injection Speed (V_{inj});
- Holding Pressure (P_h);
- Air Cavity Evacuation (E_a);
- Thickness of the Main Flow Region (t);

These parameters were considered to be the ones affecting the capabilities of the process in optimizing replication quality, as resulting from literature review.

The criteria used for selecting the upper and lower values were the recommendation of the material supplier, the literature and the experimentation. The criteria adopted for the selection of the mould temperature, the injection speed and the holding pressure are the same used for the CellDiaSP project, which are summarized in Table 8.3. The choice of the levels for all the investigated parameters is reported in Table 9.1.

During the realization of this experiments, the following parameters were fixed at a level suggested from technological consideration on the specific project and literature:

- *Material*: the injected material for this set of experiments was the *Polystyrene Total Crystal PS* 1540. All its properties and the rheological characterization has already been explained in detail in section 4.2;
- *Holding Pressure Time*: 6 s;
- *Barrel Temperature (Tollerance* $\pm$ 10 °C*)*: 240-230-220-200 °C;
- *Metering Size - Injection Plunger Stroke*: 4 mm;
- *Pre Drying*: 80 °C/ 1 hour;
- *Vacuum-Valve*:
  - *On, with Time Monitoring*;
  - *After Build Up Clamping Force*;
  - *Time Evacuate Before Injection*: 15 s;
  - *Time Evacuate After Start Injection*: 7 s;
  - *In Cavity Pressure After Air Evacuation*: $\sim 3 \div 5$ millibar.

The replicated height of the pillars was chosen as response variable for the statistical analysis of the experimental data. For each treatment, all replications were measured in three areas as shown in Figure 9.1. In each scanned area, the profiles of 5 micro pillars were considered, for a total of 15 micro pillars analyzed for each replication. Therefore, the value attributed to each measurement corresponds to the height of a characteristic micro pillar that is an average value of five pillars considered within the scanned area. The value assigned to each replication is the average of the measurements in the three scanned areas.

9.1.2 *Experimental Data*

The measurement from this set of experiment are reported in Table 9.3, where only the calculated average value and the standard deviation are given. Table 9.2 reports the codification used to uniquely identify each replication. For instance the code *HOIS*1-3 stands for the third (3) replication obtained at $T_m/\ T_g$ of 1.10 (H), 750 mm/s of

Level	T_m/T_g (°C)	V_{inj} (mm/s)	P_h (bar)	t (mm)	E_a
(-1)	0.95	450	250	1	Off
(+1)	1.10	750	400	2	On

Table 9.1: Process parameter settings and other factors for the preliminary analysis plan - NanoBones project.

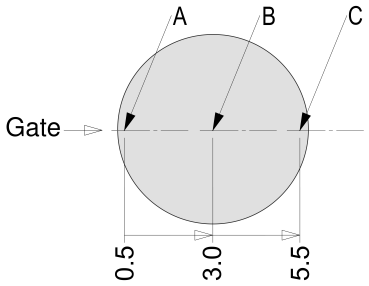

Figure 9.1: Measured areas for the characterization of the micropillars.

injection speed (O), 250 bar of holding pressure (I), with the evacuation of air from the cavity on (S) and a thickness of the main flow region of 1 mm (1).

Parameter	Code	Value
T_m/ T_g	G	0.95
	H	1.10
P_h [bar]	I	250
	L	500
V_{inj} [mm/s]	M	450
	O	750
E_a	S	on
	N	off
t [mm]	1	1
	2	2

Table 9.2: Codification for the replication of the treatments - MicroBones project.

9.1.3 *Analysis of the Factorial Plan*

The results of the *ANOVA*, reported in Table 9.4, indicate that only the thickness of the substrate and the mould temperature significantly affect the replicated height of the micro pillars. As shown in Figure 9.2a, increasing the thickness of the substrate from 1 to 2 mm yields a reduction of the average height by 19%. In fact, a higher thickness tends to limit the replication during the injection phase, due to a lower rising of cavity pressure. Indeed, the growth rate of cavity pressure is related to the pressure drop in the cavity, which is greater with a smaller thickness. Moreover, the main effect of the holding pressure resulted not significant, restraining the possibilities for the increase of the filling ratio in the packing stage. Conversely, a smaller thickness favors the increase of the replicated height of micro pillars by increasing the in-cavity pressure at the entrance of micro-cavities during the

Code	Replication	Average Value (μm)	Standard deviation (μm)
GOLN1	1	1.26	0.12
	2	1.52	0.28
	3	1.48	0.26
GOIN2	1	0.87	0.19
	2	0.99	0.31
	3	0.54	0.47
GMLS1	1	1.38	0.25
	2	1.39	0.16
	3	1.44	0.28
GMIS2	1	1.10	0.42
	2	1.13	0.43
	3	1.08	0.39
HMLN1	1	4.48	0.47
	2	4.21	0.51
	3	4.23	0.12
HMIN2	1	3.16	0.27
	2	3.21	0.20
	3	3.28	0.46
HOLS1	1	3.66	0.55
	2	3.94	0.49
	3	3.92	0.27
HOIS2	1	3.76	0.59
	2	3.60	0.42
	3	3.48	0.51

Table 9.3: Average value and standard deviation of the replications for the designed experiment - MicroBones Project.

Figure 9.2: Influence of the main factors on the replicated height of micro-pillars.

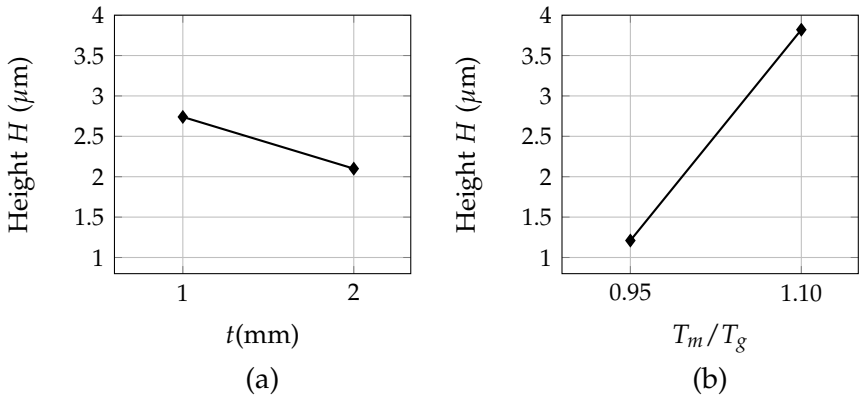

injection phase. Additionally, a thinner cavity favors a rapid filling allowing the polymer the time to fill micro features before solidification starts. In fact, the replication depends on how quickly the polymeric melt flows into the micro cavities before solidifying.

The mould temperature is also a significant parameter. As displayed in Figure 9.2b an increase of T_m/T_g from 0.95 to 1.10 lead to an increase in the average height of micro pillars from 1.2 to 3.7 μm, that is more than 300%. mould temperature is important because of its influence on the thermal gradient between the cavity surface and the injected polymer. The viscosity of the polymer melt is highly dependent on temperature, thus, it is crucial to keep the material flowing at high temperature during the filling phase. This was achieved by maintaining the highest possible value of the barrel temperature according to the materials datasheet and by adopting a rapid heat moulding cycle.

The influence of first order interactions among factors is important for a complete understanding of the effect of cavity thickness on the microinjection moulding process. Figure 9.3 shows the interactions between the thickness and the other factors implemented in the experimentation. The interaction between cavity thickness and the holding pressure is the most significant compared to others. As

Factors	SS	MS	F	P
T_m/T_g	37765903	37765903	901.84	0.000
V_{inj}	12531	12531	0.30	0.591
P_h	123710	123710	2.95	0.103
t	1631238	1631238	38.95	0.000
E_a	401	401	0.01	0.923
Error	668184	668184		

Table 9.4: Anova table for the designed experiment.

Figure 9.3: Influence of the interactions between thickness and other factors on the replicated height of micro-pillars.

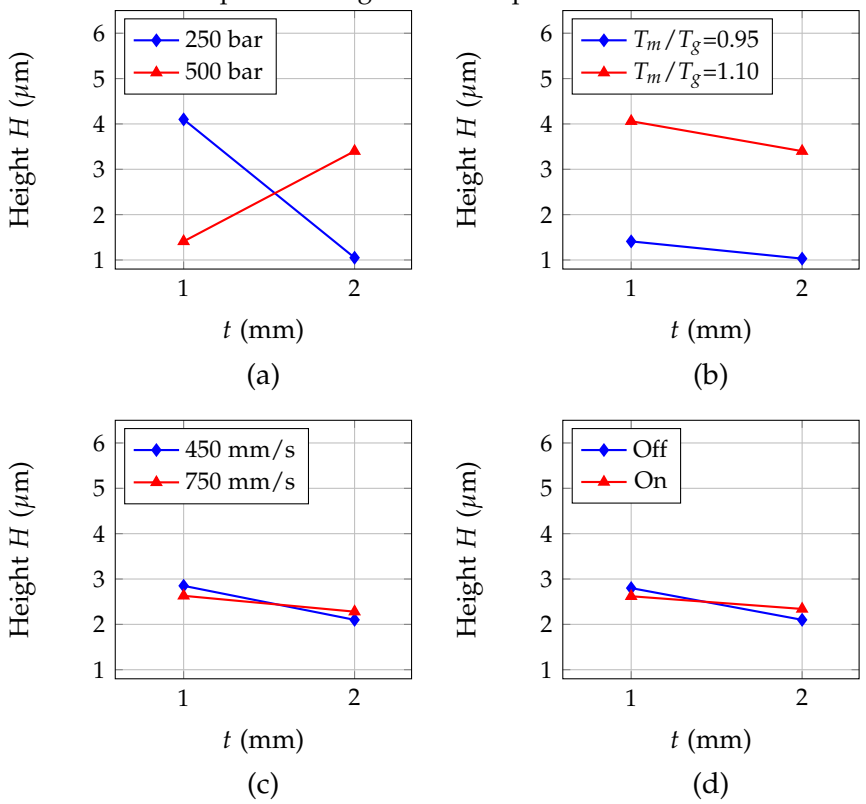

shown in Figure 9.3a, with a greater cavity thickness a higher holding pressure led to a better replication. In fact, in this case the polymer melt cools slower in the cavity thus allowing the holding pressure to have a more significant effect. In other words, a thicker cavity counteracts the effect of hesitation by slowing the cooling of the polymer melt and allowing the holding stage to be effective. Conversely, with a smaller cavity thickness the effect of the holding pressure is negligible. In fact, the cooling of the melt is faster, thus preventing the action of the holding pressure to be effective.

The interaction of cavity thickness with the mould temperature is not significant (Figure 9.3b). This result indicates that a variation of cavity thickness does not influence the positive effect of a variotherm process. In other words, a high mould temperature yields better replication results regardless of cavity design. The interactions of cavity thickness with the injection speed (Figure 9.3c) and the application of vacuum venting (Figure 9.3d) are visually slightly significant. This can be explained considering that the main effect of both the injection speed and the application of vacuum venting are not significant. However, these results suggest that with a greater thickness the replication can be improved by adopting a higher injection speed or by evacuating the air from the cavity before the injection. The

effectiveness of an higher injection speed and of vacuum venting in counteracting the negative effect of a greater cavity thickness needs to be further studied with a longer cavity, for which the main effects of these parameters is expected to be more significant. In general, the thinner the cavity is the less effective is the action of the holding pressure in pushing the polymer melt in micro cavities. This indicates that the filling of the micro features must be brought back to the injection stage and not only to the packing one, as suggested by some other researches. Cavity geometry, and in particular its thickness, controls and modifies the thermal phenomena behind the filling behavior, such as the hesitation effect and the cooling process, making the effect of the holding pressure more or less effective. Different selection of process parameters can be exploited to improve the replication but when approaching the design of an injection-moulded part with micro features the geometry of the mould cavity must be carefully considered.

9.1.3.1 *Residue Analysis*

The residues are the differences between the observed values and predicted or fitted. The residual is the part of the observation that is not explained by the fitted model. The residuals are analyzed to determine the adequacy of the model.

Figure 9.4 reports the residual plots for the variable response. The residue analysis did not reveal particular deviations from normality for all the replications. However, some unusual observation were reported (cf. Table 9.5), where R denotes an observation with a large standardized residual. All these observation refers to replication of treatments at high mould temperature. This may indicate some mistake in the experimental procedure that has been followed. However, due to the screening view followed in this analysis, the results are considered acceptable.

9.1.4 *Concluding Remarks*

The results of the preliminary analysis indicate that the thinner the cavity is the less effective is the action of the holding pressure in pushing the polymer melt in micro cavities. This indicates that the filling of the micro features must be brought back to the injection stage and

Code	Response Variable	Fit	SE Fit	Residual	St Resid
HOIS1-1	3659.40	4044.46	102.32	−385.06	−2.17 R
HMIN1-1	4481.27	4081.99	102.33	399.28	2.25 R
HOLS2-1	3755.23	3379.46	102.34	375.55	2.12 R

Table 9.5: Unusual observation in the DoE - MicroBones project.

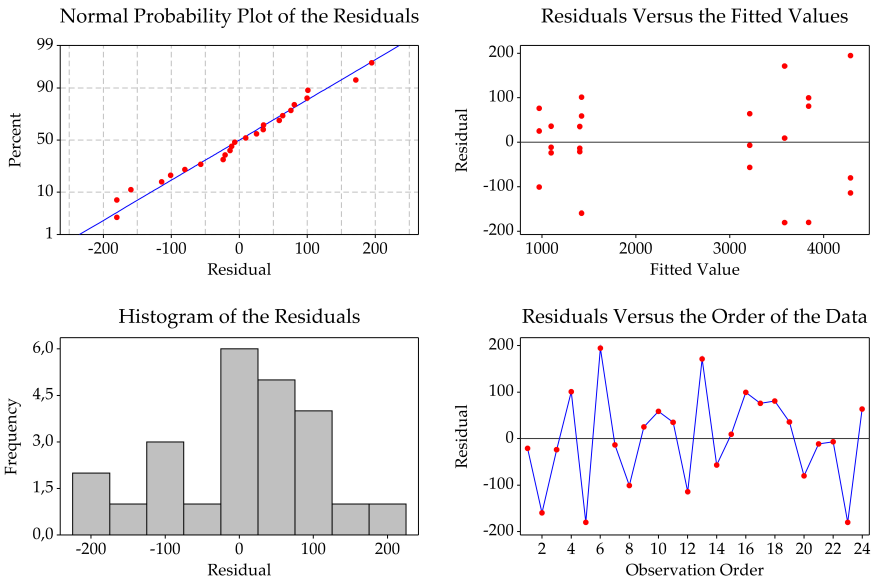

Figure 9.4: Residual Plots for the DoE - MicroBones project.

not only to the packing one, as suggested by some other researches. Cavity geometry, and in particular its thickness, controls and modifies the thermal phenomena behind the filling behavior, such as the hesitation effect and the cooling process, making the effect of the holding pressure more or less effective. Different selection of process parameters can be exploited to improve the replication but when approaching the design of an injection-moulded part with micro features the geometry of the mould cavity must be carefully considered. Considering the obtained results, the optimization analysis for the replication on nanofeatures, has been conducted using a 1mm thick mould cavity.

Moreover, the experimental results (Table 9.3) indicated a possible relation between the replicated height of the micro features and their distance from the injection location. Figure 9.5 displays the difference δ from the replicated height in the position A and the height in position B (cfr. Figure 9.1):

$$\delta = H_A - H_B \tag{9.1}$$

Positive values of δ indicates that the replication decreases moving from the injection location to the end of the cavity, while negative values of δ stand for the opposite trend of replication. Considering the influence of process parameters on δ, it can be argued that high values of the holding pressure produce a higher replication degree closer to the injection location. The pressure is higher in this region, but quickly reduces going far from the gate because of the reduced thickness of the substrate, which rapidly solidifies attenuating the effect of the holding pressure. Conversely, when moulding with a lower value of the holding pressure, the replication trend is the op-

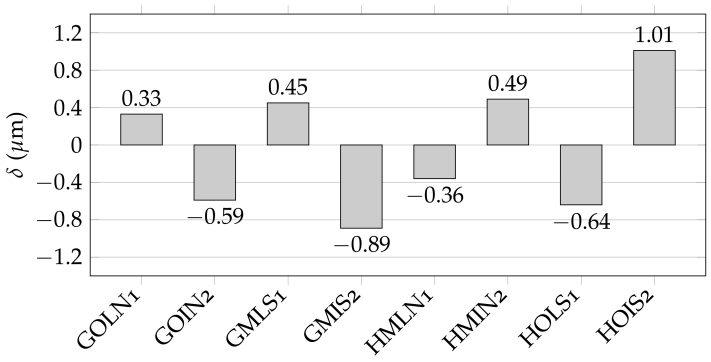

Figure 9.5: Column chart for the difference between the replicated height in position *A* and in position *B*.

posite. Indeed attributing more importance to the contribution of the filling stage to the replication.

9.2 OPTIMIZATION ANALYSIS. NANOBONES PROJECT.

9.2.1 *Analyzed Factors*

The investigation was designed according to a two-level, four-factor, 1/2 fractional plan. This fractional design is of resolution IV, hence providing sufficient information about the main effect of the factors. However, two-factor interactions are aliased. This plan allowed for a relatively reduced number of experiments to be carried out with an acceptable compromise in terms of results accuracy, only regarding the effects of main factors. For each run, the parts produced in the first 10 cycles were discarded in order to stabilize the process, and then the following part was collected for the metrological characterization. Each run was repeated 3 times in a completely randomized order for a total of 24 produced samples. In order to minimize interference from external variability sources, the polymer was taken from a single batch. The material used for the optimization analysis was PLA (*Purac, Purasorb PL*-10).

The analyzed factors were:

- The mould temperature normalized on the glass transition temperature of the injected material (T_m/T_g);
- Injection Speed (V_{inj});
- Holding Pressure (P_h);
- Air Cavity Evacuation (E_a);

These parameters were considered to be the ones affecting the capabilities of the process in optimizing replication quality, as resulting from literature review and the preliminary study.

The criteria used for selecting the upper and lower values were the recommendation of the material supplier, the literature and the experimentation. The criteria adopted for the selection of the mould temperature, the injection speed and the holding pressure are the same used for the CellDiaSP project, which are summarized in Table 8.3. The values of the levels for all the investigated parameters is reported in Table 9.6.

Being the glass transition temperature of the selected material equal to 65 °C, the high and low values of T_m/T_g correspond to a mould temperature of 61 and 72 °C respectively.

The others parameters not considering in the analysis, were fixed at the following levels:

- *Material*: *Purasorb PL 10 Poly(L-lactide)*. All its properties and the rheological characterization has already been explained in detail in section 4.6;
- *Mould insert*: the surface of the mould insert considered in this analysis was characterized by a pattern of nanoholes, having the following characteristics (cfr.section 5.4.3):
  - diameter: 200nm;
  - interspace: 300nm;
  - height: 400nm;
- *Holding Pressure Time*: 8 s;
- *Barrel Temperature (Tollerance* $\pm$ 10 *°C)*: 198-196-170-135 °C;
- *Metering Size - Injection Plunger Stroke*: 2 mm;
- *Pre Drying*: 45 °C/ 3 hour;
- *Vacuum-Valve*:
  - *On, with Time Monitoring*;
  - *After Build Up Clamping Force*;
  - *Time Evacuate Before Injection*: 15 s;
  - *Time Evacuate After Start Injection*: 7 s;
  - *In Cavity Pressure After Air Evacuation*: $\sim 3 \div 5$ millibar.

Level	T_m/T_g (°C)	V_{inj} (mm/s)	P_h (bar)	E_a
(-1)	0.95	450	250	Off
(+1)	1.10	750	400	On

Table 9.6: Process parameter settings for the optimization analysis plan in the NanoBones project.

The replicated height of the pillars was chosen as response variable for the statistical analysis of the experimental data. For each treatment, all replications were measured by means of the AFM in three areas as shown in Figure 9.1. In each scanned area, the profiles of 5 micro pillars were considered, for a total of 15 micro pillars analyzed for each replication. Therefore, the value attributed to each measurement corresponds to the height of a characteristic micro pillar that is an average value of five pillars considered within the scanned area. The value assigned to each replication is the average of the measurements in the three scanned areas.

9.2.2 *Experimental Data*

The measurement from this set of experiment are reported in Table 9.7, where only the calculated average value and the standard deviation are given.

Table 9.8 reports the codification used to uniquely identify each replication. For instance the code *CVSA*1 stands for the first (1) replication obtained at $T_m/\ T_g$ of 1.10 (C), 750 mm/s of injection speed (V), 250 bar of holding pressure (S), with the evacuation of air from the cavity on (A).

9.2.3 *Analysis of the Factorial Plan*

The *ANOVA* results for the designed plan indicate that both the mould temperature and the holding pressure have significant effect on the replication degree (p-value<0.05).

Figure 9.8a, reports the marked effect of the ratio between the mould temperature and the glass transition temperature on the average pillars height. In fact, by increasing $T_m/\ T_g$ from 0.95 to 1.10 lead to an increase in the average height of micro pillars from 66 to 342 nm. In fact, for small part volumes, like those found in micro-moulding, the melt temperature decreases at a very high rate once the polymer contacts the cavity walls. Keeping the mould temperature above the glass transition temperature of the polymer, counteract the premature material freezing and the consequent formation of the solid skin layer, allowing a better replication of the nano features. The effect of holding pressure is much less important as shown in Figure 9.8b. An increase of P_h from 250 to 400 bar yields an increment of the average height by 8%. The importance of holding pressure lies in the fact that it overcomes the tendency of the polymer melt to prematurely freeze before the injection process is complete. Premature freezing is likely to be exacerbated by the relatively high rate of heat transfer between the polymer and the mould walls for parts with nano-scaled dimensions. The effect of V_{inj} and E_a are not significant as indicate on the Pareto chart (Figure 9.7a).

Code	Replication	Average Value (nm)	Standard Deviation (nm)
FLDA	1	79.41	6.33
	2	87.03	3.30
	3	77.96	6.52
FVSA	1	46.58	5.12
	2	59.31	7.07
	3	52.47	4.55
FLSI	1	60.09	5.29
	2	46.36	4.86
	3	52.78	4.53
FVDI	1	78.02	4.35
	2	80.18	6.32
	3	76.69	4.66
CLSA	1	350.13	6.64
	2	347.51	7.46
	3	325.88	6.52
CVSI	1	350.14	3.26
	2	341.76	3.87
	3	345.42	5.27
CLDI	1	354.84	2.05
	2	350.78	3.93
	3	343.74	5.68
CVDA	1	330.16	5.21
	2	334.84	7.12
	3	339.64	5.47

Table 9.7: Average value and standard deviation for the replication of the designed experiment - NanoBones project

Parameter	Code	Value
T_m / T_g	F	0.95
	C	1.10
P_h [bar]	S	250
	D	500
V_{inj} [mm/s]	L	450
	V	750
E_a	A	on
	I	off

Table 9.8: Codification for the replication of the designed experiment - MicroBones project.

Factors	SS	MS	F	P
T_m/T_g	457873	457873	4057.87	0.000
V_{inj}	61	61	0.54	0.471
P_h	1038	1038	9.20	0.007
E_a	117	117	1.03	0.322
Error	668184	668184		

Table 9.9: Anova table for the designed experiment.

Figure 9.6: Influence of the main factors on the replicated height of nano pillars.

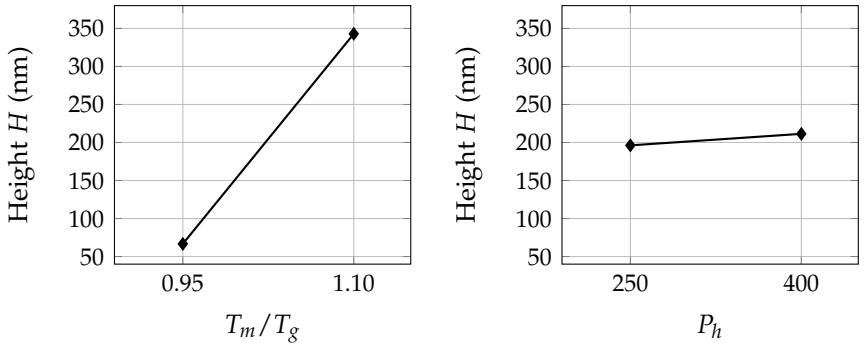

The replication quality of the nano structured surface has to be also evaluated in terms of uniformity of the replication, according to the project specification, which required both a high replication degree and the achievement of a low standard deviation in the replicated hight of the nano pillars. To maximize the height uniformity of the nano features, the standard deviation of the 3measured areas, was considered in the DOE analysis. 9.7b reports the Pareto charts for the standard deviation of the replicated nanopillars, indicating that none of the considering factors are significant.

Even if the results are consistent with those found in literature, the preponderant effect of T_m/T_g could aliased the effect of the others main factors. In fact, as shown in the Pareto chart of the average height (Figure 9.7a), the value of the standardized effect of T_m/T_g (100.52) is much more higher when compared to the values of the other considered factors (standardized effect of P_h is equal to 4.69). For this reason, a new experimental plan was designed fixing the value of T_m/T_g at 1.10. The analyzed factors and their levels were the same considering in the previous analysis (Table 9.6).

The *ANOVA* results of the new factorial plan indicate that only the cavity air evacuation affects the average height of the replicated nanofeatures, as reported in Table 9.10. The main effect of the air evacuation is to reduce the average height of the nano features (H) by 5%, as shown in Figure 9.8.

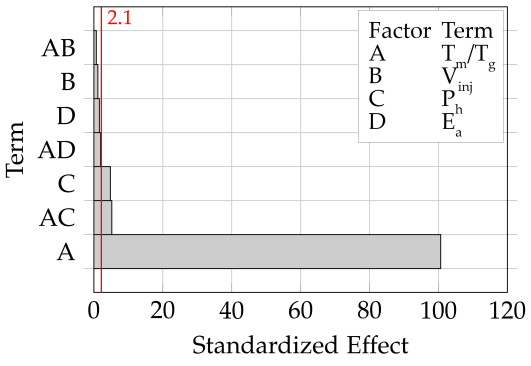

(a)

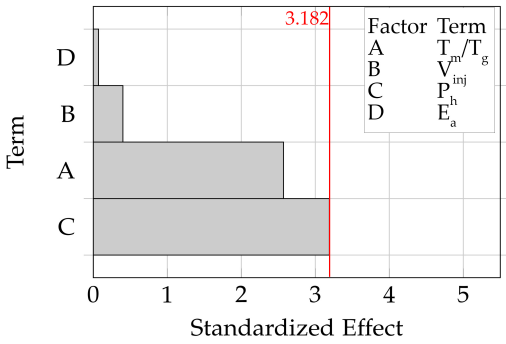

(b)

Figure 9.7: Pareto chart of the standardized effect. The response is (a) the average height and (b) the standard deviation of the replicated nanopillars. (Alpha=0.05).

Factors	SS	MS	F	P
V_{inj}	79.67	79.67	1.28	0.291
P_h	3.9	3.9	0.06	0.809
E_a	285.38	285.38	4.59	0.045
Error	497.58	497.58		

Table 9.10: Anova table for the designed experiment.

Figure 9.8: Influence of the main factors on the replicated height of nano pillars.

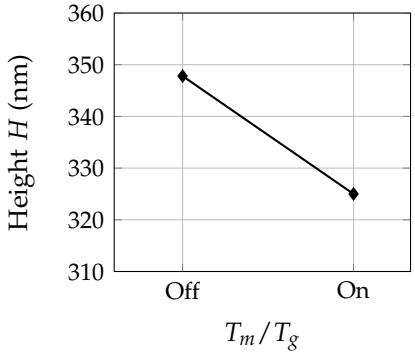

To understand this, it should be noted that air evacuation could lead to a decrease of the surface temperature in nanofeatures due to the warm air removal from the cavity. As suggested by Sha et al. [52], with the increase of the surface-to volume ratio in nano cavities air evacuation could have a detrimental effect on the melt fill for polymers that are sensitive to changes of T_m, such as polystyrene [78].

Due to the resolution of the considered factorial plan, the analysis of variance was not able to evaluate the statistical significance of first order interactions. Their influence on the response variable has been investigated only graphically, by the means of the interaction plots.

Figure 9.9 shows the significant interactions between holding pressure and the other factors. The significant interaction between P_h and V_{inj}, shown in Figure 9.9(a) shows that the effect of the holding pressure increases for low values of V_{inj}. Figure 9.9(b) reports the interaction between E_a and P_h indicating that the presence of cavity air evacuation decreases the average hight (H) for high values of holding pressure.

It should be noted that the interpretation of these graphs should be made only on a qualitative level, since differences to the average values is comparable to the values of the standard deviations obtained for the various experimental points.

Figure 9.9: Influence of the interactions between the holding pressure and the injection speed on the average height of the replicated microchannels for the CellDiaSP optimization analysis.

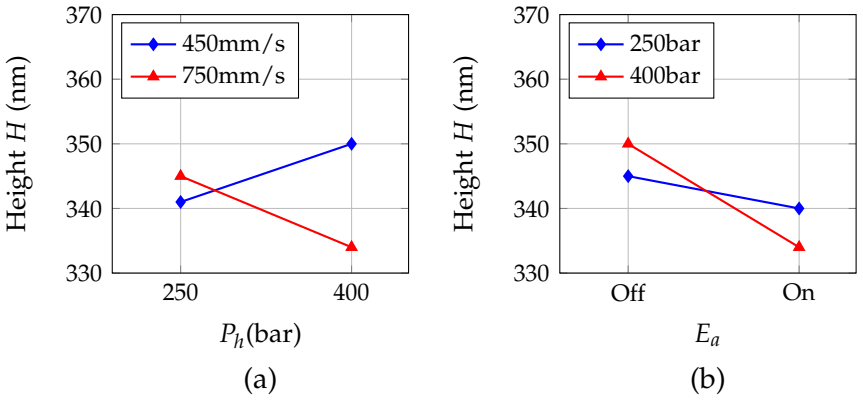

9.2.3.1 *Residue Analysis*

Also in this study, the residuals were analyzed to determine the adequacy of the model considering the complete factorial plan. Figure 9.10 reports the residual plots for the response variable. The residue analysis did not reveal particular deviations from normality for all the replications. However, one unusual observation was reported. This observation refers to replication of treatments at low mould temperature. However, due to the screening view followed in this analysis, the results are considered acceptable.

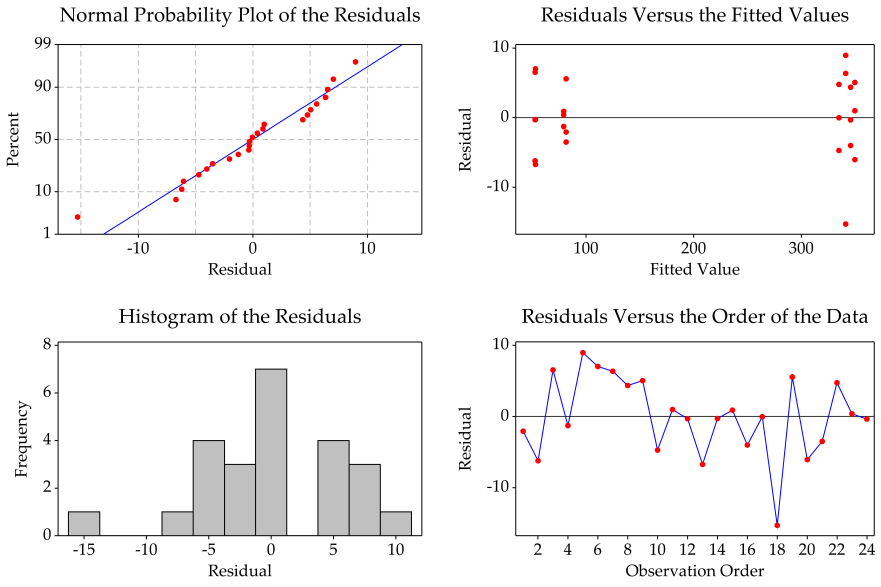

Figure 9.10: Residual Plots for the DoE -NanoBones project.

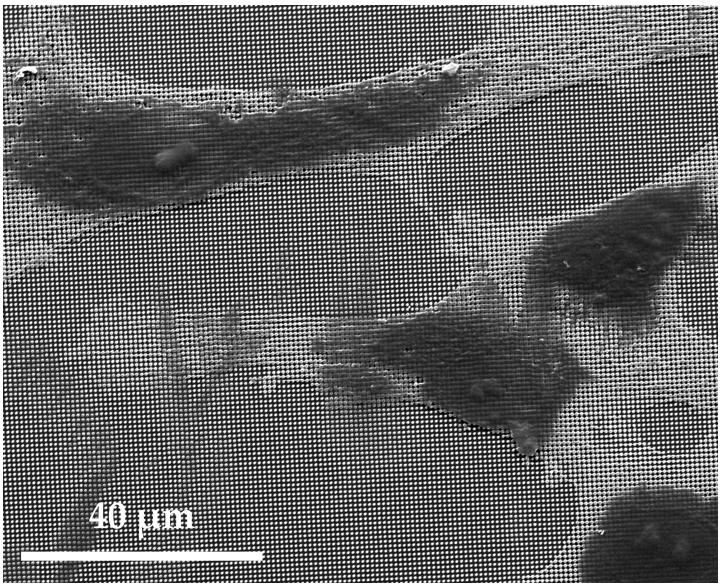

Figure 9.11: SEM picture of hMSCs culture on 4-8 nano structured PLA support after 72h from seeding.

9.2.3.2 *Concluding remarks*

The micro injection molding process of nano pillared PLA surfaces, performed on directly patternable silica-zirconia hybrid nano structured mold inserts, was optimized to increase the degree of nano structures replication. With the optimized process setting, 300 PLA samples were produced for each nano structures geometry for analyzing the hMSC behavior and differentiation (Figure 9.11).

The experimental and procedures used for the hMSC cultures are reported in Appendix A. The results obtained from nano pillared surfaces show that cells adhesion and proliferation is more positively promoted on nano pillared surfaces compared to flat surfaces.

10

DISCUSSION OF THE EXPERIMENTAL RESULTS

In the previous chapter the experimental investigations that have been carried out were explained, details on the design and analysis were given. However, the discussions of the results were related to the single project. In this chapter, the results of the experimental investigations of both the project are resumed and compared in a more comprehensive discussion which aims to clarify some aspects of the micro-injection moulding process of challenging micro and nano features.

10.1 MOULD TEMPERATURE

In this study the mould temperature is clearly confirmed to be the most influent process parameter on the replicated height of micro and nano features. Its importance that results from the experimental analysis is comparable to other researches reported in literature.

Mould temperature is important due to its influence on the thermal gradient between cavity's surface and the injected polymer. The viscosity of the polymer melt is highly dependent on temperature. Therefore it is crucial to keep the material flowing at high temperature during the filling phase. This was achieved by maintaining the highest possible value of the barrel temperature according to material's datasheets and by adopting a rapid heat cycle moulding. The latter, allows the polymer to fill both nano and micro-features from the very beginning of the process.

For the CellDiaSP project, by varying the ratio T_m/T_g from 0.95 to 1.10, the average height increased by 313%. The growth trend of micro-features height with mould temperature is almost the same for the NanoBones project preliminary analysis, where the replicated micro pillars were characterized by a diameter of 4μm and interspace of 10μm. In fact, by increasing T_m/ T_g from 0.95 to 1.10 lead to an increase in the average height of micro pillars by 315%. The replication of nanostructures is more sensitive to the increase of temperature; moulding at higher values of mould temperature lead to an increase in the average height of nano pillars by 513%.

In conclusion, it is fundamental to adopt high mould temperatures in order to improve the fluidity of the molten and consequently the height of micro-features. The disadvantage of higher cycle times can be mitigated by the adoption of a rapid heat cycle moulding.

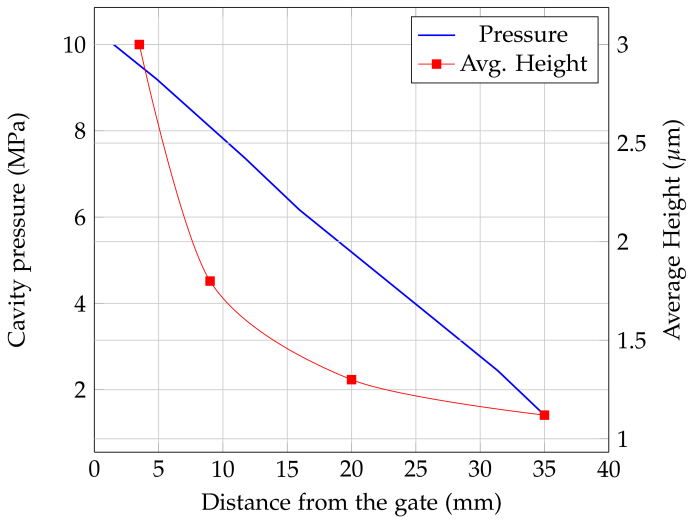

Figure 10.1: Comparison between micro features height and pressure distribution along the cavity in the CellDiaSP project.

10.2 THICKNESS OF THE MAIN FLOW REGION

The thickness of the main cavity resulted important from both projects. In the NanoBones project, the preliminary experimental results clearly indicates that a greater thickness reduce the replicated height of micro-features. Increasing cavity thickness from 1 mm to 2 mm resulted in a reduction of the average height by 19%.

In the ErytroChip this factor has not been directly investigated, due to technological limitations. Despite this some evidence of its influences emerges, in particular considering the results of the optimization analysis. As described in chapter 8.2, the distribution of the micro features height values along the cavity is extremely uneven. The replication is much better for micro features closer to the gate, as in this region the holding pressure is higher, but it quickly worsens within the first 10 mm. The high lenght to thickness ratio (46/1), that characterizes the cavity of the chip, greatly affects the uniformity of the height of micro-channels along the chip. This uneveness in replication quality is stricly related to the in-cavity pressure. In fact the high lenght to thickness ratio hinders the pressure to be uniform in the cavity.

10.3 INJECTED MATERIAL

The effect of the injected materials has been investigated only for the CellDiaSP project. This preliminary analysis aim to investigate the influence of injected material and its interaction with process parameters on the replication quality of high aspect ratio micro features. The results shown that using COC instead of PS, the average height

Figure 10.2: Different sensitivity of PS1540 and COC 5013L-10 to mould temperature variations.

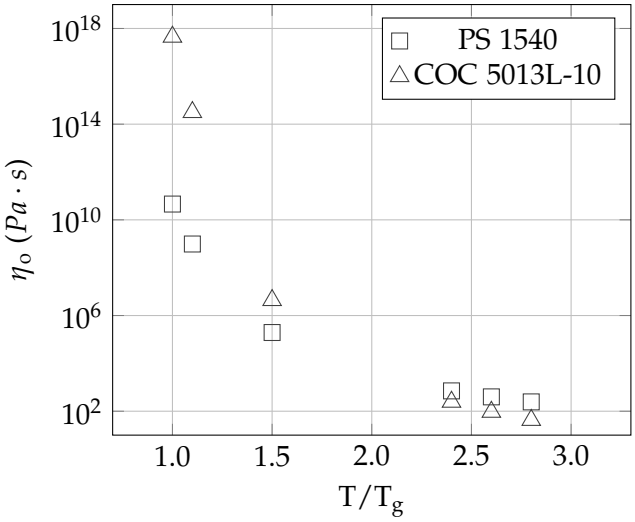

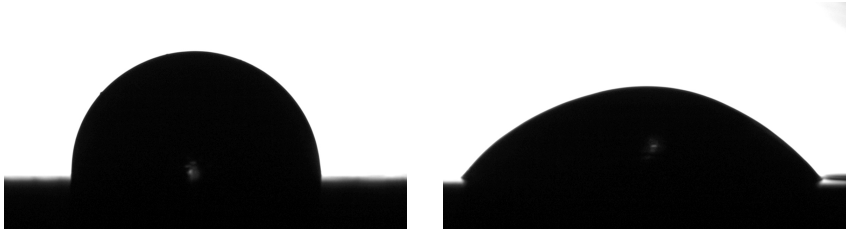

(a) (b)

Figure 10.3: Image of PS drop (a) and COC drop (b) after 10 minutes.

of the micro features increases from 1.02 to 1.25 μm. The different effect of the materials is due to their rheological properties. Indeed, PS 1540 is more viscous than COC 5013L-10 at melt temperature which is at least two times higher than T_g for both the materials. The effect of the low viscosity is markedly higher close to the gate, where the injection pressure is higher.

In conclusion, a combination of low viscosity and high wetting properties is an ideal condition to improve the replication of micro features. As emerged from the replication of nickel micro features on COC parts, the combination of higher temperature dependence of viscosity and higher wetting properties facilitate the replication and allow vacuum venting to significantly enhance the filling ratio.

10.4 HOLDING PRESSURE AND INJECTION SPEED

Experimental results showed a dependence of the replication degree on the holding pressure only when replicating nano features. In fact, in the NanoBones optimization analysis, the effect of holding pres-

sure is to increase the average height of replicated nano pillars by 8%. The importance of holding pressure lies in the fact that it overcomes the tendency of the polymer melt to prematurely freeze before the injection process is complete. Premature freezing is likely to be exacerbated by the relatively high rate of heat transfer between the polymer and the mould walls for parts with nano-scaled dimensions.

The effect of injection speed was not significant for both the replicated geometries.

10.5 CAVITY AIR EVACUATION

The efficiency of cavity air evacuation has been evaluated for both projects. The obtained results are contrasting. In the ErytroChip project it resulted a significant factor; in particular the evacuation of air from the cavity made the average height of replicated microchannels increase by 24%.

This positive effect on replication by applying the evacuation of the air, could be caused by:

1. cavity air evacuation removes the air trapped inside the high aspect ratio micro features, which increase the resistance to the flow, causing an incomplete replication;

2. being the channels placed perpendicular to the flow direction (Figure 10.4a), the evacuation of the air from the cavity, could promote the filling of the high aspect ratio micro features. A schematic representation of this phenomena is represented in Figure 10.4b).

Conversely, in the NanoBones project, the main effect of the air evacuation is to reduce the average height of the nano features (H) by 5%. This is probably due to the fact that cavity air evacuation could lead to a decrease of the surface temperature in nano features due to the warm air removal from the cavity. As speculate by Sha et al. [52], with the increase of the surface-to-volume ratio in nano cavities air evacuation could have a detrimental effect on the melt fill for polymers that are sensitive to changes of T_m, such as polystyrene [78].

Therefore, the effect of cavity air evacuation is not completely clear. As described in section 3.5.2, many authors try to understand the effect of removing the air from the cavity during the μIM process, producing mixed results.

In the following section, a step forward is taken, by analyzing the effect of cavity air evacuation, monitoring mould and polymer temperature evolution during the micro injection moulding process.

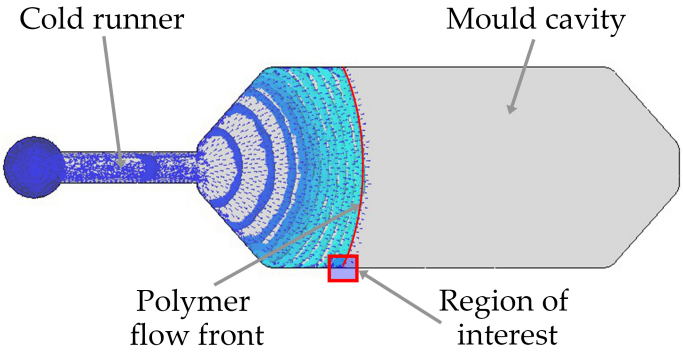

(a)

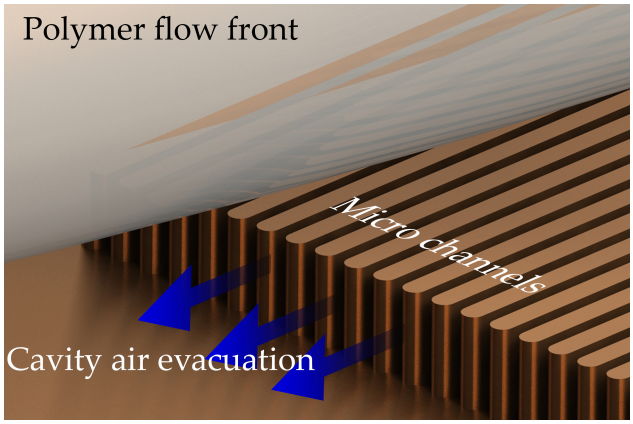

(b)

Figure 10.4: (a)Flow front shape during the filling stage of the Erytrochip, (b) schematic representation of the effect of the cavity air evacuation.

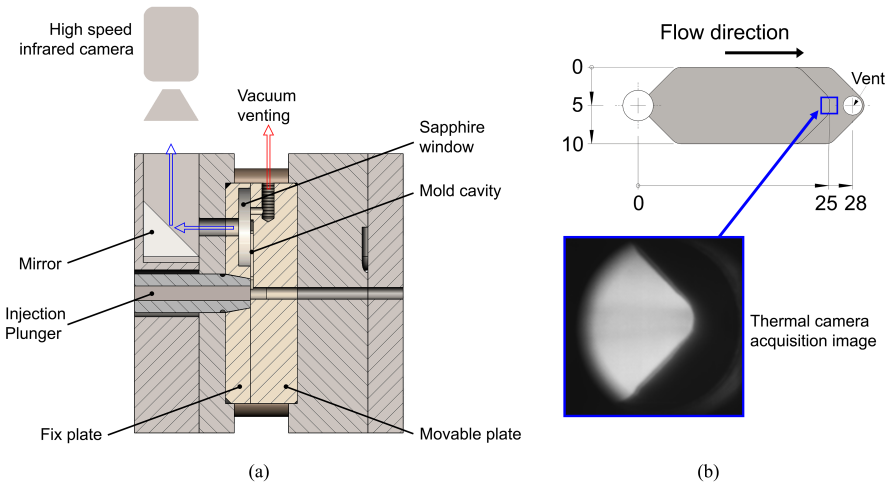

Figure 10.5: Mould design for the investigation of the influence of cavity air evacuation on mould temperature. (a) schematic representation of the experimental setup; (b) schematic top view of the part design and the image from the IR camera.

10.6 INFLUENCE OF VACUUM VENTING ON MOULD SURFACE TEMPERATURE

In this analysis, the effect of air evacuation on the mould/polymer temperature was experimentally investigated using an experimental setup developed at *Bradford University*. A high speed infrared camera system and a sapphire window in the mould were used to monitor the mould and polymer temperature during the μIM process.

10.6.1 *Experimental Setup*

The tool used to perform the experiments was based on the Hasco K-standard modular system. However, the standard system was modified to integrate a sapphire window and a mirror for the mould/melt temperature monitoring. As shown inFigure 10.5a, a pocket was machined on the fixed plate of the mould to accommodate a 45° tilted first surface gold mirror, which was aligned with the sapphire window overlooking the mould cavity.

The test part design used in this study was characterised by overall dimensions of 10 mm x 25 mm x 1 mm thickness as shown in Figure 10.5b. The cavity was vented by means of an evacuation system. A channel was machined on the moving plate of the mould to host an O-ring, which surrounds the cavity and seals the mould-parting plane. A vacuum pump was connected to the mould with a vent that was machined on the opposite side of the gate and placed inside the sealed area. The channel for the evacuation of the air from the cavity has a thickness of 50 μm and it covers all the width of the mould cavity.

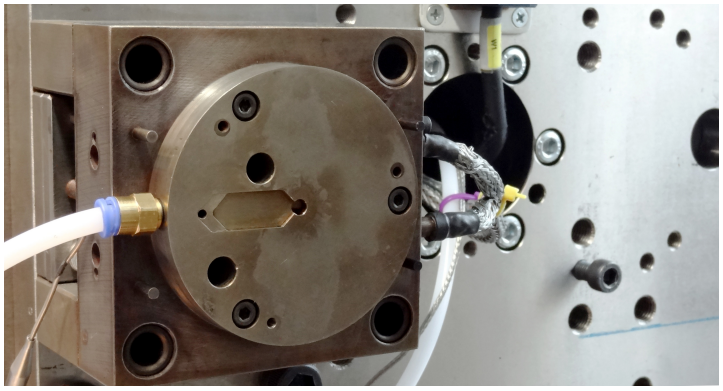

(a)

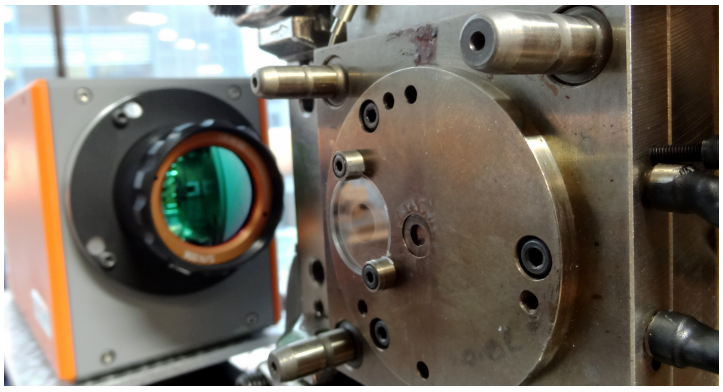

(b)

Figure 10.6: Experimental setup used for analyzing the effect of cavity air evacuation on the mould temperature. (a) Mould movable plate, (b) mould fix plate.

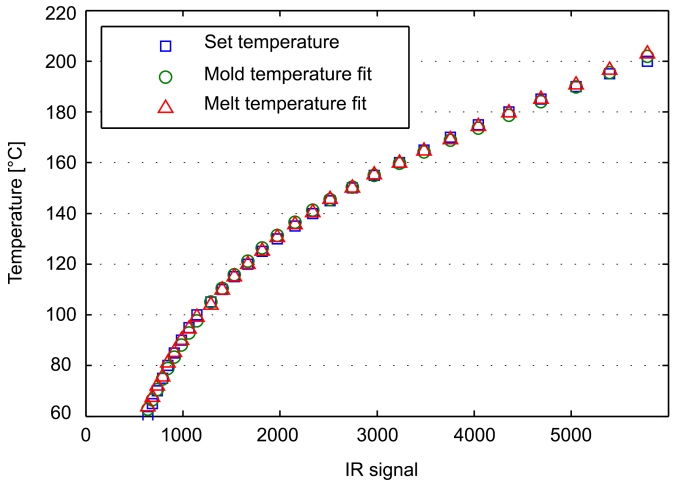

Figure 10.7: IR camera calibration for mould (○) and melt (△) temperature

The heating stage was realised using 4 electrical resistive heaters: 2 in the fixed plate and 2 in the movable one.

A commercial cyclic olefin copolymer (*Topas, COC 5013 L-10*) was used for the experimental work.

In this analysis the effects of the cavity air evacuation on the melt flow front temperature was investigated using a high-speed, high sensitivity infrared camera (Ircam Equus 81k SM). The camera has a cooled indium antimonide (InSb) detector with the spectral range of 1.5 to 5.0 μm. It can capture 386 frames per second at the full frame size of 320 x 256 pixels, and can achieve 30000 frames per second in a windowing mode. This very fast IR camera was used to measure the flow temperature of the polymer inside the mould cavity during the μIM process.

The IR camera was calibrated before the injection moulding experiments for both the mould and the polymer temperature. In the first case, the mould temperature was set using the control system integrated on the injection moulding machine and after a thermal stabilisation of 300 s, an IR signal was recorded. A similar procedure was used for the calibration with the polymer. In this case, the polymer was injected inside the mould cavity where it was left for 300 s to thermally stabilise before acquiring the IR signal. The calibration temperature ranged from 60 °C to 200 °C with increments of 5 °C and each acquisition was repeated three times. The experimental data were fitted with a general exponential model (Eq. 10.1):

$$f(x) = a \cdot \exp(b \cdot x) + c \cdot \exp(d \cdot x) \tag{10.1}$$

The coefficients of Eq. 10.1 and the parameters regarding the goodness of fit are reported in Table 10.2. In particular, the goodness of fit is related to the *R-square* value, equal to 0.9997, which means that the fit explains 99.97% of the total variation in the data about the average.

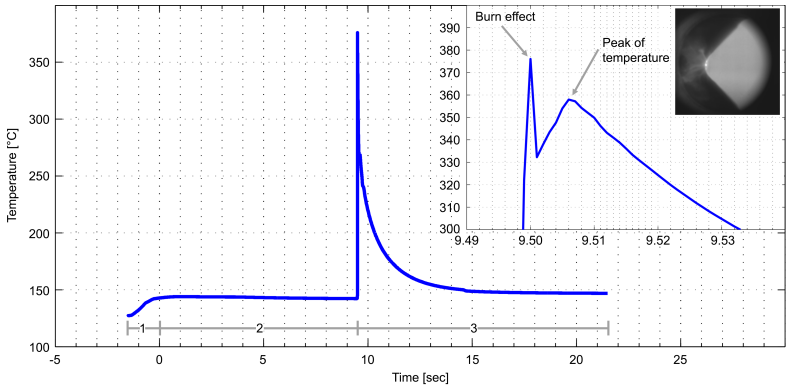

Figure 10.8: Temperature profile: (1) Mould closure; (2) Injection delay; (3) Filling and packing stage. On the upper right corner, the magnification of the temperature profile in the injection zone.

Level	T_m [°C]	V_{inj} [mm/s]	E_a
(+1)	140	850	On
(-1)	80	350	*Off*

Table 10.1: Factors and levels for the design of the factorial plan

As shown in Figure 10.7, there are no significant differences between the two considered models. For this reason, the mould temperature fitted model was chosen for the entire work.

10.6.2 *Experimental Design*

A design of experiments (DoE) approach was applied to design and analyse the experimental campaign. A two-level, three-factor, full factorial plan was used. For each run, the data collected on the first 10 cycles were discarded in order to stabilise the process. Each treatment of the DoE was repeated three times in a completely randomised order for 24 runs, with the aim of minimising the interference of external variability sources. Factors investigated were the mould temperature (T_m), the injection velocity (V_{inj}) and the presence of air evacuation (E_a). The choices of the upper and lower levels for the factors were derived from a literature review, recommendations of the material supplier and the technological limits of the available experimental setup. The range values for each factor are summarised in Table 10.1.

The parameters that were not considered as design factors were fixed at levels suggested from literature:

- Barrel temperature: 240 - 280 - 300 - 320 °C;
- Shot size: 220 mm^3;

General exponential model $f(x) = a \cdot \exp(b \cdot x) + c \cdot \exp(d \cdot x)$			
Coefficients (with 95% confidence bounds)			
For mould temp.		For melt temp.	
a	126.1	a	131.8
b	$8.16E-05$	b	$6.877E-05$
c	-139.5	c	-120.1
d	-0.00107	d	-0.00098
Goodness of fit			
For mould temp.		For melt temp.	
SSE	47.7300	SSE	6.738
R-square	0.9991	R-square	0.9997
Adjusted R-sq.	0.9989	Adjusted R-sq.	0.9997
RMSE	1.3820	RMSE	0.5955

Table 10.2: Coefficients of the fitted general exponential model and goodness of fit parameters

- Holding pressure: 40 MPa for 9 s;

The cavity pressure before the injection was set at 3 mbar. The vacuum venting was applied for 10 s before the injection and for all its duration. The response variable for this analysis was chosen to be the peak of temperature of the flow front inside the mould cavity ($\bar{T}_{\text{peak}}$). As shown in Figure 10.8, the higher peak of temperature is related to the burn effect caused by the rapid compression of the air ahead of the flow front, while the second peak of temperature is related to the maximum flow front temperature. For each test, the signal acquired with the IR camera, was elaborated using the software Works from Ircam. The signal was extracted from a region of interest (ROI) of the size of 70 x 50 pixels as shown in Figure 10.9 and it has been applied the general exponential model (Eq. 10.1) in order to obtain the temperature profile.

10.6.3 *Results and Discussions*

The factorial design was analysed in order to comprehend which factors and interactions are statistically significant for the variation of the flow front temperature inside the mould cavity.

Table 10.3 presents the results obtained from the experiments. For each level of the experimental design, the average peak temperature ($\bar{T}_{\text{peak}}$) and the standard deviation are reported. A general linear model was used to perform an univariate analysis of variance, includ-

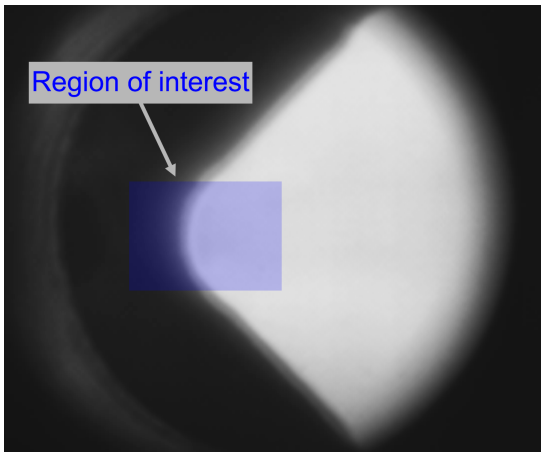

Figure 10.9: Thermal camera acquisition image and the region of interest (ROI)

T_m [°C]	V_{inj} [mm/s]	E_a [°C]	$\bar{T}_{peak}$ [°C]	Std. dev [°C]
80	350	Off	269.0	2.84
140	350	Off	309.7	2.34
80	850	Off	293.7	3.00
140	850	Off	370.2	2.48
80	350	On	260.9	2.61
140	350	On	297.6	2.14
80	850	On	274.2	2.58
140	850	On	331.6	3.12

Table 10.3: Results of the experimental campaign

Figure 10.10: Main effect plots of (a) air evacuation, (b) injection speed and (c) mould temperature.

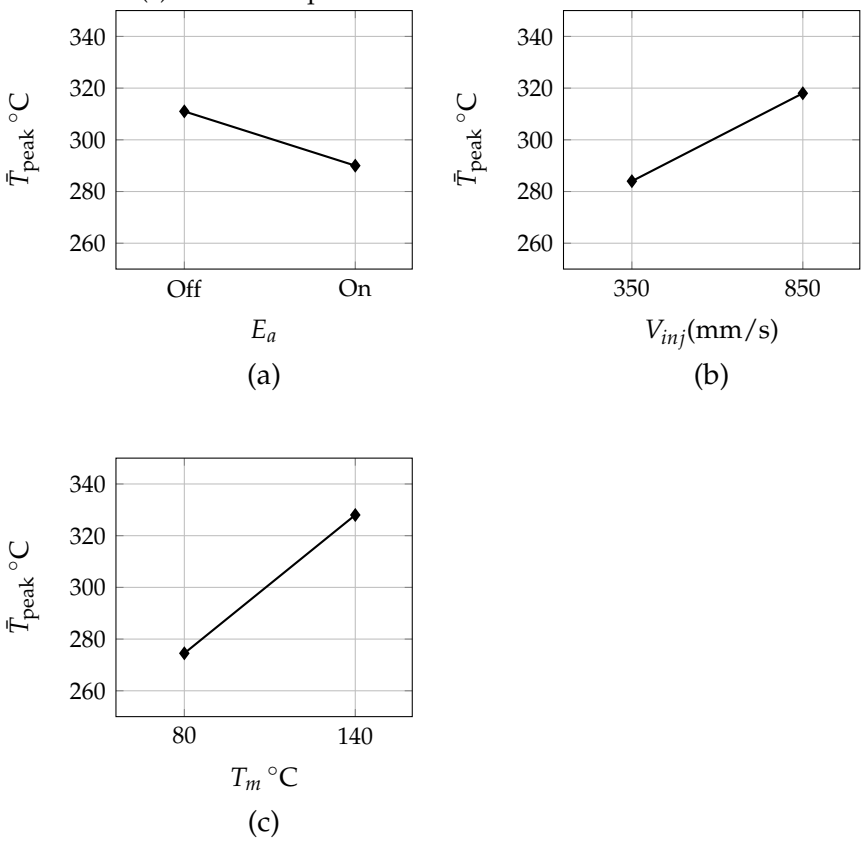

ing all the main factors and their interactions. The *ANOVA* results of the experimental plan indicate that all of the main factors are significant (Table 10.4).

Interestingly, it was observed that the effect of applying vacuum venting before the injection, resulted in a significant reduction of the melt flow temperature as shown in Figure 10.10a. In particular, when evacuating the air from the cavity the average value of the flow front temperature decreases by 7%. The air trapped inside the cavity is subjected to a rapid compression between cavity walls and the polymer melt injected at high speed. This phenomena is particularly relevant in small cavities, typical of μIM applications. The heat that is produced increases both the temperature of the flow front and the mould temperature. Therefore, when applying vacuum venting the consequent reduction of the melt and mould temperature should be considered, as it directly affects the thermal gradient between the melt and the mould. This effect can be particularly significant for the μIM process, in which mould temperature plays a fundamental role in determining the filling length of the polymer in narrow cavities and micro/nano features. In particular, a lower temperature, and thus a higher viscosity of the melt, can significantly hinder the

Source	SS	MS	F	P
T_m	16757.7	16757.7	2372.97	0.000
V_{inj}	6594.2	6594.2	933.77	0.000
E_a	2297.9	2297.9	325.40	0.000
$T_m \cdot V_{inj}$	1198.5	1198.5	169.71	0.000
$T_m \cdot E_a$	199.9	199.9	28.30	0.000
$V_{inj} \cdot E_a$	536.0	536.0	75.90	0.000
$T_m \cdot V_{inj} \cdot E_a$	87.1	87.1	12.33	0.003
Error	113.0	113.0	7.1	

Table 10.4: ANOVA results for the experimental plan

filling of micro cavities even when applying high values of holding pressure.

By increasing the injection speed from 350 to 850 mm/s the temperature of the flow front increases by +12% on average (Figure 10.10b). This effect is related to the higher shear rates that characterise the flow and produce a higher viscous heating.

The main effect of the mould temperature on the melt flow temperature is reported in Figure 10.10c. This is related to the thermal flux between the mould and the polymer melt. By increasing the mould temperature from 80 °C to 140 °C the temperature at the flow front increases from 274 °C to 327 °C (+19% on average).

To completely understand the influence of process parameters on the temperature at the flow front, the effects of first order interactions have to be considered as shown by the analysis of variance (Table 10.4).

When the polymer is injected at a higher mould temperature, the effect of injection velocity is more evident (Figure 10.11a). This is related to the thermal conduction rate of the mould. Indeed,moulding at high value of injection speed, the air compression rate is greater causing higher temperature rise. This effect is amplified by higher mould temperature, at which the thermal gradient between the mould and the polymer is smaller and so the heat conduction.

The interaction between the injection speed and the evacuation of air from the cavity is reported in (Figure 10.11b). When vacuum venting is not applied, at a high value of injection speed the air in the cavity is compressed at a higher rate thus the increase of the flow front temperature is greater. The evacuation of the air from the cavity contrasts the rapid compression and as a result it lessens the increase of the polymer flow front temperature.

As shown in (Figure 10.11c) , the effect of applying vacuum venting is more significant when moulding at a higher mould temperature, both for low and high injection speeds. This is more evident in Fig-

Figure 10.11: Interaction plots of (a) injection speed and mould temperature, (b) injection speed and air evacuation, (c) mould temperature and air evacuation.

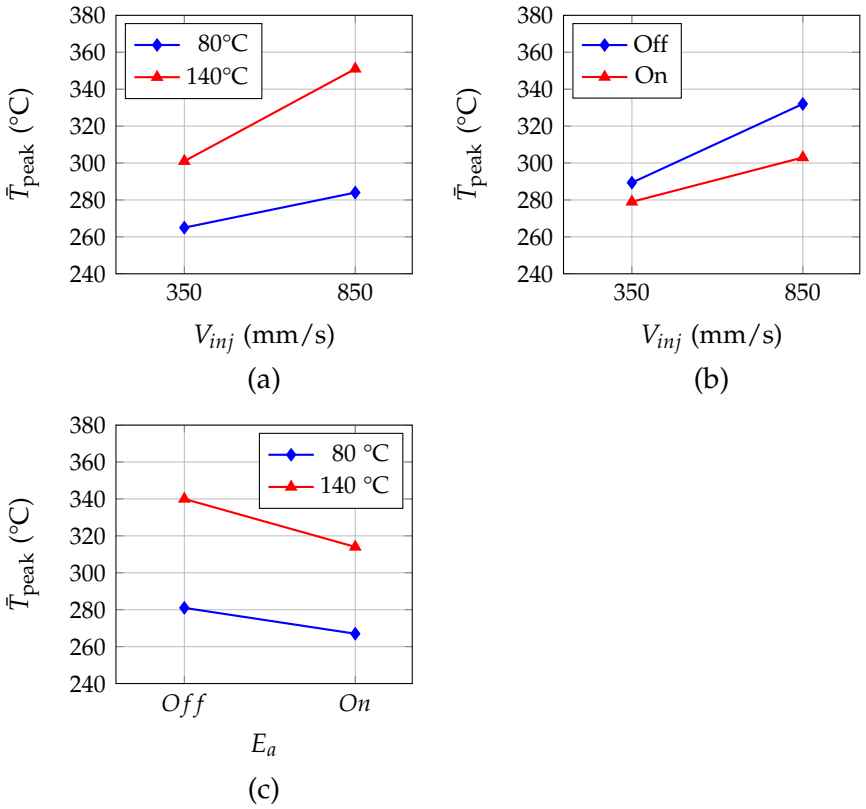

ure Figure 10.12, which shows the experimental average temperature data for the different moulding conditions at 80 °C (Figure 10.12a) and 140 °C (Figure 10.12b). At lower mould temperature, the pressure drop during the filling phase is higher, due to the higher viscosity of the polymer and to the thicker solidified layer. Therefore, the melt flow front velocity decreases according to the polymer compressibility. In fact, as reported in Figure 10.12a, when injection moulding at lower value of mould temperature and without applying vacuum venting, the burn effect, which is caused by the rapid compression of the air ahead of the polymer flow front, occurs only at high value of injection velocity. Conversely at high value of mould temperature (Figure 10.12b) and without cavity air evacuation, the burn effect occurs for both high and low value of injection speed causing an increment of the mould surface temperature.

10.6.4 *Concluding Remarks*

In this analysis, the effect of cavity air evacuation was experimentally investigated, monitoring mould and polymer temperature evolution during the micro injection moulding process by means of a high speed infrared camera and a sapphire window which forms part of the mould wall.

The results of the experimental tests showed that when evacuating the air from the cavity the average value of the measured temperature decreases by 7%. In particular, when applying vacuum venting the consequent reduction of the flow front temperature should be considered, as it directly affects the thermal gradient between the mould and the melt. It was observed that the effect of applying vacuum venting is more evident when moulding at a higher mould temperature, both for low and high injection speed. The main effect of injection speed and mould temperature are significant as well. In particular, by increasing the injection speed from 350 to 850 mm/s the temperature of the flow front increases by +12% on average due to the higher shear rates that characterise the flow and produce a higher viscous heating. The main effect of the mould temperature on the melt flow temperature is related to the thermal flux between the mould and the polymer melt. By increasing the mould temperature from 80 °C to 140 °C the temperature at the flow front increases by +19% on average. Interestingly, it was observed that moulding at high value of injection speed, the air compression rate is greater causing higher temperature rise. This effect is amplified by higher mould temperature, at which the thermal gradient between the mould and the polymer is smaller and so the heat conduction. Moreover, at lower mould temperature, the pressure drop during the filling phase is higher, due to the higher viscosity of the polymer and to the thicker solidified layer. Therefore, the melt flow front velocity decreases according to the polymer com-

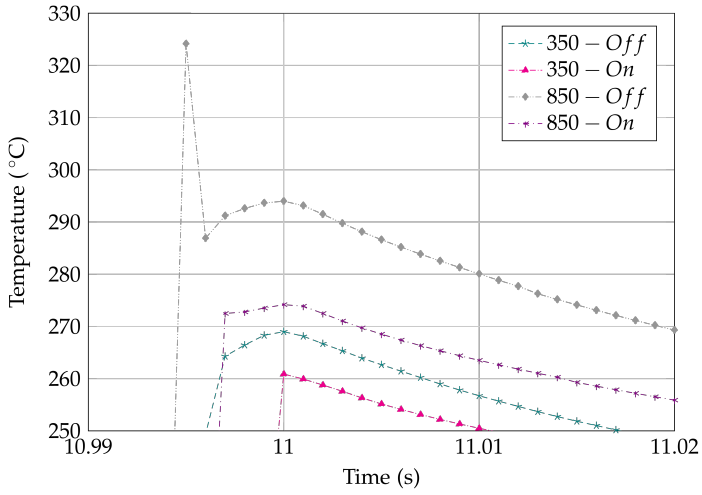

(a)

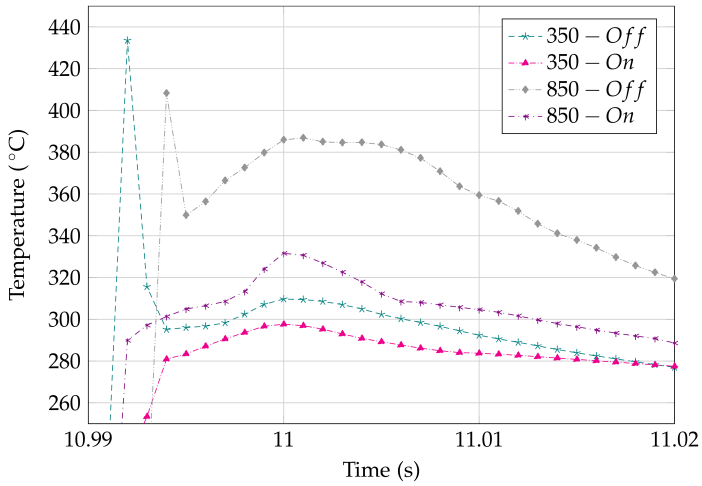

(b)

Figure 10.12: Experimental temperature data for different moulding conditions at (a) 80 °C and (b)140 °C. The maximum standard deviation for the average value is 4.02 °C.

pressibility. This effect can be particularly significant for the micro injection moulding process for which it is well-known that the temperature plays a fundamental role in determining the filling length of the polymer in micro/nano features.

Part IV

CONCLUSION

11

CONCLUSIONS

In this work, the micro injection moulding process for the manufacturing of nano features and high AR micro features was characterized, focusing on the challenges and limitations in the replication. The experimental investigation considered two projects characterized by different geometry and dimensions of the macro- and nano- cavities.

Among process parameters, mould temperature is clearly confirmed to be the most influent on the replicated height of micro and nano features. Considering the CellDiaSP project and the preliminary analysis of the NanoBones project, where the features were characterized by a diameter of 4μm and a depth of 5μm, by increasing T_m/T_g from 0.95 to 1.10, lead to an increase in the average height of the replicated micro features of $\sim$310%. Moreover, the experimental results indicate that the replication of nano structures is more sensitive to the increase of temperature. In fact, when moulding at higher values of mould temperature, the average height of nano pillars increased by 513%.

Mould temperature is important due to its influence on the thermal gradient between cavity's surface and the injected polymer. Therefore it is crucial to keep the material flowing at a temperature higher than the transition temperature of the injected material during the filling phase. In μIM it is fundamental to adopt high mould temperatures in order to improve the fluidity of the molten and consequently the height of micro- and nano features. The disadvantage of higher cycle times can be mitigated by the adoption of a rapid heat cycle moulding.

The effect of the holding pressure and of the injection speed were found to be less significant. In particular, the experimental results showed a dependence of the replication degree on the holding pressure only when replicating nano features. In fact, in the NanoBones optimization analysis, the effect of holding pressure is to increase the average height of replicated nano pillars by 8%. The importance of holding pressure lies in the fact that it overcomes the tendency of the polymer melt to prematurely freeze before the injection process is complete. Premature freezing is likely to be exacerbated by the relatively high rate of heat transfer between the polymer and the mould walls for parts with nano-scaled dimensions. Conversely, the effect of injection speed was not significant for both the replicated geometries.

The analysis of the efficiency of cavity air evacuation produced contrasting results. When replicating high aspect ratio micro features, the use of vacuum venting lead to an increment of the replication degree

by 24%. This is due to the fact that cavity air evacuation removes the air trapped,which increase the resistance to the flow, causing an incomplete replication. Otherwise, when replicating nano features, the effect is the opposite. Applying vacuum venting, lead to a decrease of the average height of the nano features by 5%, due to the fact that cavity air evacuation lead to a decrease of the mould surface temperature. This effect was experimentally investigated using a high speed infrared camera and a sapphire window overlook in the mould cavity in order to monitor the mould and polymer temperature during the μIM process. The results of the experimental tests showed that when evacuating the air from the cavity the average value of the measured temperature decreases by 7%. In particular, when applying vacuum venting the consequent reduction of the flow front temperature should be considered, as it directly affects the thermal gradient between the mould and the melt.

In μIM, the quality of the replication is not only affected by process parameters but also by interfacial effects, in particular the wettability between polymer melt and the tool is critical. Wetting of the mould surface by the polymer melt may be an additional driving for a favorable combination of polymer and mould materials. The adhesion of the polymer is expected to be influenced by the chemistry of the mould surface, which can affect the initial contact between the hot polymer melt and the cold mould surface, and thus the filling of the cavity. Good wettability behavior can promote the replication, because of the strong interaction between the melt and the mould. Thus, wetting properties are relevant for the analysis of the μIM replication results, in particular for the understanding of the different relation between the material and a particular selection of process parameters. The experimental results indicate that a combination of low viscosity and high wetting properties is an ideal condition to improve the replication of micro features. As emerged from the replication of nickel micro features on COC parts, the combination of higher temperature dependence of viscosity and higher wetting properties facilitate the replication and allow vacuum venting to significantly enhance the filling ratio. In particular, the experimental results indicate that using COC instead of PS, the average height of the micro features increases from 1.02 to 1.25 μm.

In addition to process parameters and injected materials, also the geometry of the molded part can influence the melt filling by directly affecting the pressure profile in the macro cavity. In particular, the thickness of the substrate, which is much larger compared to the micro features, affects the replication quality by changing the evolution of the cavity pressure generated during the injection phase. Moreover, substrate thickness is critical because it determines the cavity filling time for a given injection speed. Experimental results indicate that the thinner the cavity is the less effective is the action of the holding pres-

sure in pushing the polymer melt in micro cavities. In the NanoBones project, the preliminary experimental results clearly indicates that a greater thickness reduce the replicated height of micro-features. Increasing cavity thickness from 1 mm to 2 mm resulted in a reduction of the average height by 19%. This indicates that the filling of the micro features must be brought back to the injection stage and not only to the packing one, as suggested by some other researches. Cavity geometry, and in particular its thickness, controls and modifies the thermal phenomena behind the filling behavior, such as the hesitation effect and the cooling process, making the effect of the holding pressure more or less effective.

In conclusion, this research completely characterized the μIM technology, not only considering the process parameters, but also considering the material properties, the interaction between polymer and mould material, and the use of auxiliary technologies like cavity air evacuation and rapid heat cycle moulding. The carried out work confirms previous findings and contributes to extend the state-of-the-art knowledge about the μIM process, which is considering nowadays a reliable and cost effective means of producing a wide range of micro components in thermoplastics materials.

Part V

APPENDIX

A

MESENCHEMICAL STEM CELLS IN VITRO CULTURES

An industrially feasible process for the fast mass-production of molded polymeric nano-patterned substrates was the main aim of the NanoBones project. Nano structured PLA surfaces were obtained through micro injection molding (μIM) technique on directly patterned stamps realized with a new zirconia-based hybrid spin-on system able to withstand 300 cycles. Among the different obtainable geometries, PLA replicas reporting 200 and 400 nm diameter pillars with 300, 400, 600, 800 nm center-to-center distance respectively, were manufactured (Table A.1.

Code	Diameter [nm]	Interspace [nm]	Aspect Ratio
2-3	200	300	2
2-4	200	400	2
4-6	400	600	2
4-8	400	800	2

Table A.1: Nanostructured support dimnesions for the MSC in vitro cultures.

Moreover, 300 PLA supports without any structures were realized as control for the MSC culture analysis.Whit the nano structured PLA substrates, the effect of the substrate topography on human mesenchymal stem cells behavior without any osteogenic growth factors was analyzed.

A.1 FACTORS AFFECTING HMSCS DIFFERENTIATION

The physical and chemical properties of materials in the local cellular micro environment are increasingly appreciated as key players in stem-cell fate decisions, that is the cell ability of self renewing and differentiating[1]. Cells interact with surfaces typically through the creation of attachment points linking the cytoskeleton (cells mechanical framework) to extracellular binding sites. For this reason the basic understanding of cell-substrate interaction represents a crucial factor in

1 Watt, F. M.et al., Role of the Extracellular Matrix in Regulating Stem Cell Fate. Nat. Rev. 2013, 14, 467

the fields of tissue engineering, drug development, and regenerative medicine[2].

Traditionally, substrate materials were simply considered as inert context that carry biochemical supplements (such as growth factors) for cell growth, differentiation promotion, or both. However, more recently, intrinsic material properties that mimic physiologically relevant extracellular matrix (ECM) characteristics have been proven to regulate stem cell fate (from adhesion to proliferation and differentiation). In particular, substrate mechanical stiffness, micro- and nanometer-scale topography, and simple chemical functionality each have been reported to play a fundamental role in driving human mesenchymal stem cell (hMSC) differentiation[3].

Topography was first identified to influence cell behavior as early as 1911, when the guidance of cells along the fibers of a spider's web was observed: the cells followed the fibers of the web in a phenomenon called stereotropism, or physical guidance [4]. Since this discovery, numerous studies have been conducted to analyze cell behavior on various micro- and nano-features such as lines, wells, holes, and more. After that, topography, independent from substrate chemistry, was found not only to have a strong effect on cell morphology[5], but also to provide physical, geometrical, mechanical, and structural signals that act together as a smart entity for guiding cell adhesion, orientation, migration, proliferation, viability, cytoskeletal organization, gene expression, and differentiation[6]. Moreover, MSCs specify lineage and commit to phenotypes with extreme sensitivity to tissue level elasticity. Soft matrixes that mimic brain are neurogenic, stiffer matrixes that mimic muscle are myogenic, and comparatively rigid matrixes that mimic collagenous bone prove osteogenic. According to this, influencing cell behavior from proliferation to differentiation using the material design of the substrate or implant topography has been found to be a desirable approach for many regenerative medicine applications.

As an example, the development of a new family of implantable bio-inspired materials that better mimic the natural bone extracellular matrix, a naturally nanocomposite tissue, can stimulate stem cell differentiation toward osteogenic lineages in the absence of specific chemical treatments.In particular, interactions between MSCs and surfaces with specific micro- and nano patterns can stimulate the cells to produce in vitro bone mineral.

---

2 De Angelis,F. et al., Water Soluble Nanoporous Nanoparticle for in Vivo Targeted Drug Delivery and Controlled Release in B Cells Tumor Context. Nanoscale 2010, 2, 2230-2236

3 Murphy, W. L. et al., Materials as Stem Cell Regulators. Nat. Mater. 2014, 13, 547

4 Harrison, R. G. On the Stereotropism of Embryonic Cells. Science 1911, 34, 279-281

5 Flemming, R. G.et al., Effects of Synthetic Micro- and Nano-Structured Surfaces on Cell Behavior. Biomaterials 1999, 20, 573-588

6 Bruinink, A. et al., Grooves Affect Primary Bone Marrow but Not Osteoblastic MC3T3-E1 Cell Cultures. Biomaterials 2001, 22, 2465-2473

A.2 MATERIALS AND METHODS

After the realization of 300 PLA substrate for each nano structured geometries, the adhesion, the cell viability and differentiation were analyzed at the *Dep. of Pharmaceutical Science* of Padova University.

MTS Assay

To test cell viability, the MTS test (*CellTiter 96 AQueous One Solution Cell Proliferation Assay; Promega, Austria*) was used, according to the manufacturer instructions. Briefly, at 24 h and 3, 7, 14, and 21 days from seeding, 200 μL of cell media, containing 10% MTS, were added into each well, and cells were incubated at 37 °Cfor 4 h. Optical density of purple formazan produced in living cells was measured at 490 nm, using a Microplate autoreader EL 311 (*BIO-TEK Instruments, Inc., Winooski, VT*). Results were expressed as number of cells. The linearity of absorbance of formazan over a range of 2.5x103 to 20x103 cells was established by determining the linear coefficient (0.999).

Alizarin Staining

At 7, 14, and 21 days from seeding, cultures were rinsed with phosphate buffered solution and fixed in 3.7% formaldehyde. To each well was then added 40 mM Alizarin red solution (*Alizarin Red S, Sigma-Aldrich*), which was then incubated at room temperature for 20 min. The dye was extracted by 10% acetic acid (200 μl/well). Acetic solutions were heated at 85°Cand lyophilized using Savant (*Savant Speed Vac Concentrator, Thermo Scientific, Rockford, IL*). Each sample was then resuspended in 10% acetic acid (pH 4.1), and optical density was determined at 405 nm using a Microplate Autoreader EL 311. Results were expressed as μM alizarin. 2

Reverse Transcription Polymerase Chain Reaction (RTPCR)

At 21 days, total *RNA* was extracted using TRIzol method according to the manufacturer's instructions (*Invitrogen, Paisley, United Kingdom*) and quantified using NANODROP 2000 (*Thermo Scientific*). RT-PCR was carried out through the Qiagen One Step RT-PCR Kit (*Qiagen, Crawley, United Kingdom*) according to manufacturer's protocol and using total *RNA* at concentration of 500 ng/reaction for each sample. The thermal cycling program consisted of 50°Cfor 30 min (reverse transcription), 95°Cfor 15 min (DNA-polymerase activation), 40 two-step cycles of 95°Cfor 30 s (denaturation), 50°Cfor 1 min (annealing) and 72°Cfor 1 min (elongation). The procedure was carried out using the iCycler iQ (*Bio Rad*). To obtain a semiquantitative assessment of gene expression, data were expressed as normalized ratios by comparing the integrated density values for osteocalcin (OC) gene with those for GAPDH. The PCR products were separated by 2% agarose gel electrophoresis and visualized by Gel Red Nucleic Acid staining 1:10000 (*Biotium, Hayward, California*).

Statistical Analysis

Triplicate experiments were performed. The results were expressed as the arithmetic mean ± standard deviation. Their statistical comparison was performed by analysis of variance, followed by Student's t test.

A.3 HMSC IN VIVO CULTURE RESULTS

Cell Adhesion

It is well-known that MSCs adhesion on biomaterials occurring through integrin receptors regulates growth and differentiation. Surface topography modulating focal adhesion assembly and cytoskeletal stress can both activate signaling cascades and modify the organization of nuclear components, leading to changes in gene expression.

Cell adhesion was evaluated by means of SEM and MTS assay after 24 h from seeding on nano patterned and control substrates. It must be pointed out that control substrates (code *C*)were obtained by replicating a flat steel stamp with polystyrene with the same microinjection conditions selected for the nanostructured surfaces. As shown in Figure A.1 MSCs well adhered onto all types of arrays, showing an elongated shape. A more flattened phenotype was visible on control, compared to that observed on 200-300, 200-400, 400-600 and 400-800 where cells showed an elongated shape. It has been observed that a relationship exists between cell morphology and MSC differentiation, that is, high-spread cells are often committed to an osteoblastic fate. SEM analysis revealed that on all surfaces cells formed an almost confluent monolayer at 7 days and then stratified at 14 and 21 days. At 21 days, the cell number on all pillar-structured PLA surfaces were significantly higher than that determined on control cultures.

Osteogenic Differentiation of hMSC

Osteogenic differentiation of hMSCs was verified by evaluation of calcium deposition and osteocalcin mRNA expression. Figure A.3 shows that all the nanostructured surfaces have osteoinductive properties. In particular at 7 days from seeding, the surfaces 2-4 and 4-8 induced a significant increase in the inorganic component compared to control. However, for all geometries, the greatest percentage changes, compared to the unmodified surfaces, were recorded at 14d. Conversely, at 21d a significant increment was observed only for the surfaces 2-4 and 4-6. It should be noted that this last result was partially expected, as the MSC when reach the confluence and begin to stratify, spontaneously differentiate into osteoblast.

The experimental results obtained from nano-pillared surfaces show that cells adhesion and proliferation is more positively promoted on nano-pillared surfaces compared to flat surfaces.

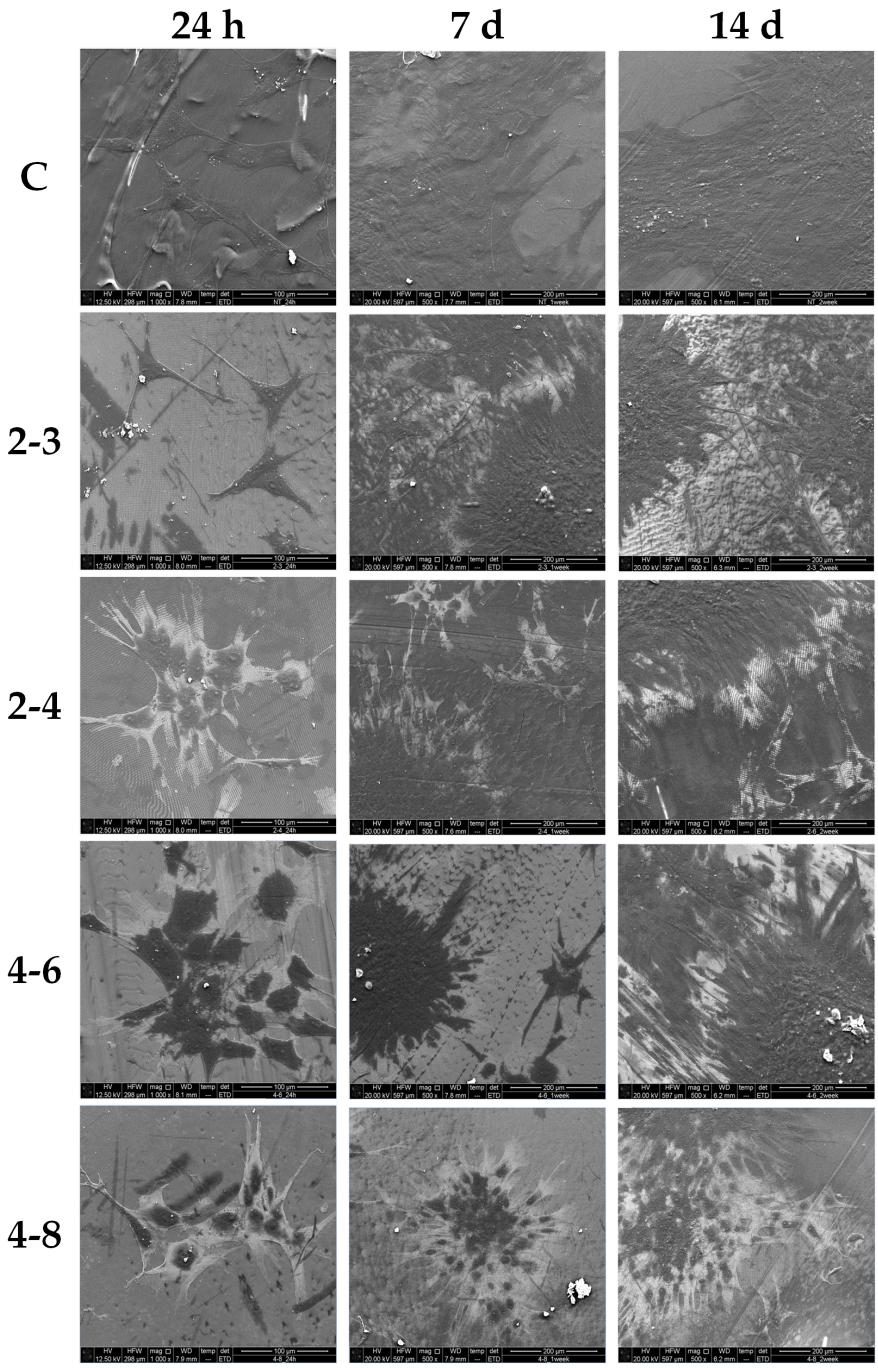

Figure A.1: Cell adhesion on nanopillar-structured PLA surfaces and control ones at 24h, 7d and 14d from seeding.

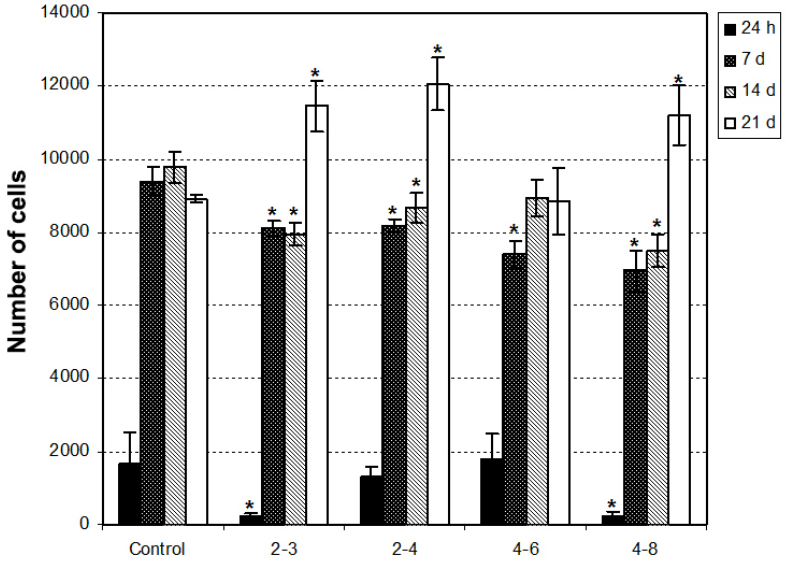

Figure A.2: Cell proliferation at 1, 7, 14, and 21 days after seeding on pillar-structured PLA surfaces and control ones. Results, expressed as cell number, are means ± SD of three independent experiments. * = $p < 0.05$ vs control cultures, Student's t test.

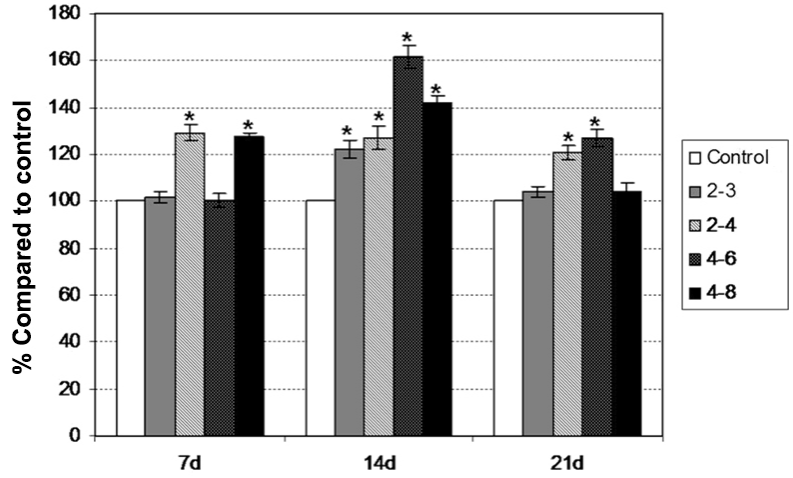

Figure A.3: Effects of pillar-structured surfaces on mineralization of MSCs at 7, 14, and 21 days after seeding. Results, expressed as % compared to control, are means ± SD of three independent experiments. * = $p < 0.05$ vs control cultures, Student's t test.

RINGRAZIAMENTI

Questo lavoro di tesi rappresenta il termine del percorso di dottorato in Ingegneria Industriale intrapreso tre anni fa.

Molte sono le persone che desidero ringraziare per il loro supporto, per gli insegnamenti ricevuti e soprattutto per la loro amicizia.

Innanzitutto desidero ringraziare il Prof. Giovanni Lucchetta, il quale, oltre a supportarmi e a guidarmi durante tutti e tre gli anni, mi ha tramandato una grande passione per la ricerca.

Desidero poi ringraziare tutti i miei colleghi del Laboratorio Te.Si. tra cui Luca, Davide, Federico, Ruggero, Riccardo e Filippo con i quali ho instaurato un profondo legame di amicizia.

Un grazie va anche al Prof. Ben Whiteside e a tutto il suo gruppo di ricerca per avermi ospitato presso i loro laboratori all'Università di Bradford.

Infine, ho desiderio di ringraziare con affetto i miei genitori Marta e Ruggero per il grande sostegno e aiuto che mi hanno sempre dato.

Un grazie a Laura per essermi stata vicina in ogni momento.

M. S.

BIBLIOGRAPHY

[1] R Surace, G Trotta, I Fassi, V Bellantone, *The micro injection moulding process for polymeric components manufacturing*, INTECH Open Access Publisher, **2012**.

[2] Wittmann Battenfeld GmbH, Micro-Moulding: Battenfeld Injection Molding, Kottingbrunn, Austria, **2010**, pp. 1–70.

[3] M. Oliveira, V. Neto, M. Fonseca, T. Zhiltsova, J. Gracio in A. Z. El-Sonbati, *Thermoplastic Elastomers*, InTech, **2012**.

[4] H Guckel, *Proceedings of the IEEE* **1998**, *86*, 1586–1593.

[5] E. Becker, W. Ehrfeld, P. Hagmann, A Maner, D Münchmeyer, *Microelectronic engineering* **1986**, *4*, 35–56.

[6] Y. Xia, J. A. Rogers, K. E. Paul, G. M. Whitesides, *Chemical reviews* **1999**, *99*, 1823–1848.

[7] E. Delamarche, H. Schmid, B. Michel, H. Biebuyck, *Advanced Materials* **1997**, *9*, 741–746.

[8] Y. Xia, E. Kim, X.-M. Zhao, J. A. Rogers, M. Prentiss, G. M. Whitesides, *Science* **1996**, *273*, 347–349.

[9] P. Rai-Choudhury, *Handbook of microlithography, micromachining, and microfabrication: microlithography*, *Vol. 1*, Iet, **1997**.

[10] J. Ming, F. J. Smith, *Speech Communication* **2001**, *34*, 41–55.

[11] S. Y. Chou, *Mrs Bulletin* **2001**, *26*, 512–517.

[12] C. S. Torres, S Zankovych, J Seekamp, A. Kam, C. C. Cedeno, T Hoffmann, J Ahopelto, F Reuther, K Pfeiffer, G Bleidiessel, et al., *Materials Science and Engineering: C* **2003**, *23*, 23–31.

[13] H. N. Hansen, R. Hocken, G. Tosello, *CIRP Annals-Manufacturing Technology* **2011**, *60*, 695–714.

[14] Y. Qin, *Micro-manufacturing engineering and technology*, Elsevier, 1a, **2010**, pp. 1–414.

[15] J. Greener, R. Wimberger-Friedl, *Precision Injection Molding*, Hanser, **2006**, pp. 1–328.

[16] M Heckele, W. Schomburg, *Journal of Micromechanics and Microengineering* **2004**, *14*, R1.

[17] K. Monkkonen, J. Hietala, P. Paakkonen, E. J. Paakkonen, et al., *Polymer engineering and science* **2002**, *42*, 1600.

[18] M. Matschuk, N. B. Larsen, *Journal of Micromechanics and Microengineering* **2013**, *23*, 025003.

[19] H. Suzuki, T. Takayama, H. Ito in International Journal of Modern Physics: Conference Series, *Vol. 6*, World Scientific, **2012**, pp. 563–569.

[20] A.-C. Liou, R.-H. Chen, *The International Journal of Advanced Manufacturing Technology* **2006**, *28*, 1097–1103.

[21] M. Yoshii, H. Kuramoto, K. Kato, *Polymer Engineering & Science* **1994**, *34*, 1211–1218.

[22] R Wimberger-Friedl, *Specialized Molding Techniques: Application Design Materials and Processing* **2008**, 149.

[23] L. Yu, C. G. Koh, L. J. Lee, K. W. Koelling, M. J. Madou, *Polymer Engineering and Science* **2002**, *42*, 871.

[24] H.-Y. Lin, C.-H. Chang, W.-B. Young, *International Communications in Heat and Mass Transfer* **2010**, *37*, 1477–1486.

[25] H.-Y. Lin, W.-B. Young, *Applied Mathematical Modelling* **2009**, *33*, 3746–3755.

[26] M.-C. Yu, W.-B. Young, P.-M. Hsu, *Materials Science and Engineering: A* **2007**, *460*, 288–295.

[27] C.-S. Chen, S.-C. Chen, W.-H. Liao, R.-D. Chien, S.-H. Lin, *International Communications in Heat and Mass Transfer* **2010**, *37*, 1290–1294.

[28] H. Pranov, H. K. Rasmussen, N. B. Larsen, N. Gadegaard, *Polymer Engineering & Science* **2006**, *46*, 160–171.

[29] C. Griffiths, S. Dimov, E. Brousseau, R. Hoyle, *Journal of Materials Processing Technology* **2007**, *189*, 418–427.

[30] U. M. Attia, S. Marson, J. R. Alcock, *Microfluidics and Nanofluidics* **2009**, *7*, 1–28.

[31] G. Tosello, A. Gava, H Hansen, G. Lucchetta in ANTEC conference proceedings, *Vol. 4*, **2007**, p. 2002.

[32] C. A. Griffiths, S. S. Dimov, S Scholz, H. Hirshy, G. Tosello, *Journal of Manufacturing Science and Engineering* **2011**, *133*, 031007.

[33] W. Michaeli, A. Schreiber, *Advances in polymer technology* **2009**, *28*, 65–76.

[34] Y. Shen, S. Yeh, S. Chen, *International communications in heat and mass transfer* **2002**, *29*, 643–652.

[35] V. Bellantone, R. Surace, G. Trotta, I. Fassi, *The International Journal of Advanced Manufacturing Technology* **2013**, *67*, 1407–1421.

[36] H. A. Barnes, J. F. Hutton, K. Walters, *An introduction to rheology*, *Vol. 3*, Elsevier, **1989**.

[37] C. W. Macosko, R. G. Larson, **1994**.

[38] X Han, H Yokoi, *Polymer Engineering & Science* **2006**, *46*, 1590–1597.

[39] Y.-K. Shen, C.-Y. Chang, Y.-S. Shen, S.-C. Hsu, M.-W. Wu, *International Communications in Heat and Mass Transfer* **2008**, *35*, 723–727.

[40] C. Gornik in Macromolecular Symposia, *Vol. 217*, Wiley Online Library, **2004**, pp. 365–374.

[41] D. Yao, *Journal of injection molding technology* **2002**, *6*, 11.

[42] Y. Yeong-Eun, K. Tae-Hoon, J. Tae-Jin, C. Doo-Sun, K. Chang-Wan, K. Sun-Kyung, *Transactions of Nonferrous Metals Society of China* **2011**, *21*, s148–s152.

[43] W.-B. Young, *Applied mathematical modelling* **2007**, *31*, 1798–1806.

[44] G. Xu, L. Yu, L. J. Lee, K. W. Koelling, *Polymer Engineering & Science* **2005**, *45*, 866–875.

[45] O Rötting, W Röpke, H Becker, C Gärtner, *Microsystem Technologies* **2002**, *8*, 32–36.

[46] J. G. Lee, B.-K. Lee, T. G. Kang, T. H. Kwon, *Polymer Engineering & Science* **2010**, *50*, 1186–1198.

[47] G. Fu, S. B. Tor, D. E. Hardt, N. Loh, *Microsystem technologies* **2011**, *17*, 1791–1798.

[48] S. Kuhn, A. Burr, M. Kübler, M. Deckert, C. Bleesen, *Journal of Micromechanics and Microengineering* **2011**, *21*, 025024.

[49] N. S. Ong, H. Zhang, W. H. Woo, *Materials and Manufacturing Processes* **2006**, *21*, 824–831.

[50] U. M. Attia, J. R. Alcock, *Microsystem technologies* **2009**, *15*, 1861–1872.

[51] H. Becker, C. Gärtner, *Analytical and bioanalytical chemistry* **2008**, *390*, 89–111.

[52] B Sha, S Dimov, C Griffiths, M. Packianather, *Journal of Materials Processing Technology* **2007**, *183*, 284–296.

[53] R.-D. Chien, *Sensors and Actuators A: Physical* **2006**, *128*, 238–247.

[54] B. Sha, S. Dimov, C. Griffiths, M. S. Packianather, *The International Journal of Advanced Manufacturing Technology* **2007**, *33*, 147–156.

[55] Y.-C. Su, J. Shah, L. Lin, *Journal of Micromechanics and Microengineering* **2004**, *14*, 415.

[56] H Schift, C David, M Gabriel, J Gobrecht, L. Heyderman, W Kaiser, S Köppel, L Scandella, *Microelectronic Engineering* **2000**, *53*, 171–174.

[57] U. A. Theilade, H. N. Hansen, *The International Journal of Advanced Manufacturing Technology* **2007**, *33*, 157–166.

[58] G Lucchetta, M Fiorotto, P. Bariani, *CIRP Annals-Manufacturing Technology* **2012**, *61*, 539–542.

[59] K. Miller, K. Ramani, *Advances in Polymer Technology* **1998**, *17*, 251–257.

[60] D. Yao, T. E. Kimerling, B. Kim, *Polymer Engineering and Science* **2006**, *46*, 938.

[61] G Fu, N. Loh, S. Tor, B. Tay, Y Murakoshi, R Maeda, *Microsystem Technologies* **2005**, *11*, 1267–1271.

[62] M.-C. Jeng, S.-C. Chen, P. S. Minh, J.-A. Chang, C.-s. Chung, *International communications in heat and mass transfer* **2010**, *37*, 1295–1304.

[63] S.-H. Yoon, P Padmanabha, N.-G. Cha, J. Mead, C. Barry, *International Polymer Processing* **2011**, *26*, 346–353.

[64] R. Ruprecht, W. Bacher, J. H. Hausselt, V. Piotter in Micromachining and Microfabrication, International Society for Optics and Photonics, **1995**, pp. 146–157.

[65] G. Menges, W. Michaeli, P. Mohren, G. Menges, W. Michaeli, P. Mohren, *How to make injection molds*, Carl Hanser Verlag GmbH & Co. KG, **2001**.

[66] C. Griffiths, S. S. Dimov, S Scholz, G. Tosello, *Journal of Manufacturing Science and Engineering* **2011**, *133*, 011006.

[67] Z. Lu, K. Zhang, *The International Journal of Advanced Manufacturing Technology* **2009**, *40*, 490–496.

[68] R. Thiruvenkataswamy, *Controlling dimensions when injection molding microfluidic devices*, University of Massachusetts Lowell, **2007**.

[69] N. Lee, Y.-K. Kim, S. Kang, *Journal of Physics D: Applied Physics* **2004**, *37*, 1624.

[70] S. J. Lee, G. Khang, Y. M. Lee, H. B. Lee, *Journal of colloid and interface science* **2003**, *259*, 228–235.

[71] P. Mosaddegh, D. C. Angstadt, *Journal of Micromechanics and Microengineering* **2008**, *18*, 035036.

[72] H Yokoi, X Han, T Takahashi, W. Kim, *Polymer Engineering & Science* **2006**, *46*, 1140–1146.

[73] K. Kolind, A. Dolatshahi-Pirouz, J. Lovmand, F. S. Pedersen, M. Foss, F. Besenbacher, *Biomaterials* **2010**, *31*, 9182–9191.

[74] R. Artigas in *Optical Measurement of Surface Topography*, Springer, **2011**, pp. 237–286.

[75] J. Melngailis, *Journal of Vacuum Science & Technology B* **1987**, *5*, 469–495.

[76] D. C. Montgomery, D. C. Montgomery, D. C. Montgomery, *Design and analysis of experiments*, *Vol. 7*, Wiley New York, **1984**.

[77] T. A. Osswald, L.-S. Turng, P. J. Gramann, *Injection molding handbook*, Hanser Verlag, **2008**.

[78] A. J. Lasprilla, G. A. Martinez, B. H. Lunelli, A. L. Jardini, R. Maciel Filho, *Biotechnology advances* **2012**, *30*, 321–328.